August 2018

Studies in Molecular Recognition: Non-proteogenic Amino Acids for Antibiotic Studies and Chemosensors for Recognition and Reporting of Metal-ions

Sarah Anne Oehm
University of Wisconsin-Milwaukee

MOLECULAR RECOGNITION:

NON-PROTEOGENIC AMINO ACIDS FOR ANTIBIOTIC STUDIES

AND CHEMOSENSORS FOR RECOGNITION AND REPORTING OF METAL IONS

by

Sarah Oehm

A Dissertation Submitted in

Partial Fulfillment of the

Requirements for the Degree of

Doctor of Philosophy

in Chemistry

at

University of Wisconsin – Milwaukee

May 2018

ABSTRACT
STUDIES IN MOLECULAR RECOGNITION:
NON-PROTEOGENIC AMINO ACIDS FOR ANTIBIOTIC STUDIES AND
CHEMOSENSORS FOR RECOGNITION AND REPORTING OF METAL-IONS

by

Sarah Oehm

The University of Wisconsin – Milwaukee, May 2018
Under the Supervision of Professor Alan W. Schwabacher

The field of molecular recognition focuses on the selective and reversible binding of small guest molecules to larger host molecules. This dissertation describes synthesis of small molecules as binding guests for enzymatic substrates as well as molecules as host chemosensors to detect and identify metal ions. Two approaches to new antibiotic drugs have been explored, and an array of sensors for the quantitation of aqueous metals is being commercialized.

As strains of deadly bacteria emerge with evolved resistance to known antibiotics, new drugs are needed with novel mechanisms of action. Natural product antibiotics containing enduracididine, a non-canonical amino acid derived from arginine, have been found effective against resistant organisms. Recently, the biosynthesis of enduracididine has been elucidated by the Silvaggi group. Various derivatives of arginine are of interest as guest molecules for the Mpp family of proteins. We have developed a particularly succinct route to γ-hydroxy-arginine, which has also been used as a precursor to other oxidized arginine derivatives. Our route provides quantities of arginine derivatives which have been synthesized via a four step route utilizing an isoxazoline intermediate. The synthetic methods for formation and subsequent reduction of the isoxazoline have been studied extensively; and this succinct and versatile synthesis yields either γ-hydroxy-arginine or the keto acid derived from it by changing the conditions of the reduction.

In another approach to developing new antibiotic treatment, we have pursued the inhibition of the β-barrel assembly machine (BAM), through a small molecule scaffold that binds β-sheets. BAMa is the only known β-barrel protein that spontaneously folds, while all others require the help of BAMa. The β-barrel membrane proteins include efflux pumps, proteins for active transport that allow bacterial survival by ejection of antibiotic drugs. Inhibition of BAMa may itself prove bactericidal, or used in combination therapy increase efficacy of drugs rendered previously ineffective due to acquired resistance.

We have also developed metal ion chemosensors for simulataneous identification and quantitation of multiple metals. These are useful for monitoring metal ion concentrations in industrial wastewater. Current limitations in measuring metal concentration in wastewater can lead to increased costs and excess solid waste in order to meet compliance standards. Our goal is a simple system to allow continuous, real-time measurement of multiple metals on site to decrease over-treatment and detect spikes in pollutant metals. Utilizing UV/VIS absorption an array of semi-selective sensors each with its own spectral response to metal ions allows identification and concentration of pollutants to be determined. Toward this end, we have prepared chemosensors, demonstrated their sensing ability, and covalently attached them to transparent polymers and transparent supports in several ways that allow repeated use for metal-ion measurement. These dyes have been studied in solution and when covalently bound to polymers. Dyes with complementary metal-selectivity allow for high information from a few sensors; a model using three sensors has been demonstrated to simultaneously measure the concentration of seven metals in solution.

DEDICATION

For my Grandparents,

Who never ran out of

Vinegar and Baking Soda

TABLE OF CONTENTS

LIST OF FIGURES

LIST OF ABBREVIATIONS

AcOH	Acetic Acid
Arg	Arginine
BAM	β-Barrel Assembly Machine
Boc	*tert*-Butoxycarbonyl
BSA	*bis*-trimethylsilyl acetamide
BuOH	Butanol
CDI	Carbonyldiimidazole
DABCO	1,4-diazabicyclo[2.2.2]octane
d	Doublet (NMR)
DCC	N,N-Dicyclohexylcarbodiimide
dd	Doublet of doublets (NMR)
DIC	N,N-Diisopropylcarbodiimide
DIPEA	Diisopropylethylamine
DMAP	Dimethylaminopyridine
DMF	Dimethylformamide
DMSO	Dimethylsulfoxide
EDTA	Ethylenediaminetetraacetic acid
End	Enduracididine
eq.	Equivalent
EtOH	Ethanol
h	Hour
HOBT	Hydroxybenzotriazole

IPA	Isopropyl alcohol
IR	Infrared Spectroscopy
J	Coupling constant (NMR)
LCMS	Liquid Chromatography Mass Spectrometry
m	Multiplet
MeOH	Methanol
min	Minute
Mpp	Mannopeptimycin (gene cluster)
MRSA	Methicillin-resistant Staphylococcus aureus
MW	Molecular Weight
NMP	N-Methyl-2-pyrrolidone
NMR	Nuclear Magnetic Resonance
PBP	Penicillin-Binding Proteins
PLP	pyridoxal 5'-phosphate
rt	Room Temperature
s	Singlet (NMR)
SwMppP	*Streptomyces wadayamensis* MppP
t	Triplet (NMR)
TFA	Trifluoroacetic acid
THF	Tetrahydrofuran
TLC	Thin Layer Chromatography
Ts	*para*-toluenesulfonyl
UV	Ultra Violet

Chapter 1. Introduction

1.1 Molecular Recognition

Intermolecular forces such as hydrogen-bonding, Van der Waals forces, dipole-ion, and π-π interactions contribute to the macroscopic physical properties of pure compounds and influence the behaviors of compounds in mixtures. Large host molecules exhibit reversible and selective binding of smaller guest molecules: the specificity and affinity for the binding event depends on the intermolecular forces that contribute positively and negatively to the binding. These factors influence the complexation equilibrium, (Figure 1[1]) described by an association constant, K_a, or dissociation constant, K_d, which can be measured by variety of instrumental and titration methods.
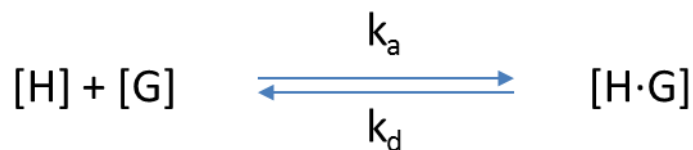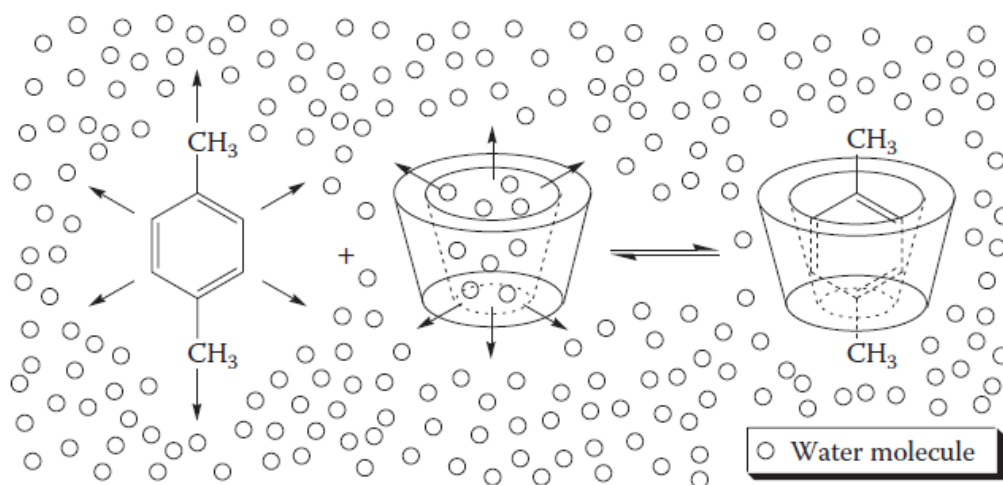
Figure 1. Host Guest Complexation

Intermolecular forces lead to recognition and binding events that create the chemical basis for all biology. Non-covalent interactions of solvated molecules in aqueous media is especially impressive. Increased favorability for complexation is achieved through rigid scaffolds with pre-organized conformations to contribute to positive binding interactions for the host and guest molecules. Selectivity effects can be steric, relying on the Van der Waals radius of a substrate in size exclusion, or selectivity can be achieved through the electronic effects of polar and ionic interactions. Molecular recognition in nature is selective and specific, such as enzyme-substrate or antibody-antigen. Complex biological events can be understood and modeled by mimicking biology with simpler synthetic systems and making small variations in structure.

Molecular recognition has been studied in diverse systems. Host molecules, such as the families of crown ethers, calixarenes, and cyclodextrins are well-known for their ability to reversibly bind substrate guest molecules and offer a wide variety of applications ranging from ion-recognition[2] to more complex sensing[3], including but not limited to catalysis[4] and enzyme mimetics.[5] This dissertation describes the synthesis of small molecules for molecular recognition to biological host proteins as well as metal-ion guests.

Chapter 2. Antibiotic Studies: Lipid II Inhibition and Oxidized Derivatives of Arginine

2.1 Introduction to Lipid II Inhibition

The challenges in antibiotic research are many.[6] The bacterial cell wall presents a challenge for the diffusion of drugs into the cytoplasm, and in gram-negative bacteria a second outer-membrane compounds this challenge. An electron micrograph of a thin section of the bacterial cellular envelope[7] (Figure 2) shows the inner membrane (Arrow 1), barely visible next to the highly stained inner layers of the peptidoglycan cell wall (Arrow 2), which is surrounded by the external membrane (Arrow 3) found in Gram-negative bacteria.
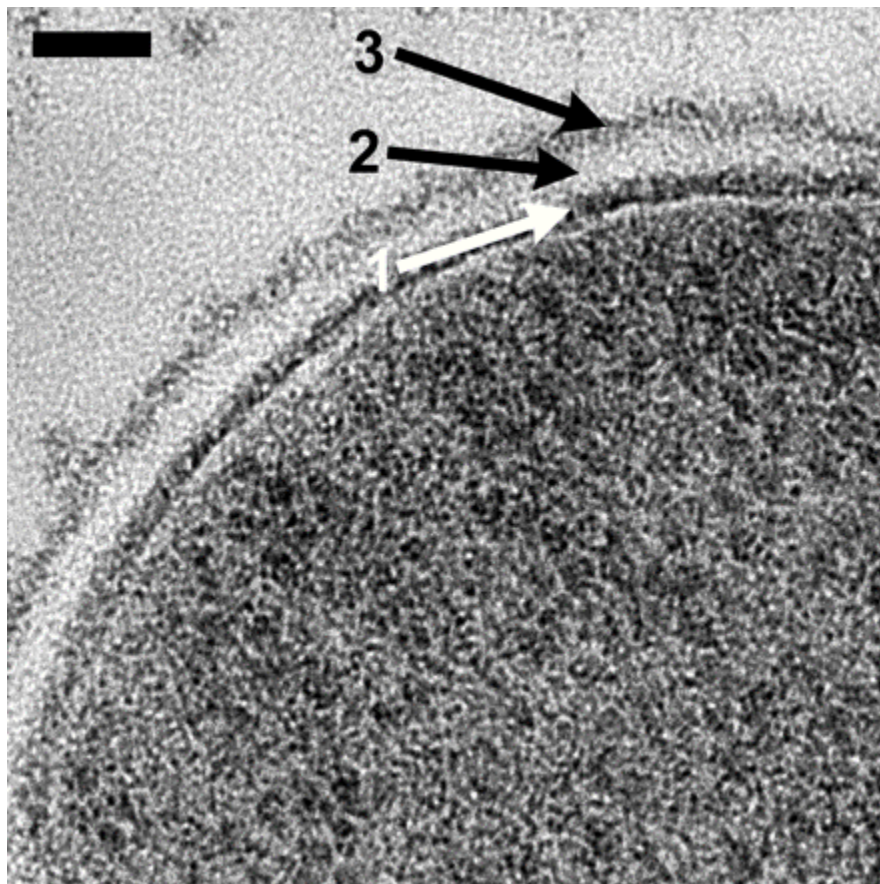
Figure 2. Electron Micrograph of a Gram-Negative Bacterium

The cell wall is not found in mammals, making the cellular envelope an attractive target for antimicrobial drugs. Ideal candidates for antibiotics target components of the outer membrane and cell wall of bacteria, the peptidoglycan layer. These non-mammalian organelles are on the cellular exterior and more readily accessed, without relying on active transport or diffusion into the cell. As these molecular targets are specific to bacteria, little toxicological off-target effects are expected in animals.

Commonly prescribed treatments target structures of the cell wall. Lipid II is the monomer that makes up the peptidoglycan cell wall of bacteria (Figure 3). It is polymerized by a DD-transpeptidase, commonly referred to penicillin-binding protein (PBP), as shown in Figure 4. This transpeptidase catalyzes the condensation of lipid II monomers, by recognizing the acyl-D-alanyl-D-alanine sequence.[8]
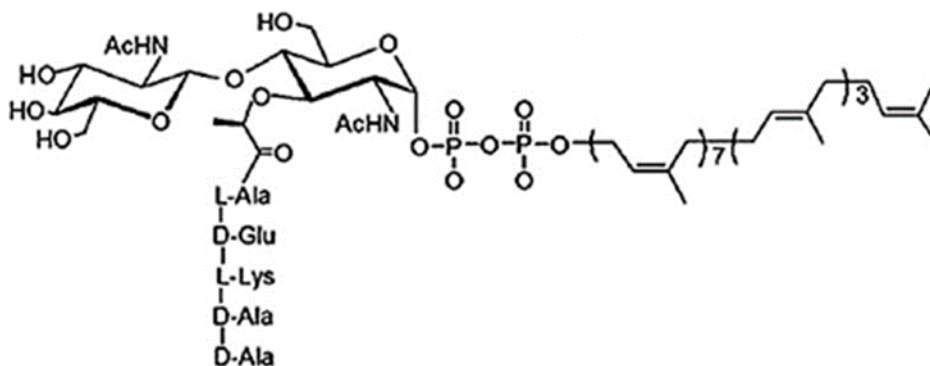
Figure 3. Structure of Lipid II
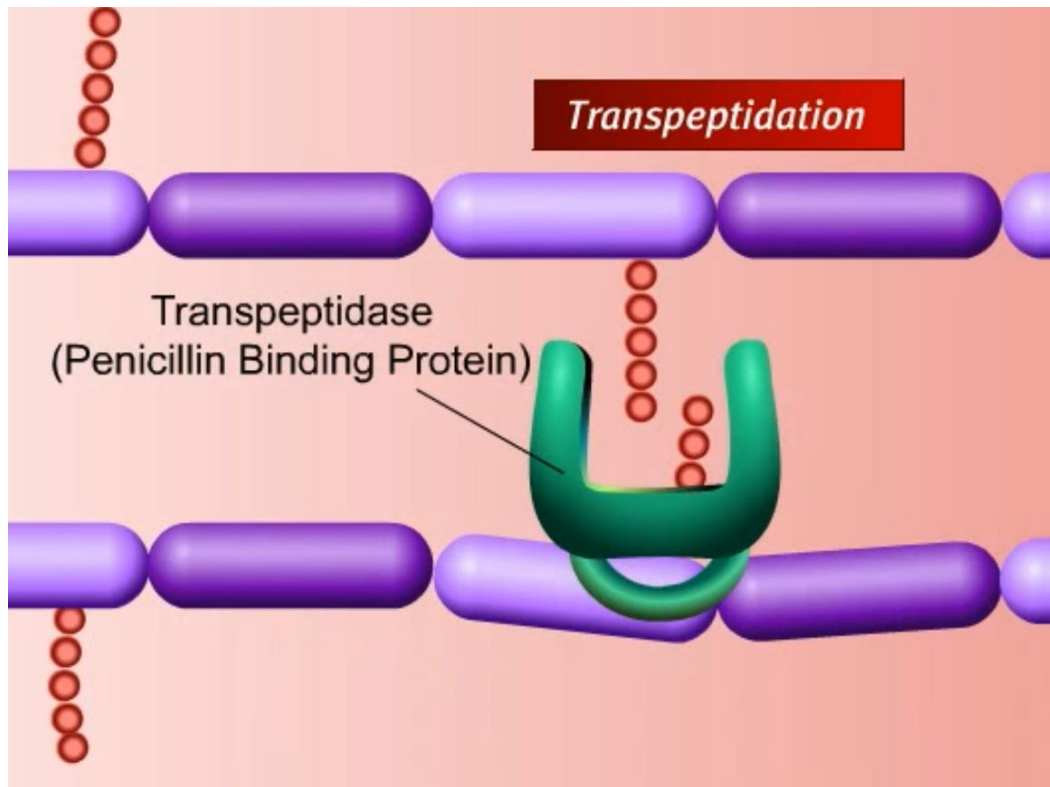
Figure 4. Lipid II units are connected by Penicillin Binding Protein to form the peptidoglycan cell wall of bacteria.

The β-lactam antibiotics, penicillin and methicillin (Figure 5, left and right respectively), contain a ring conformationally locked in a similar geometry to the D-ala-D-ala binding mode, and bind covalently to the transpeptidase, inhibiting the organism's ability to repair the cell wall. As β-lactam antibiotics inhibit the crosslinking of lipid II,[9] enzymes which hydrolyze the cell wall are still active, leading to cell death.

Bacterial generation time is short and resistant individuals are able to survive, giving rise to another challenge in antibiotic development: the race to develop drugs to compete with the evolution of resistance. Resistance to penicillin G has evolved through hydrolysis of penicillins by β-lactamases, however methicillin is resistant to these enzymes. In methicillin resistant

organisms, such as Methicillin-Resistant *Staphylococcus aureus* (MRSA), gene-modification of PBP has been observed.[9] Drug-resistant bacteria are a rising problem due to the increased use of antibiotics and antiseptics, through use in livestock feed and over-prescription, leading to the evolution of stronger microorganisms. MRSA infections are difficult to treat with currently available drugs and an estimated 1.7 million healthcare-associated infections are responsible for 99,000 deaths annually in the US.[10] There is a need for new antibiotics which function through new mechanisms to which the organisms have not yet adapted a tolerance.
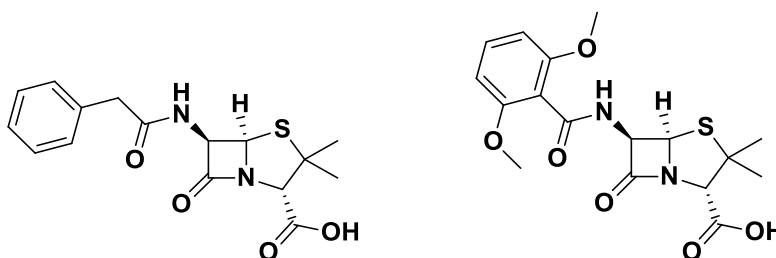
Figure 5. Penicillin G and Methicillin

Lipid II Inhibiting Natural Products

Vancomycin has emerged as a drug of a new class of glycopeptide antibiotics, and is the leading treatment for MRSA. Vancomycin disrupts cell wall synthesis by binding directly to the lipid II.[11] The crystal structure of vancomycin in blue with the D-Ala-D-Ala terminus of lipid II in green (Figure 6) shows how the pentapeptide tail of lipid II fits into the cavity of the cyclic antibiotic.[12] The cyclic structure of vancomycin pre-organizes five hydrogen-bonding interactions (shown with dotted lines) between the hydroxyl groups of the host antibiotic and carbonyls of the lipid II peptide backbone of the guest molecule resulting in high affinity binding to the bacterial target.
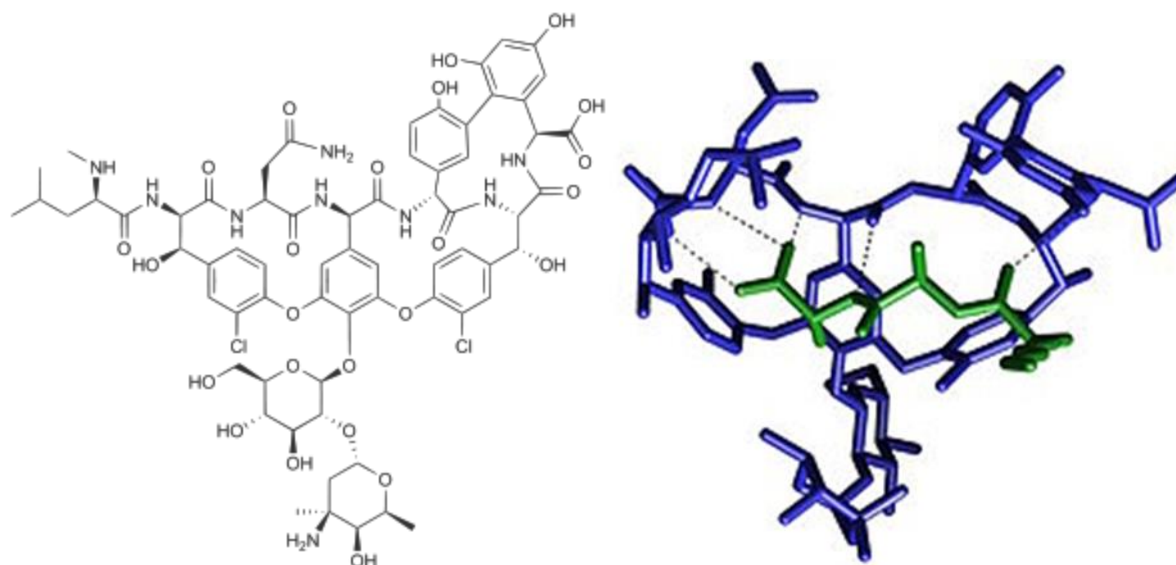
Figure 6. Vancomycin and its crystal structure bound with pentapeptide of lipid II

Despite favorable binding, modification by methylation and amidation of the amino acids of lipid II has rendered vancomycin ineffective in highly resistant strains of *Staphylococcus aureus*.[13]

A new class of lipid II-binding inhibitors has been identified.[14] Enduracididine-containing natural products: the cyclic lipopeptide enduracidin[6,15,16] (Figure 7), cyclic glycopeptide mannopeptimycin[17–19] (Figure 8), and cyclic peptide teixobactin[20,21] (Figure 9), have been of recent interest.[14] Due to their cyclic structure, they are similar to vancomycin in their resistance to digestion by proteases and pre-organized in conformations with limited rotational freedom resulting in good selectivity for binding their biological targets. These natural products contain many non-proteogenic amino acids. We have focused on the synthesis and biosynthesis of enduracididine (L-End) and its diasteromer L-*allo*-End, which are incorporated into these antibiotics.
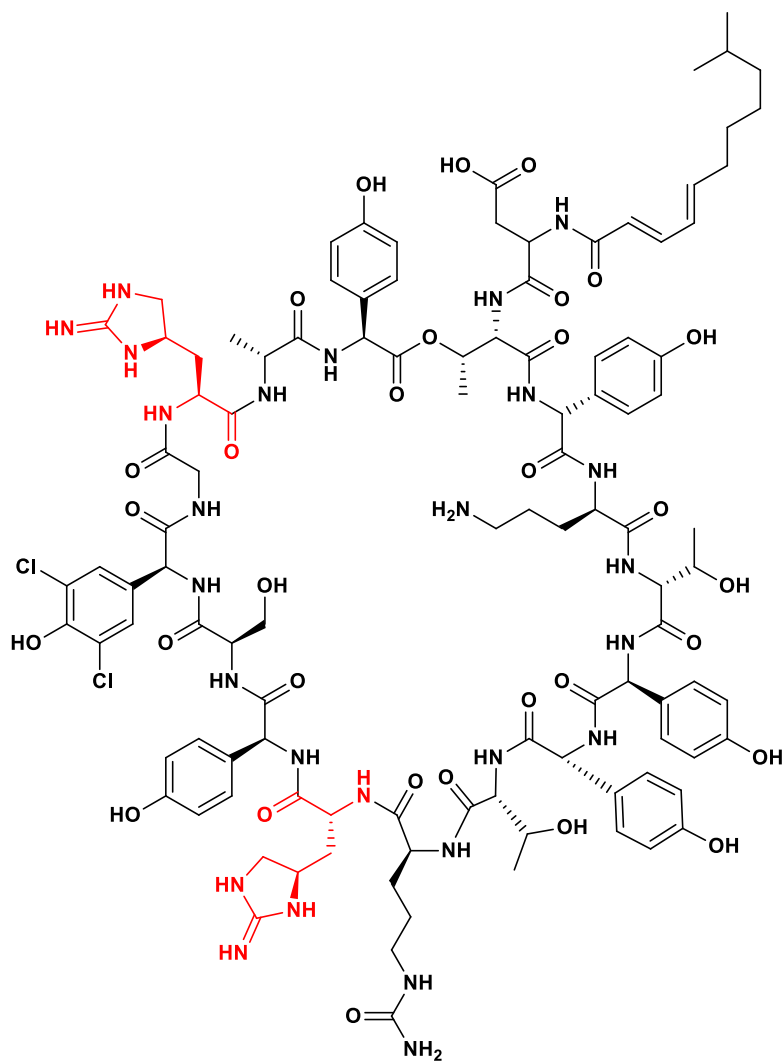
Figure 7. Enduracidin
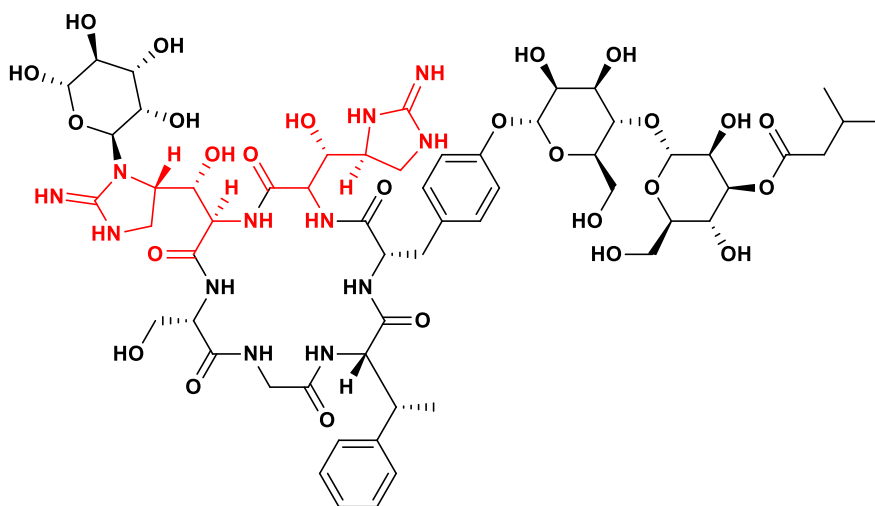
Figure 8. Mannopeptimycin
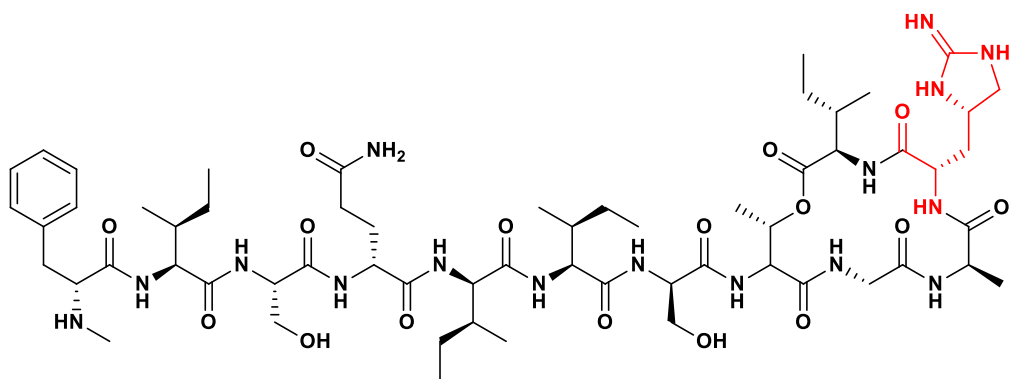
Figure 9. Teixobactin

Enduracididine is a cyclic guanidine-containing amino acid, analogous to conformationally restricted arginine (Figure 10). The conformational restriction of the L-End compared to L-Arg appears to enhance efficacy of the antibiotic activity. In studies with teixobactin, substitution of L-*allo*-enduracididine with L-Arg raised the minimum inhibitory concentration (MIC) of the drug by a factor of 8, from 0.2nM to 1.6nM,[22] leading to the hypothesis that the conformation of L-Arg is influential to activity, and the limited rotational freedom of the guanidinium moiety in L-*allo*-End is influential to activity. Our efforts in understanding these antibiotics is through the study of oxidized arginines involved in the biosynthesis of enduracididine, with the long-term goal of a semi-biosynthetic route to novel analogues of enduracididine.
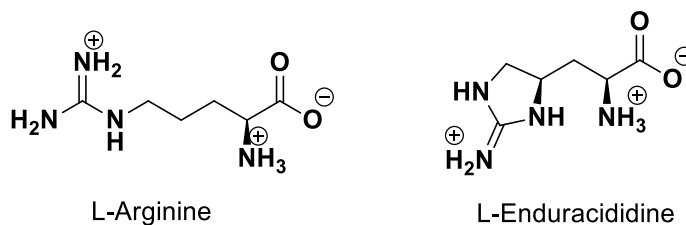
Figure 10. L-Arginine and L-Enduracididine

Synthesis of Diasteromeric L-Enduracididine

Synthesis of diastereomeric enduracididine was first reported by Tsuji in 1975[23] (Figure 11). Beginning from L-histidine methyl ester and using steps that include expensive precious metal catalysis and harsh conditions, including hydrolysis by anhydrous hydrofluoric acid, L-End and L-*allo*-End were prepared as a mixture in 18% yield over five steps.
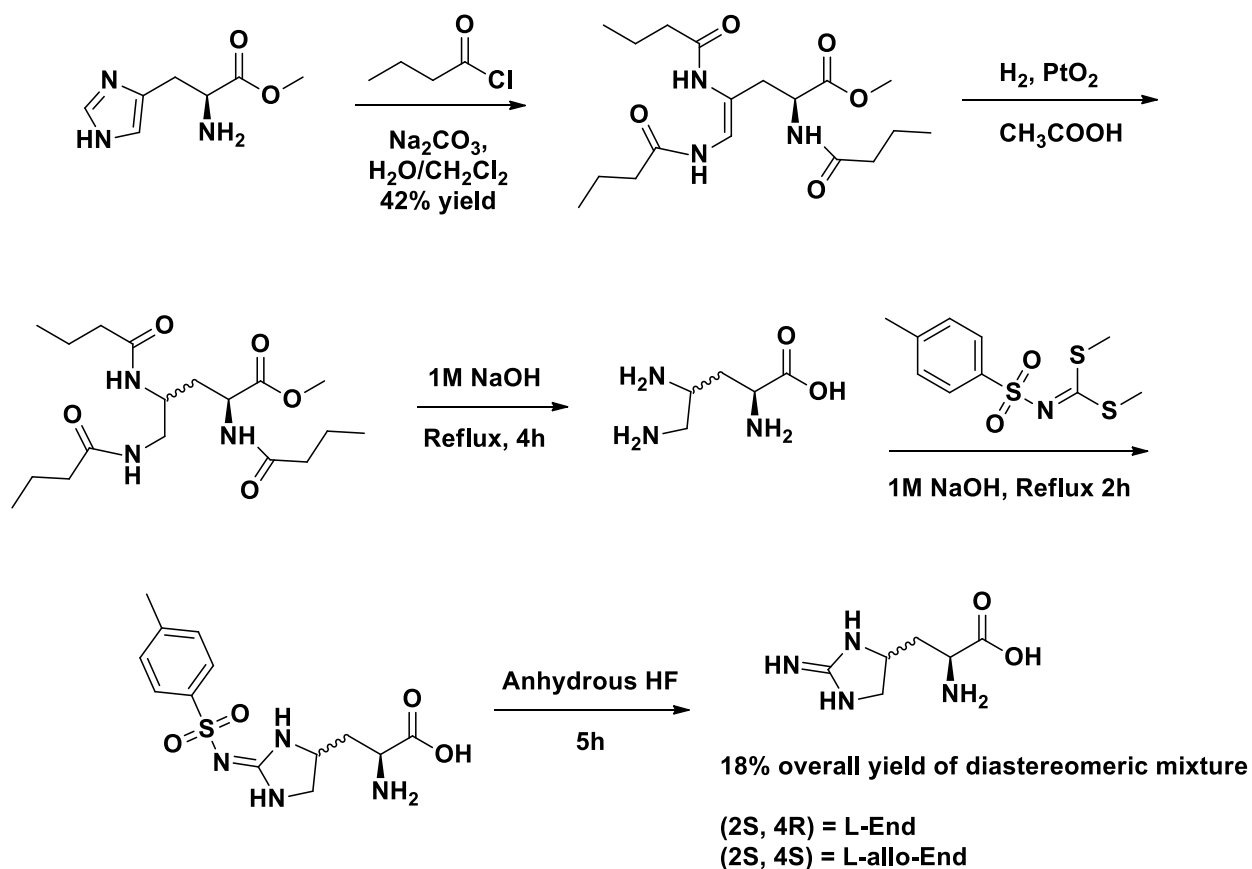
Figure 11. Synthesis of Diastereomeric L-Enduracididine

Synthesis of L-allo-Enduracididine

The stereoselective synthesis of L-*allo*-End (Figure 12) was reported by Craig in 2015.[24]

Beginning from a chiral precursor, (4R)-N-(tert-butoxycarbonyl)-4-hydroxyproline, undergoes a

ten-step synthesis to yield the trifluoroacetate salt of L-allo-End in roughly 31% overall yield.
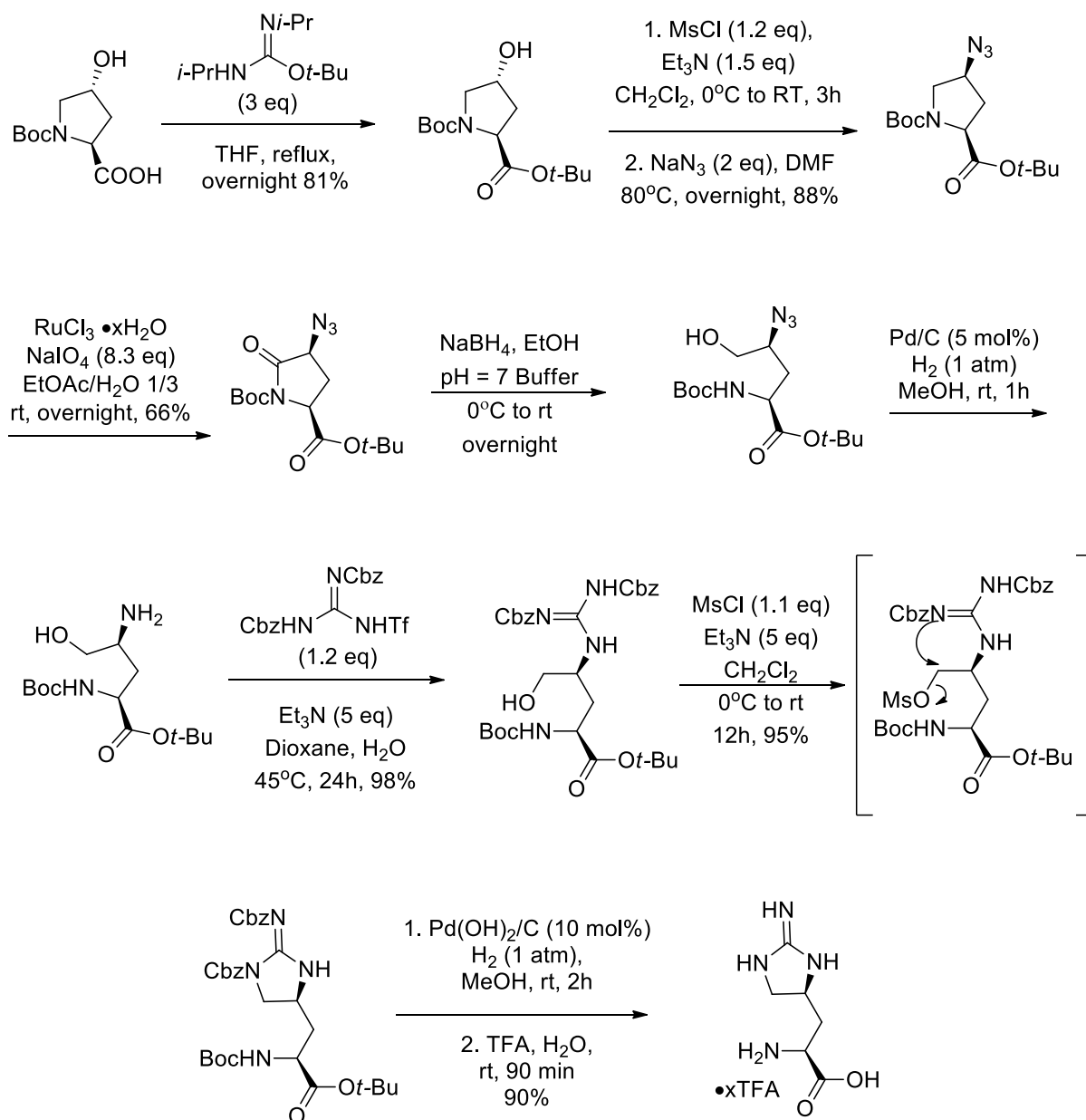
2.2 Enduracididine Biosynthesis

The MppPRQ gene cluster identified in the Mpp Pathway converts L-Arg to L-End (Figure 13).[16] The pathway is referred to as the Mpp Pathway, as these genes were first discovered in the total biosynthesis of mannopeptimycin.[18]
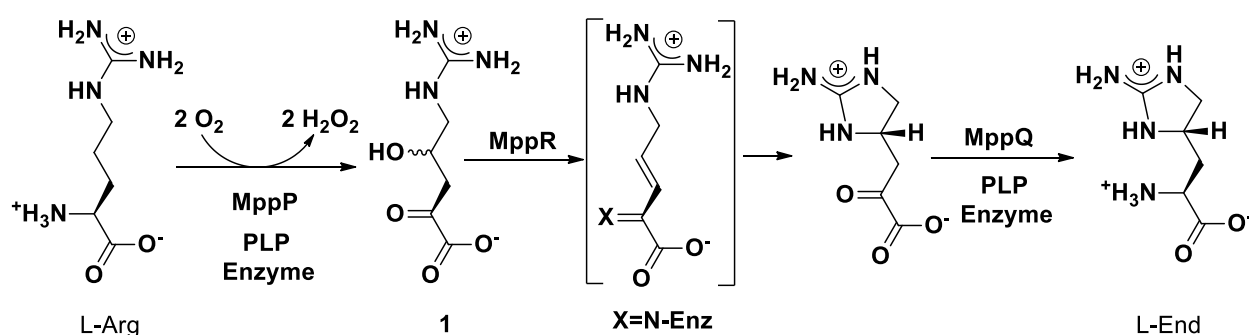
Figure 13. Streptomyces wadayamensis MppPRQ Pathway

The first enzyme in the pathway, MppP, is the first known PLP enzyme to catalyze hydroxylation as well as the more familiar PLP-enzyme function of converting an amino acid to its ketoacid. Its conversion of L-Arg to its γ-hydroxy-keto acid is incomplete; a ratio of 1.7:1 of the hydroxy-keto acid **1**: keto acid **3** (Figure 14) has been measured.

Our mechanism (Figure 14) takes into account all of the experimental data currently available.[25] The first steps up to **Q1** are common steps in PLP-dependent enzymes. The extreme stability of **Q1** in the absence of dioxygen ($t_{1/2}$ of several hours) suggests the active site of SwMppP is designed to stabilize this electron-rich intermediate until it encounters dioxygen. The formation of the superoxide anion and subsequent H-abstraction steps at C3 and C4 (**IV** and **V** in Figure 14) are speculative, and the same transformation could be accomplished in other ways, for

12

example, with a hydroperoxy-PLP adduct at Cα. Hydrolysis at this point leads to formation of **3** after consumption of one molecule of dioxygen and producing one molecule of H_2O_2.

If water is effectively excluded from the catalytic center, loss of the first molecule of peroxide leads to the second quinonoid intermediate (**Q2**), which after reacting with a second molecule of dioxygen, leads to a species like the hydroperoxy speculated in **VIII** (Figure 14) that can be displaced by water to give the fully oxidized product **1** and a second molecule of H_2O_2.

The colored boxes indicate the species that can be detected spectroscopically: **I**, internal aldimine (415 nm); **II**, external aldimine (425 nm); **Q1**, first quinonoid intermediate (510 nm); **Q2**, second quinonoid intermediate (560 nm). The species in grey boxes are not observed directly. The branch leading to **3** is speculative. Nonenzymatic deamination would give **3**, H_2O_2, and ammonia as observed experimentally. The oxygen atoms in the branch leading to **1** originate with H_2O, and do not come from dioxygen.[25] Pre-steady state kinetics studies are underway to test the current hypothetical mechanism, and if possible, assign rate constants to the observable steps. The γ-hydroxy-keto acid **1** goes on to react as the substrate for MppR which gives the cyclized substrate for MppQ (Figure 13). Presumably, the cyclization occurs through olefin intermediate shown in brackets. MppQ is a PLP enzyme catalyzing the transamination of keto acid to amino acid.
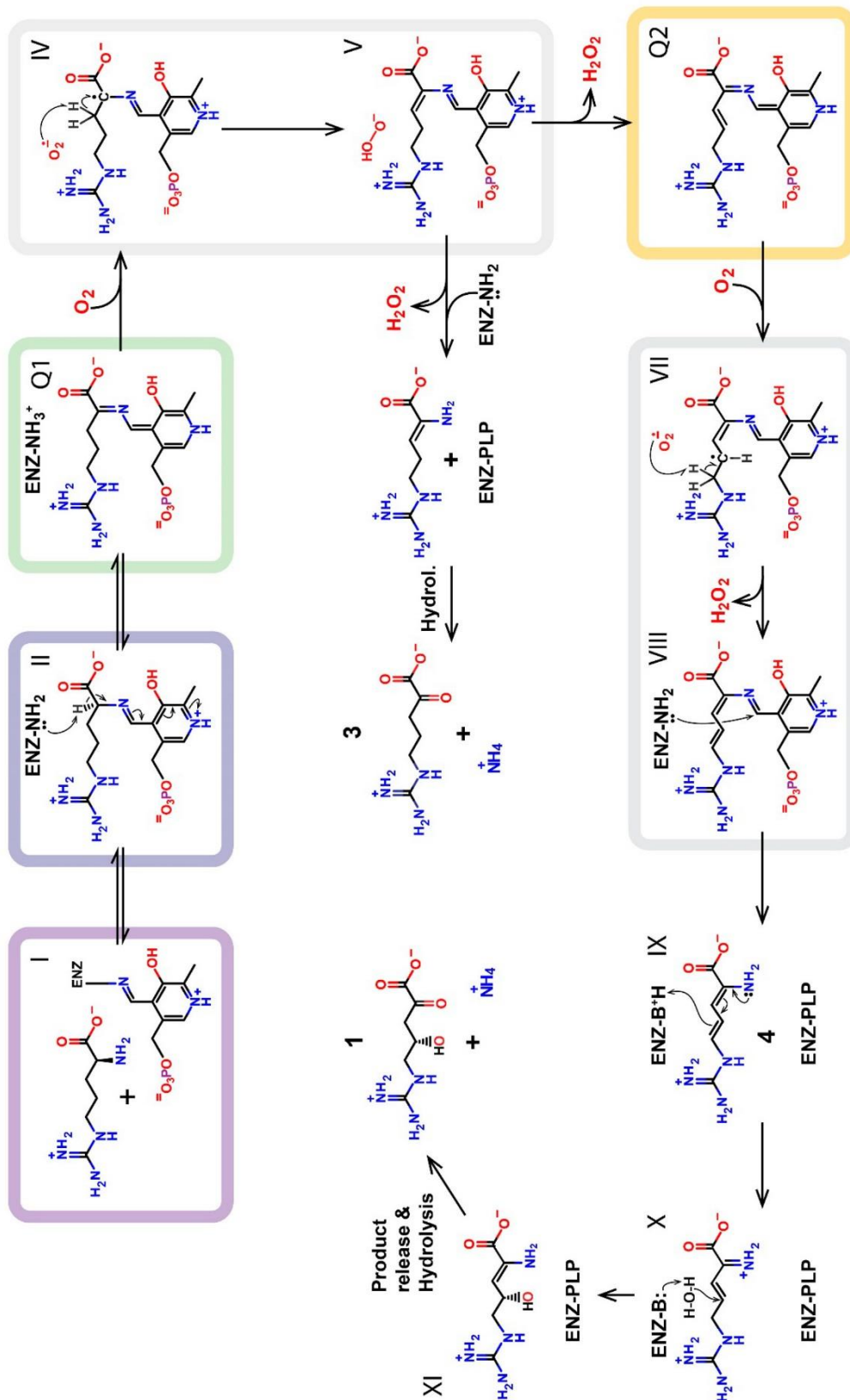
Figure 14. MppP Mechanism

14

Our efforts have focused on understanding MppP and MppR and our studies require significant amounts of γ-hydroxy arginine **2**, which is commercially unavailable, necessitating the synthesis of **2**. Yoon's synthesis of **2**[26] (Figure 15), starts with iodolactonizition of Boc-allyl glycine ($900/g Sigma-Aldrich) with good diastereomeric excess in one step. The iodide is substituted with azide and reduced to amine which is then guanidinylated with ^{13}C-containing diBoc-thiourea for radiopharmaceutical studies. The lactone is hydrolyzed in base and deprotected to yield 60mg **2** as its dicationic hydrochloride salt in 30% overall yield.
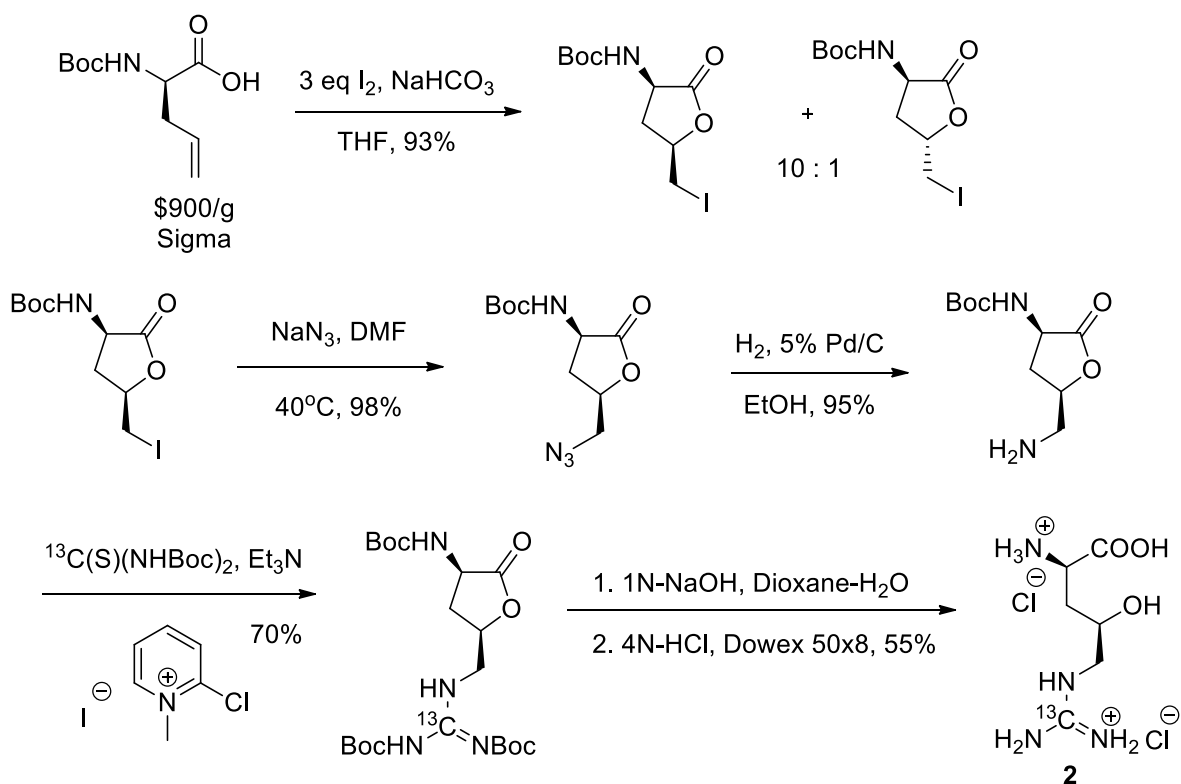
Figure 15. Yoon's Synthesis of γ-Hydroxy Arginine

Product **2** has been treated with L-amino acid oxidase (L-AAO) to give **1** by Robert Hoppe in the Schwabacher Lab.[27]

The structure and function of MppP from *Streptomyces wadayamensis* (SwMppP) has been probed extensively through X-ray crystallography and kinetic studies of the wild-type and 5

mutants.[25] Orthogonal views of the active site of SwMppP with keto acid of γ-hydroxy-arginine (**1, 4HKA** in Figure 16) and PLP are shown covalently bound to the enzyme as the aldimine. The glutamic acid residue (E15) is hydrogen-bonded to the carboxylate of **1**. The hydroxyl of threonine (T12) is hydrogen-bonded to the guanidine group. The imidazole ring of histidine (H29) hydrogen-bonds to the hydroxyl of the **1**. Water molecules in the crystal structure are shown as blue spheres and participate in hydrogen-bonding interactions as well. These hydrogen-bonding interactions are highlighted in dashed green lines. The hydrogen-bonding of E15 and T12 appear essential for hydroxylation to occur. In SwMppP with point mutations of these residues to alanine, formation of **1** was not observed. Without the N-terminus there appears to be premature hydrolysis of the aldimine, and **1** is not observed.
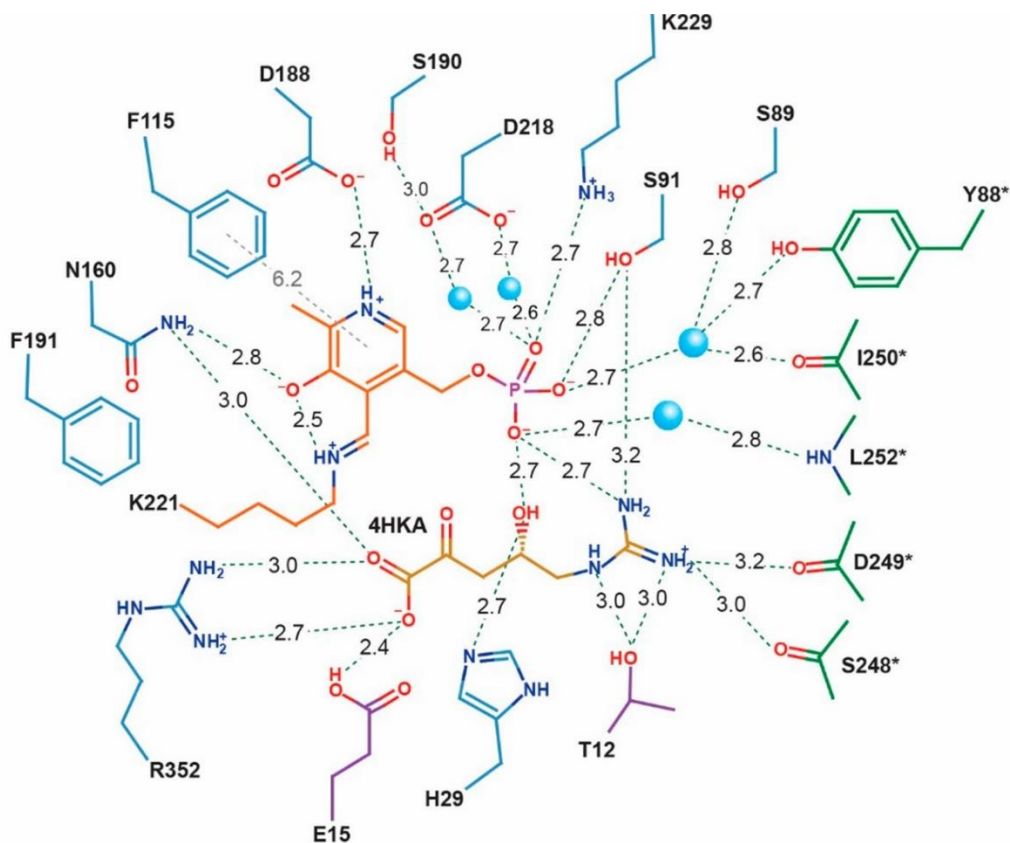
Figure 16. Active Site of MppP

16

The rate of consumption of O_2 was compared among SwMppP and its point mutants, again decreased activity was observed in 4 of the mutants, with E15Q being the only mutant comparable to the wild-type. Incorporation of ^{18}O from $^{18}O_2$ into **1** confirmed the oxidase activity of MppP. The production of H_2O_2 as a product of SwMppP was assayed by the addition of catalase, and the amount of O_2 generated by catalase is always half that consumed by MppP, indicating that each molecule of O_2 used to oxidize L-Arg is reduced to H_2O_2.

2.3 Oxidized Derivatives of Arginine for the Study of Enduracididine Biosynthesis

To further probe the mechanism of enduracididine biosynthesis, we are preparing non-commerically available derivatives of arginine. Originally, γ-hydroxy-arginine **2** was proposed as an intermediate in the Mpp pathway. The first enzyme in the sequence, MppP acts on arginine to give the keto acid **1** as its product, **1** goes on to be the substrate for MppR. However, MppP yields a mixture of keto acids (Figure 14, **1** and **3**) in which complete hydroxylation does not occur at the γ-position, necessitating a chemosynthesis to complement our studies.
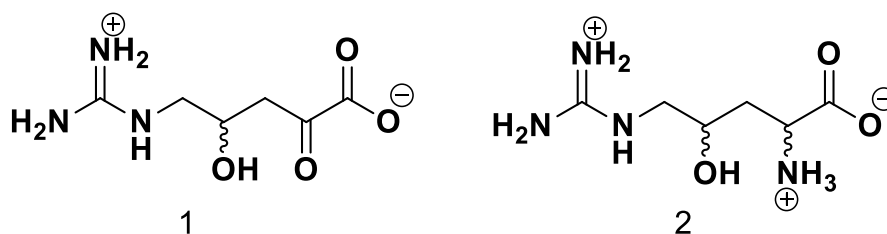
Figure 17. Oxidized Derivatives of L-Arg

Given the significance of ketoacid **1** and amino acid **2** (Figure 17) to the biosynthesis of enduracidin, we set out to prepare one or both of these substances in a cost-effective and scalable synthesis. Since compound **1** has been prepared from **2**[28] and ^{13}C-labelled **2** has been shown to incorporate label into Enduracidin,[28] we gave highest priority to preparation of **2**, but followed a route potentially leading to either **1** or **2** (Figure 18).
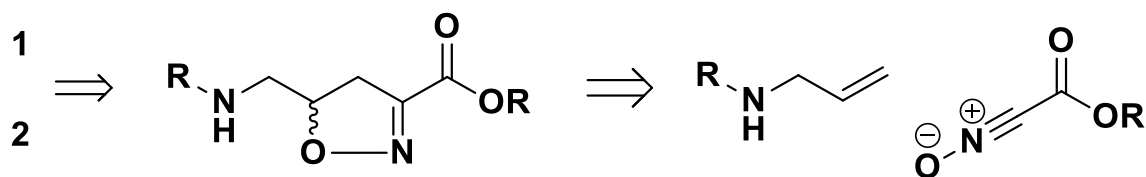
Figure 18. Retrosynthetic Analysis

We built the carbon skeleton of the arginines **1** and **2** from a functionalized isoxazoline. Isoxazolines are known to be converted by hydrogenolysis to imine alcohols, which undergo either hydrolysis to keto alcohol or further reduction *in situ* to amino alcohols.[29] Our isoxazoline gives access to a structure with several heteroatoms in one step. Formation of isoxazolines has been well-investigated by cycloaddition of nitrile oxides and alkenes,[29] and more recently demonstrated with nitro compounds.[30]

Isoxazolines for the Synthesis of γ-Hydroxy-Arginine

Isoxazolines are formed by the cycloadditions of alkenes (dipolarophiles) with nitrile oxides (strong dipoles).[29,31] The needed highly reactive nitrile oxides are usually formed by treatment of a nitroalkane with a powerful dehydrating agent such as phenyl isocyanate[32] (Figure 19) or by treatment of a halo-substituted oxime with base.[31]
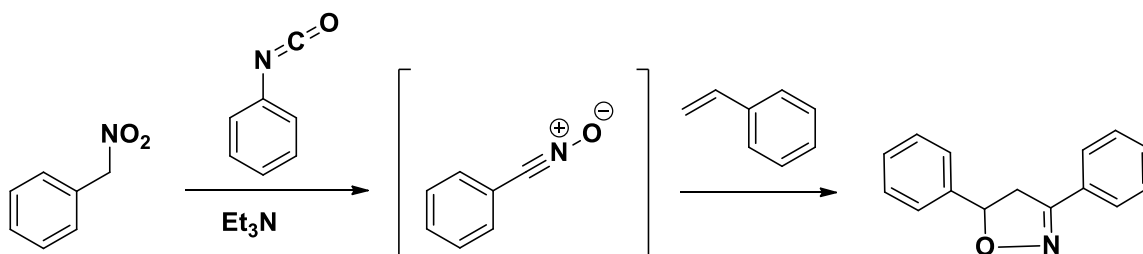
Figure 19. Nitrile Oxide Cycloaddition

19

However, in the case of ethyl nitroacetate a powerful dehydrating agent is not needed:

Machetti reported isoxazolines are formed in CDCl₃, but faster in aqueous solution (Figure 20),

though prolonged reaction times are needed in both solvents.[30,33,34]
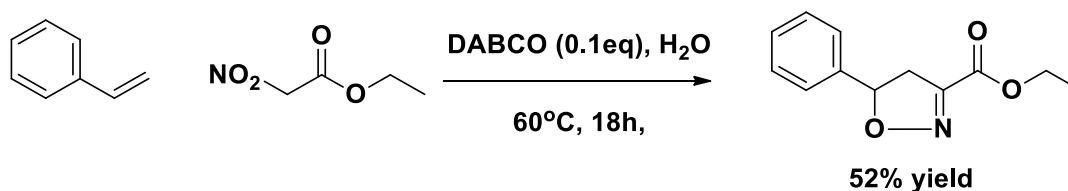
Figure 20. Machetti-DeSarlo Reaction

Spontaneous dehydration to nitrile oxide in aqueous solution seemed unlikely. Silyl

nitronates are known to cycloadd intramolecularly to alkenes with subsequent elimination to

isoxazolines, so an analogous mechanism was proposed in water.[30] To enhance the rate of

reaction, we tried silylation in organic solvent. In our case, the silyl nitronate was not reactive:

exposure of allylamine and ethyl nitroacetate in CDCl₃ with *bis*-trimethylsilyl acetamide (BSA)

led to silylation, and no further changes were observed by NMR.

Looking more closely at the scope of the Machetti's reported reactions, no allylamines or

amino-olefins were reported. His group achieved good yields with non-nucleophilic alkenes, and

of those with substituents more complex than alkyl and aryl groups, most substrates were

electron-poor with electron-withdrawing functionalities such as esters and nitrates. During this

time, a model reaction using 4-pentenoic acid to give isoxazoline **4** was also pursued. I

considered that allyl ammonium salts would make more favorable dipolarophiles than allyl

amine and began exploring reaction conditions using allyl ammonium chloride. After making

this change, trace isoxazoline formation was observed for the first time (Figure 21).
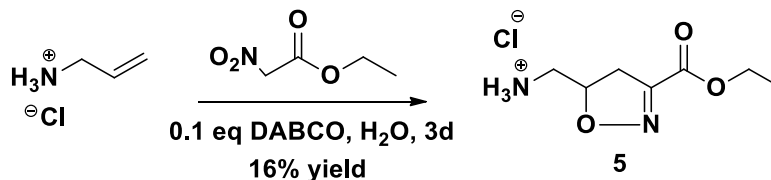
Figure 21. Isoxazoline 5 Machetti Conditions

Base catalysis was investigated thoroughly by Machetti,[30] and while they reported DABCO to promote high yields; we found that there was little difference in rate using other bases. We screened bases: DABCO, 2-pyridone, and allyl amine as catalysts and found 16%, 29%, and 30% yields respectively when allyl ammonium chloride, ethyl nitroacetate and 10mol% base were heated at 60°C in water for 3 days. Reasonable yields were afforded when using the conjugate base of our dipolarophile, and its presence simplified purification as it remains soluble under our trituration and crystallization conditions.

Effect of pH was studied using buffers as well as by varying ratios of allyl amine and its ammonium chloride. I found a trend of better yield with higher ratio of the ammonium chloride, but that a minimum amount of base enhanced the rate of reaction. In studies of isoxazoline **4**, we confirmed that pH effected our yields, and that the acidic alkenes were helpful to promote reaction. Moving forward in the synthesis of **5**, the standard procedure became to add 0.1 eq of allyl amine as a base catalyst.

Counter-ion effect was briefly explored using allyl ammonium chloride and allyl ammonium tosylate. No preference for an anion was found, both affording yields ranging from 25-35%. Since chloride does not interfere in the ^{1}H-NMR spectra, allyl ammonium chloride was chosen for simplicity while screening the conditions described below.
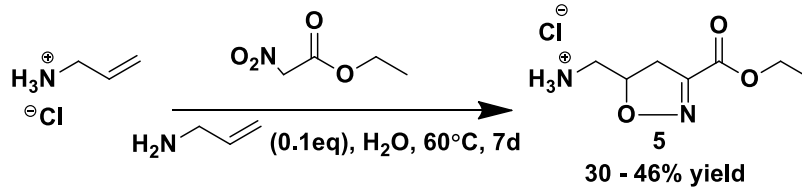
Figure 22. Isoxazoline 5 Condition Optimization

Further progress in optimized yield was achieved through screening temperature, solvents, concentration, and time (Figure 22). Temperatures of 45-70°C were favorable, and 60°C chosen as the optimum. Less than 1% product was observed without sufficiently elevated temperature, and decomposition of starting materials observed at reflux in water, ethanol, and *t*-butanol yielded reactions below 2%. At 60°C H_2O was found to be the best solvent; reactions in EtOH and *t*-BuOH showed less than 10% conversion by ¹H-NMR over the same time period. Concentrations below 1M of either the ethyl nitroacetate or alkene were detrimental to rate and yield. Reaction times longer than one week (168h) offered no increase in yield.

Machetti and coworkers had observed an induction period in their reactions[34] as did we. Exposure of ethyl nitroacetate to allyl ammonium chloride and 10% allyl amine in aqueous solution led very slowly to isoxazoline **5**, isolated as the crystalline HCl salt. While direct, this reaction took several days and led to yields 30-46%, other solvents and conditions working much less well. At this point in our studies, the Blackmond group published a proposed mechanism[35] that accounted for the induction period: she showed a dramatic effect of added nitrite, and suggested the induction period was due to slow formation of nitrite from the ethyl nitroacetate.

Furthermore, Blackmond demonstrated that ¹⁵N-labelled nitrite is incorporated into the cycloadduct. She proposed several roles for nitrite incorporation, including the elimination of water in aqueous media proposed earlier by Machetti.[30] We have been skeptical of suggestions

that cycloaddition followed by dehydration is energetically favorable in aqueous media. We

favor Blackmond's ideas proposed in Figure 23.
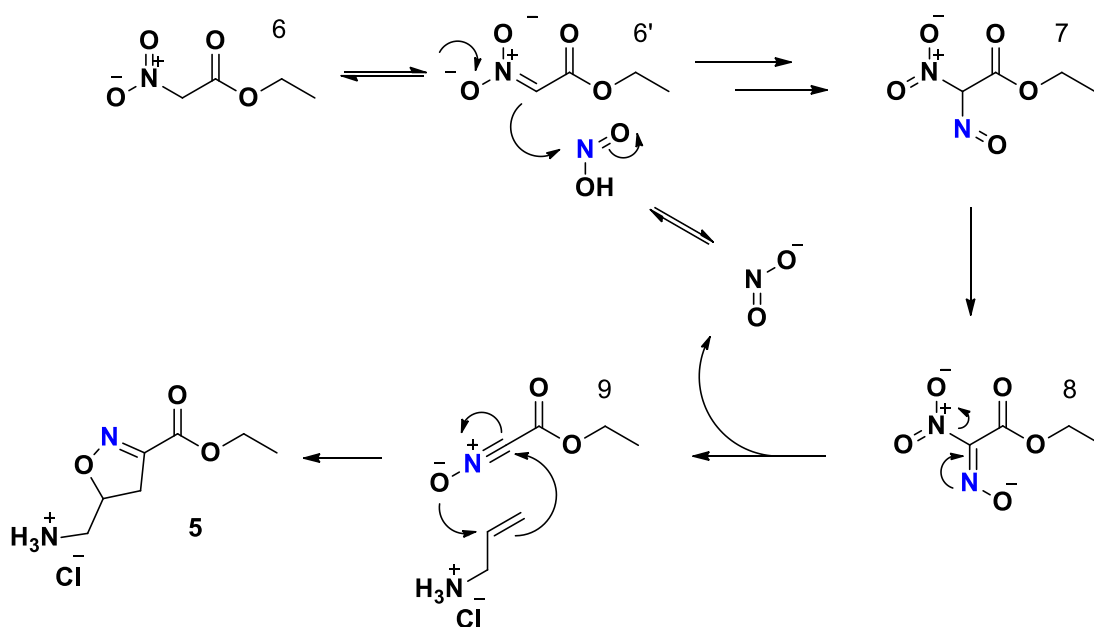
Figure 23. Blackmond Mechanism of Isoxazoline Formation

The utility of the mechanism (Figure 23) has allowed better understanding for our

reaction. The conjugate base **6'** of ethyl nitroacetate **6** adds to nitrous acid and loses water to

form the nitro-nitroso intermediate **7** which can be deprotonated to its conjugate base **8**. Nitrite is

lost to generate nitrile oxide **9** and regenerate the catalytic cycle of nitrite incorporation. Finally

the cycloaddition of **9** and alkene occurs in an irreversible step to form **5**.
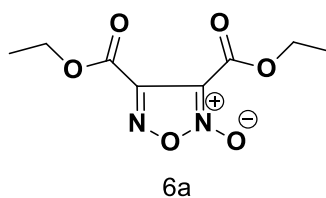
Figure 24. Nitrile Oxide Dimer 6a

I hypothesize that the low yields of my reaction have been due to competition of cylcoaddition of **9** with itself, giving the undesired dimer side product **6a**, Figure 24. Upon work up, various amounts of **6a** have been observed in the ^{1}H-NMR (CDCl$_3$) of the filtrate and on TLC along with unreacted alkene. Until recently, **6a**, had been mistaken for unreacted ethyl nitroacetate, but an in-house preparation of ethyl nitroacetate that was disrupted by an unknown contaminant yielding almost exclusively **6a** and provided an authentic sample for comparison. Isoxazoline formation saw no increase in yield by using excess ethyl nitroacetate or by adding small portions of excess ethyl nitroacetate over the course of the reaction; yield in relation to ethyl nitroacetate conversion increased when the alkene and ethyl nitroacetate were used in 1:1 molar equivalents. In light of our proposed mechanism (Figure 23), it may improve yield to start the reaction with a deficiency of ethyl nitroacetate and add more over time to limit concentration of nitrile oxide in solution, but this has not yet been attempted.
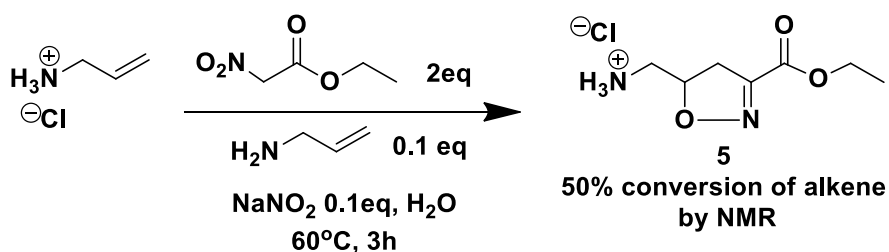
Figure 25. Isoxazoline 5 and Nitrite Catalysis

We added sodium nitrite to our standard isoxazoline procedure and found 50% conversion of allyl ammonium chloride to **5** within 3h, as determined by ^{1}H-NMR (Figure 25). A 1:1 molar ratio of allyl ammonium chloride to isoxazoline was observed, this was using an excess of ethyl nitroacetate, as the advantage of lower ethyl nitroacetate had not been well understood at that time. It is difficult to assess conversion based on ethyl nitroacetate because it

24

is only sparingly soluble in D_2O, and the product is insoluble in $CDCl_3$. An estimated yield

based on ethyl nitroacetate is 25%. Isolation of **5** is achieved by evaporating to dryness,

trituration in minimal CH_3CN, and filtration to give a beautiful white crystalline solid.

Separation of **5** from sodium salts required a new purification procedure, therefore t-butyl nitrite

has been used as catalyst and we were able to isolate comparable yields of **5** after a reaction time

of 24h or less, which under earlier conditions took 120h or more.

Guanidinylation

The next step in the synthesis of **2** is the addition of the guanidine group (Figure 26). The guanidinylating agent,[36] N,N'-diboc-1*H*-pyrazole-1-carboxamidine reacts readily with the amine group of **5** under basic conditions. Et$_3$N is used to convert the **5** to its free amine *in situ* and this substitutes the pyrazole to give 80-98% isolated yield of **10** after crystallization.
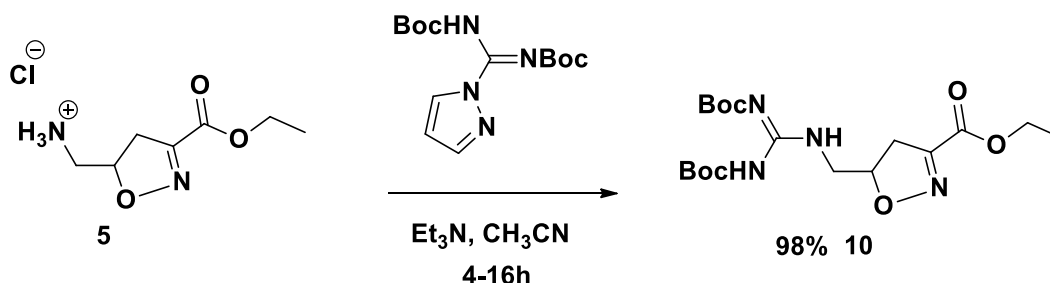
Figure 26. Guanidinylation

The above reaction was carried out using CH$_2$Cl$_2$ in an effort to simplify the workup, as **10** is purified by crystallization from a mixture of CH$_2$Cl$_2$ and hexanes. However, the reaction is faster in CH$_3$CN and gives higher yields. The reported range of reaction times and 80-98% isolated yields takes these solvent effects into account. Complete removal of CH$_3$CN is necessary for efficient crystallization and high product recovery. Excellent purification of **10** can eliminate the need for chromatography in the entire synthesis of **2**.

Deprotection
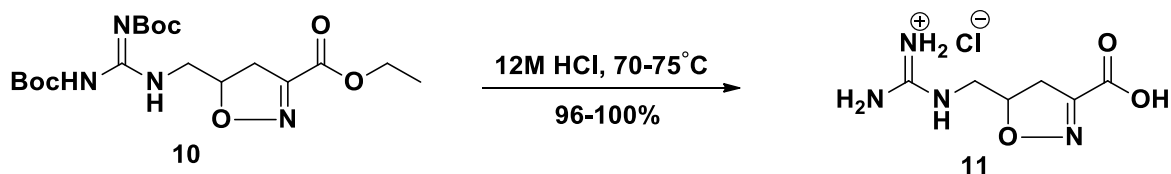
Figure 27. Deprotection of Isoxazoline 10

The deprotection of both Boc groups and the ethyl ester of **10** can be achieved in one convenient step leading to the deprotected iosoxazoline **11** (Figure 27). Selective deprotection of **10** by saponification in 1M NaOH gives its carboxylate salt; the hydrolysis of only the Boc groups can be achieved using trifluoroacetic acid with gentle heating.

In the following reduction studies, I have employed the use of isoxazoline **10** and its deprotected analogue **11**. We are ultimately interested in amino acid **2**, necessitating the eventual removal of protecting groups. Reductions of isoxazolines **10** and **11** to arginine derivatives **2'** and **2**, respectively (Figure 28), were pursued under a variety of conditions. **2'** can be deprotected to **2**. It is important to note that reactions in pursuit of keto acid **1** are not expected to withstand deprotection conditions, as elimination of **1'** to **1a** is highly likely. Attempts to reduce and hydrolyze protected isoxazoline **10** to protected hydroxyl ketone **1'** were used as model reactions, in pursuit of a substrate similar to keto acid **1** that would be compatible with isolation by normal phase chromatography for the purpose of characterizing **1**.
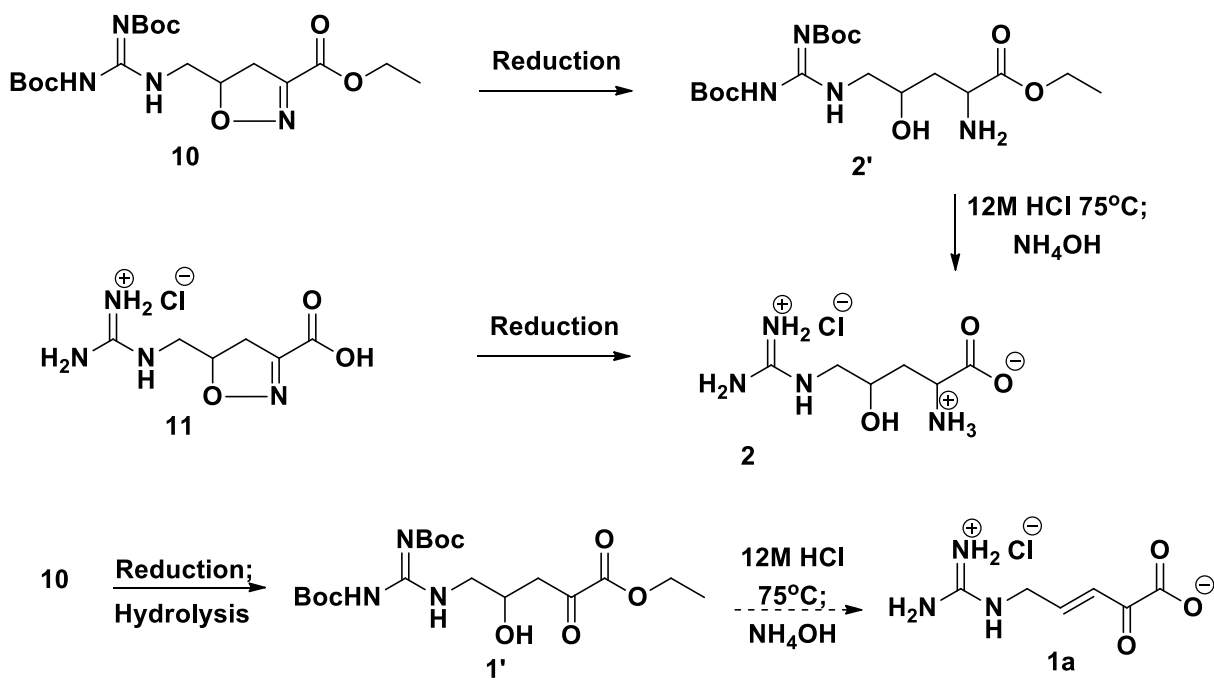
Figure 28. Deprotection of Reduced Isoxazolines

Reduction
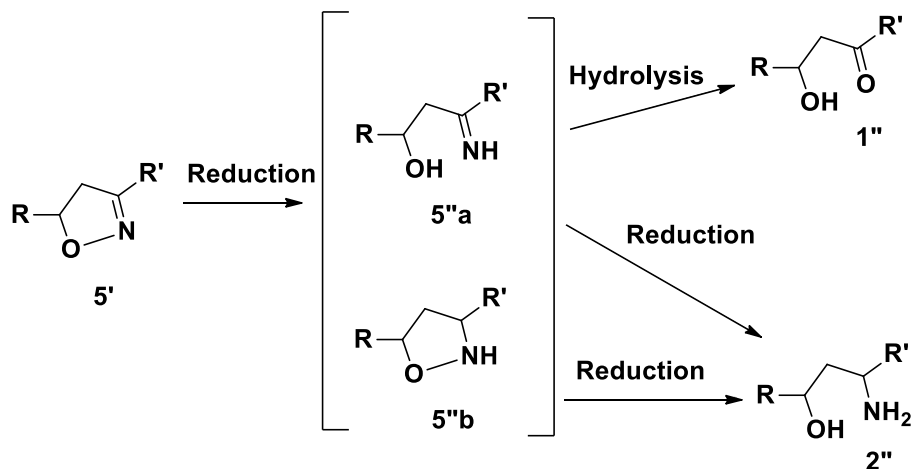
Figure 29. Divergent Reduction Pathway of Isoxazoline

The general utility of isoxazolines **5'** as building blocks for β-hydroxy ketones **1"** and β-hydroxy amines **2"** is well described (Figure 29).[29] The reduction of an isoxazoline proceeds through two possible intermediates: imine or isoxazolidine. The reduction of the N-O bond of **5'** provides the intermediate imine **5"a**, which has been reported under a variety of conditions.[29] The pathway is divergent from imine **5"a**, as the C=N bond of **5"a** is susceptible to hydrolysis[37] resulting in **1"** or further reduction[29] resulting in **2"**. Reduction of the C=N bond of **5'** provides the intermediate isoxazolidine **5"b**, which may only reduce further to **2"** and has been reported under Lewis acidic conditions in the presence of $NaBH_4$ or $LiAlH_4$.[38]

Following the work of Dennis Curran,[37] my first efforts were the conversion of deprotected isoxazoline **11** to β-hydroxy ketone **1**. The reaction was carried out under the conditions shown in Figure 30: **11** was exposed to Raney Ni and boric acid dissolved in a mixture of hydrous methanol under 1atm H_2. By mass spectrometry we observed partial

29

reactions of **11** to **1** directly, but found isolation from aqueous media difficult, and focused on work towards **1'** as we believed this crude product would allow for extraction from water and further purification by normal phase column chromatography. Conversion of **11** to **1** under Curran's conditions were inconclusive; no hydroxy-ketone was isolated for definitive characterization under variations of this work. Molecular ion +190 (which corresponds to protonated **1**) was detectable by MS, but always in the presence of +187 [**11+H**]. Due to the highly polar nature of starting material and product, separation by normal phase chromatography was not practical.
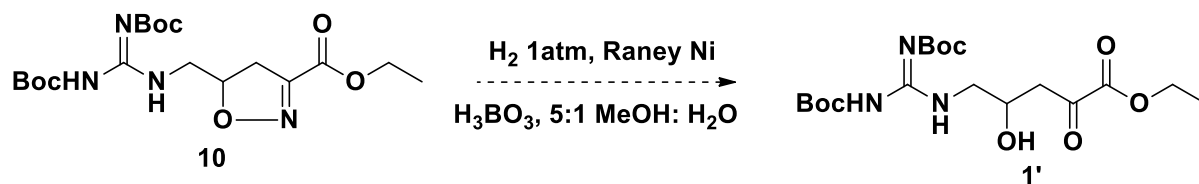
Figure 30. Curran's Conditions Ineffective

Isoxazoline **10** to β-hydroxy ketone **1'** was first explored by reaction with H_2 (g) at 1atm, Raney Ni, H_3BO_3 in 5:1 MeOH:H_2O (Figure 30). Several attempts at this procedure gave no observable reaction. Considering the Boc groups and ethyl ester, poor solubility of the reactant was considered a plausible reason for poor reactivity and several solvents were explored including ethyl acetate, ethanol, methanol, and mixtures of these solvents with H_2O in varying proportions. Conditions such as additives (H_3BO_3, CH_3COOH, $NaBH_3CN$, to list a few), reaction times and temperatures were varied using either Raney Ni or Pd/C.

We decided to increase the concentration of hydrogen by generating H_2 *in situ*. Various sources of hydrogen were then explored, including Et_3NH^+ $HCOO^-$ or NH_4^+ $HCOO^-$ with either

Raney Ni or Pd/C. These conditions showed no reaction in all combinations of salt and catalyst, were allowed long reaction times at room temperature and then gently heated. No change was observed by TLC.

Reducing metals were explored with acids: CH_3COOH with Zn,[39] and $NH_4^+ Cl^-$ with Fe (Figure 31).[40] The reactions with Zn and Fe resulted in new compounds observed by TLC, but workup of these reactions isolated primarily starting material. Mass Spectroscopy of crude product **1'** recovered from conditions shown in Figure 31 revealed ions that correspond to the β-hydroxy-ketone, but with varying degrees of deprotection, and was unable to be isolated.
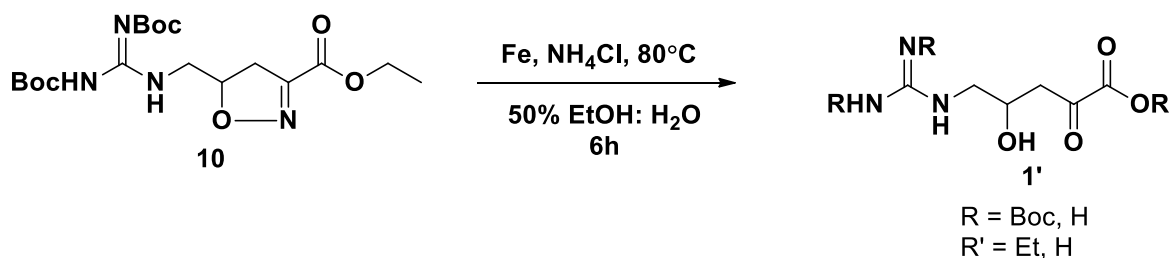
Figure 31. Model of Reduction and Hydrolysis

The presence of both the basic guanidine and labile ester of isoxazoline **10** presented an unexpected challenge in the synthesis of compounds **1** and **2**. The result of screening several reduction conditions found partial conversion of **10** to **2'** using H_2 (1atm), Pd/C, and aq. EtOH. And it was at this time that we focused our reduction efforts to the pursuit of conditions favoring the hydroxy-amines **2** and **2'**.

Generating hydrogen *in situ* using triethylsilane and Pd/C gave no reaction, so I increased pressure of H_2 using a Parr shaker apparatus at 60psi. Increasing pressure from 1atm to 60psi gave better results, under several conditions varying solvent, concentration, time, reactions with

either Pd/C or Raney Ni reliably gave partial conversion to the amines **2** and **2'**, but yields and conversions could not be reproduced. Using Pd(OH)$_2$/C to generate the active Pd surface *in situ* enhanced rate of conversion (Figure 32), 44% conversion was measured by quantitative ninhydrin test[41] and the molecular ion of **2** was confirmed by MS, but these conditions did not lend well to standard methods of purification, and separation of product from starting materials complicated further characterization. It is possible that keto acid **1** was formed but not detected by MS under these conditions as well, complicating resolution of ^{1}H-NMR spectra.
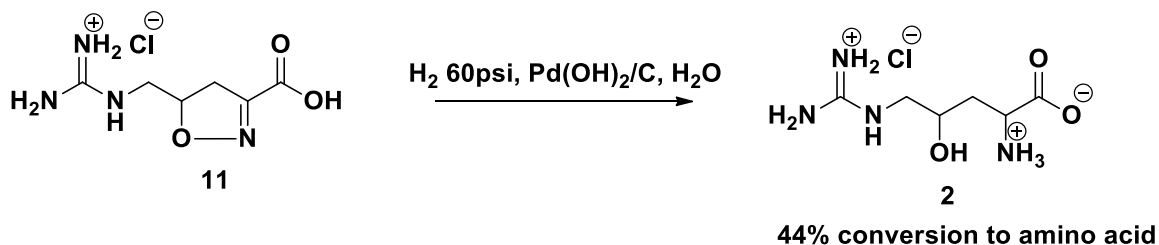
Figure 32. Pd(OH)$_2$/C as Catalyst

My early work hoped to control the reduction of **11** through the use of either hydrous or anhydrous conditions; difficulty in isolation from aqueous media made the former option a challenge, and poor solubilty of **11** in organic solvent inhibited the latter (Figures 28 and 32). We then focused on reduction followed by deprotection; methods for the reduction of protected isoxazoline **10** in organic solvent to give β-hydroxy amine **2'** were explored extensively, using several of the methods employed in our studies of reduction of **11**.

Kozikowski reported reduction of isoxazolines to β-hydroxy amines in the presence of NaBH$_4$.[38] Reduction of **10** with NaBH$_4$ with Pd/C in EtOH afforded reduction of ester, giving isoxazoline **12** as the corresponding alcohol (Figure 33). TLC clearly showed a reaction had occurred, IR confirmed the presence of O-H bond, and MS found +372 ion; our initial hope was

the formation of lactam **12a**, which had potential for use in synthesis toward **2**. ^{1}H-NMR, ^{13}C-NMR, and HSQC of **12** confirmed its identity; and while this may be an interesting reaction, it had no synthetic utility for us at this time.
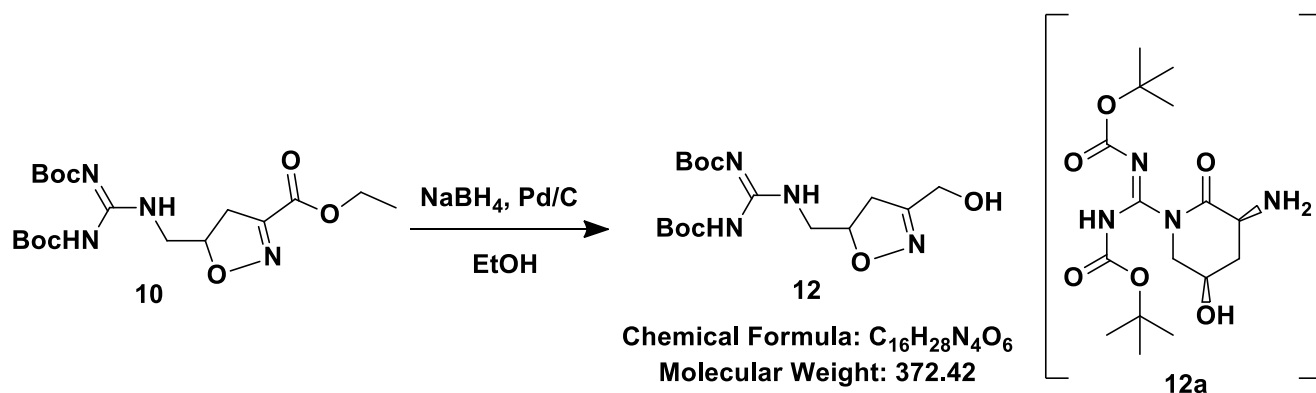
Figure 33. NaBH₄ Reduces Ester to Alcohol

Reduction conditions employed in the attempted conversions of **10** to **1'** were tested in the conversion of **10** to **2'**. These reactions were monitored by TLC, using ninhydrin to visualize amines. When new compounds were detected, they were analyzed by MS and quantified by ninhydrin.[41] The need for positive, negative, and blank controls in ninhydrin quantitation is necessary when working with guanidinium-containing compounds. Unexpectedly, Boc-protected guanidine reacts with ninhydrin, especially upon long exposure (2 min or more) to high temperature. Early in my work, several false positives were assumed to be the amine, but were only ninhydrin-positive due to long development and high heat giving a purplish color change. In the presence of a free amine the color change takes less than 30 seconds to appear, and is a vivid violet. In my ninhydrin quantitations, L-Arg was used a positive control and isoxazoline **10** as a negative control. Water was used as a blank control to ensure that no contaminants were present in the quantitation solutions, as amines are common contaminants in pyridine and we found it necessary to use distilled pyridine in our quantitation. From these experiments we

learned that EtOH and 60psi H_2 were favored variables, but still did not achieve complete conversion of **10.**

The possibility of the guanidine nitrogens poisoning the catalyst through chelation to the metal, led me to try reduction conditions in dilute acetic acid. We hypothesized that in mildly acidic solution (pH 4) the guanidinium moiety would be protonated without hydrolysis of Boc. The conditions shown in Figure 34 afforded very little of the expected products **2'** or **1'**, but resulted in a new product **13**. Low concentration of γ-hydroxy arginine **2'** was evidenced by ninhydrin quantitation. The mass spectrum showed a base peak of +463, corresponding to **13a**, as well as ions **13b** and **13c** that indicated loss of Boc groups.
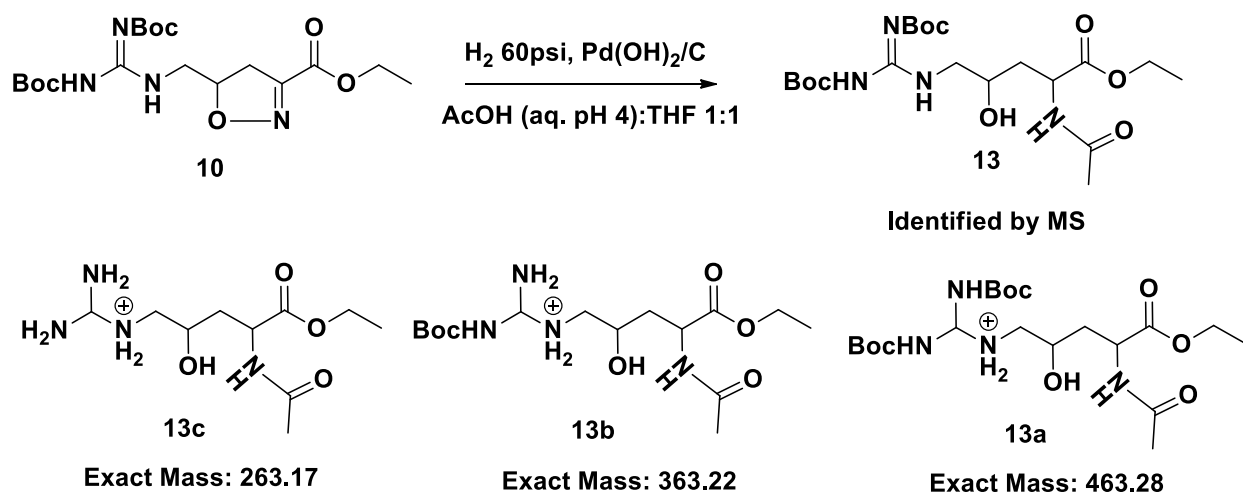
Figure 34. Acetylation of Reduced Amine

When Pd(OH)$_2$/C was used in place of Pd/C, the amino alcohol **2'** was observed to form quickly, but would reach about 50% conversion and not react further. Our hypothesis was that nitrogen was inhibiting catalysis was correct, but it was the primary amine of the reduced

product and not the guanidine itself. Boc_2O was added in a one-pot reaction such that the amino

alcohol **2'** was Boc-protected as it formed in the Parr shaker. The combination of 60psi H_2,

$Pd(OH)_2$, EtOH in the presence of Boc_2O gave full conversion of isoxazoline **10** to a

chromatographable amino alcohol **14** in a single step (Figure 35).
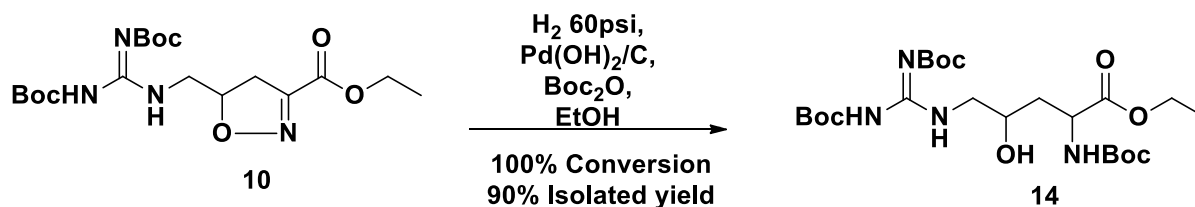
Figure 35. Reduction in the Presence of Boc₂O

These conditions are now considered the standard method for reduction and deprotection

of γ-hydroxy arginine **2** from **10**: reduction of protected isoxazoline with 60psi H_2, $Pd(OH)_2$/C,

Boc_2O, in EtOH, followed by flash chromatography, deprotection in 12M HCl and neutralization

with 10% NH_4OH (aq) to afford **2** as its monohydrochloride salt (Figure 36). The reduction has

been reproduced with full conversion at 1g scale, and scalable approaches to isolation without

chromatography has been achieved on 100mg scale.

2.4 Conclusion

Synthesis of γ-hydroxy arginine **2** has been achieved from readily available, inexpensive starting materials in 4 steps with 40% overall yield (Figure 36). This compares favorably to Yoon's earlier synthesis from allyl-glycine (cost $900/g) in 7 steps and 30% overall yield (Figure 15). However, Yoon's synthesis is stereoselective, and ours is a diastereomeric mixture. This is unlikely to hinder future work; oxidation of **2** to **1** has been carried out by L-AAO, and D-AAO is available.
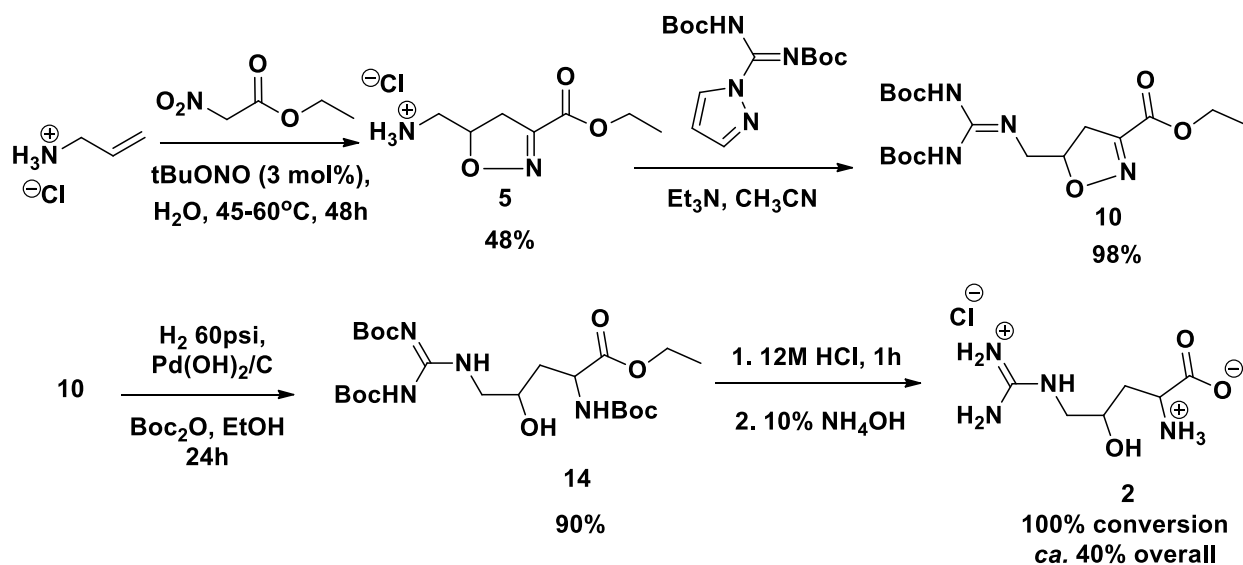
Figure 36. Synthesis of Oxidized Arginines

The synthesis of **2** can be achieved in a short sequence that is economically and environmentally friendly. The cycloaddition to isoxazoline **5** is carried out at ambient conditions in H_2O, and isolated by trituration in a minute quantity of CH_3CN. Isoxazoline **10** is formed in high yield and isolated with high purity by crystallization after an efficient organic-aqueous extraction. **2** has been isolated with high purity by filtering **14** away from catalyst through a syringe filter with a Teflon membrane and deprotection conditions and evaporation under

reduced pressure and elevated temperature (75°C) to remove excess Boc$_2$O and its byproduct, *t*-butanol. This sequence uses "green" solvents when possible and avoids the waste of solvents and silica gel by sidestepping chromatography in favor of purification by crystallization.

The sequence could be improved by increasing yield of the isoxazoline cycloaddition; to that end I propose running the reaction in as concentrated aqueous solution allyl ammonium chloride as allowed that avoids decomposition, and adding ethyl nitro acetate slowly, maintaining a deficiency of nitrile oxide in solution and increasing its probability to react with alkene. We have hypothesized that the favorable effects on reaction rate observed in H$_2$O could be due to limited concentration of nitrile oxide in aqueous solution. The reaction is biphasic, as ethyl nitroacetate is mostly insoluble in H$_2$O, and we have not attempted to quantify nitrile oxide concentration in either phase.

There are discrepancies between the NMR spectra of **2** prepared from isoxazoline and a known standard, this could be due to the formation of a 5-membered lactone or an enrichment of stereoisomers that differs from the standard.

2.5 Experimental: 2, 4, 5, 6, 10, 11, 12, 14

*γ-Hydroxy Arginine **2***
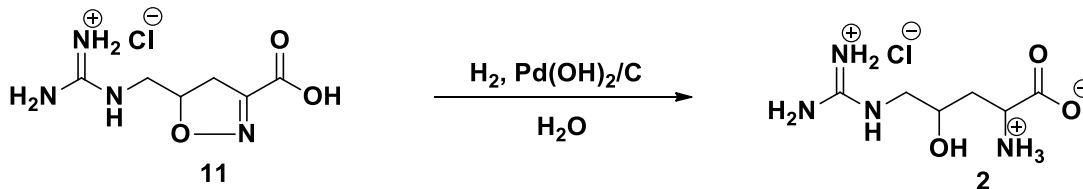
11 (0.1440g, 0.6471mmol) is dissolved in 3 mL H_2O (0.2157 M limiting reagent), and 14

mg 20% $Pd(OH)_2/C$ is added. This is reacted in the Parr shaker at 60 psi H_2 (g) for 72 h.

Ninhydrin quantitation confirms 44% conversion to amine.
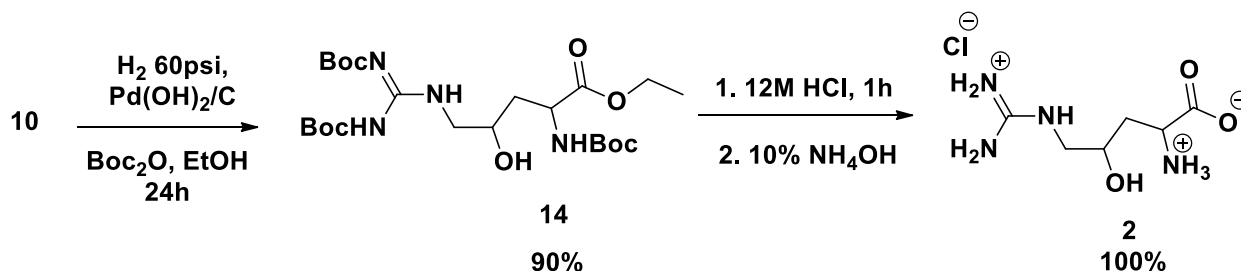
Isoxazoline **10** (0.8357 g, 2.016 mmol), 0.88g Boc_2O (2 eq), 0.08g 20% $Pd(OH)_2/C$ (10%

by mass), and 15mL of EtOH (0.133M limiting reagent) is mixed in a test tube with a glass bead

to ensure good mixing, this is placed inside of a thick-walled bottle and reacted under 60psi H_2

using a Parr shaker apparatus for 24h. Complete consumption of **10** is visualized by TLC and

mass spectrum shows high intensity base peak at +519, with no trace of **10**. Pd was removed by

filtration with a Teflon syringe filter and concentrated. Protected Hydroxy-Arg **14** (SAO-7-10)

(134mg) was dissolved in 25mL 12M HCl and heated to 75°C with stirring, after 1h it was

evaporated to dryness and then brought to pH 6 by addition of 10% NH_4OH to give **2** as its

monohydrochloride salt (SAO-7-13). The NMR spectra of **14** and **2** are attached in the appendix

at the end of this dissertation. This compound was quite literally identified days before my graduation and the spectra are not fully understood at this time. We will publishing these structures. Stay tuned!

Mass Spectrum: H_2O/CH_3CN mobile phase: SAO-5-96-03.pdf: +192 (**2**, Base peak), +174, +214
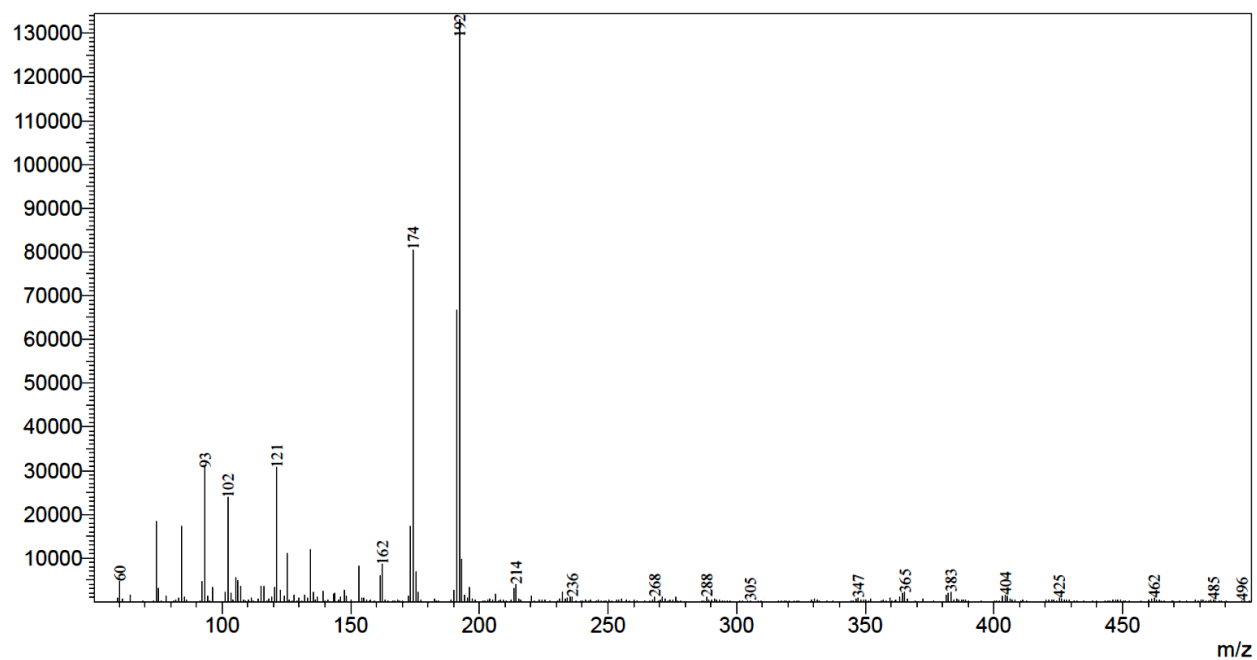
Isoxazoline 4
3-(3-(ethoxycarbonyl)-4,5-dihydroisoxazol-5-yl)propanoic acid
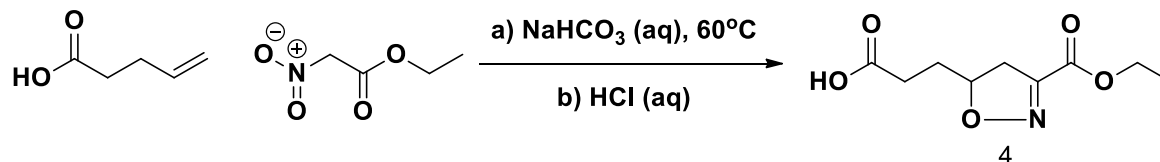
4-pentenoic acid (0.1mL), ethyl nitroacetate (0.11mL, 1eq intended), 1 mL NaHCO$_3$ [0.03M] was heated at 60°C for 7 days, then brought to pH 2 before extracting with dichloromethane. 60% yield. ^{1}H-NMR. Characterization data: ^{1}H-NMR (in CDCl$_3$) 300MHz: δ11ppm, (broad s, 1H), 4.883 (m, 1H), 4.352 (q, 2H), 3.320 (dd, 1H), 2.878 (dd, 1H), 2.561 (t, 2H), 1.994 (q, 2H) 1.371 (t, 3H). ^{13}C-NMR 300MHz: δ177.76, 160.65, 151.48, 82.33, 62.18, 38.64, 29.94, 29.42, 14.13. MS: 215.20 expected, found m/z = 214.2 [M-H]$^-$ and 429.3 [2M-H]$^-$.

Isoxazoline 5
(3-(ethoxycarbonyl)-4,5-dihydroisoxazol-5-yl)methanaminium chloride

C$_7$H$_{13}$ClN$_2$O$_3$ "ammonium isoxazoline ethyl ester" 208.64 g/mol
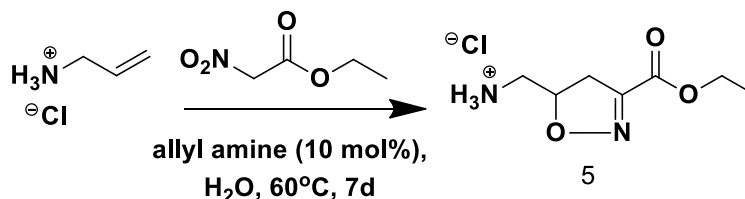
A solution of allyl amine hydrochloride (0.4963g, 5.31mmol) ethyl nitroacetate (0.6mL, 5.36mmol, 1.01eq) and allyl amine (0.040mL, 0.53 mmol, 0.10 mol eq) in H$_2$O (5mL) was heated under N$_2$ at 60°C for 7d. Removal of solvent by rotary evaporation at 40°C, trituration of the solid residue with CH$_3$CN (3mL), filtration and rinsing with cold CH$_3$CN gave 0.4586g (41%) # as a fine white powder, MP = 205-206°C. SAO-1-26a ^{1}H NMR spectrum in D$_2$O: 1H NMR Data: δ5.1 (1H, m, J = 6.6 Hz, C5-H), 4.3 (2H, q, J = 7.2, CH2CH3), 3.4 (1H, dd, J =

11.1, 18; C4-H2), 3.2 (2H, s, NH2), 3.0 (1H, dd, $J = 6.6$, 18; C4-H2), 1.2 (3H, t, $J = 6.9$,

CH2CH3). SAO-1-26a ^{13}C NMR spectrum in D_2O: δ 161.08, 153.8, 63.33, 36.75, 29.60, 13.16

SAO-5-51 ^{13}C NMR spectrum in DMSO-d_6: δ 160.31, 152.98, 79.81, 62.03, 41.88, 37.48, 14.45

R_f on TLC: 10% NH4OH/EtOH and silica plates yields Rf ~0.5

Mass Spec: +174

MP: 205-206°C, followed by decomposition, gas bubbles and turning brown.

SAO-5-92 Procedure with Nitrite Catalyst: Isoxazoline 5
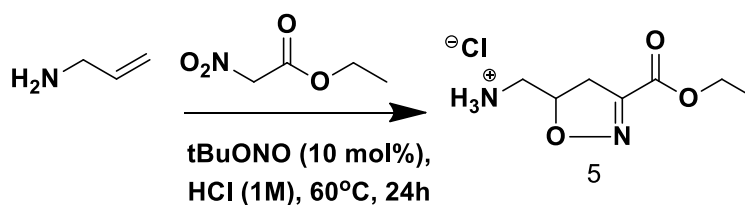
Allyl amine (1.4780g, 0.0259 mol) is charged with 25ml 1M HCl, followed by 3.2mL in-house

made ethyl nitroacetate (1.1eq). This is charged with t-butyl nitrite (0.100mL, 3.2 mol %).

Reaction is kept at 60°C for 24h, and then solvent is removed via rotary evaporator to afford

5.26g of waxy solid. This is triturated with 10mL CH$_3$CN and 1.632g of white solid product was

collected for 30% yield from the first crop, decomposition point: 209°C. The second crop

afforded 60mg to bring the total yield to 31%. Yields up to 48% have been obtained at larger

scale.

Ethyl nitroacetate 6

1) Ac$_2$O, H$_2$SO$_4$, 70% HNO$_3$, 0° C
2) EtOH, 0° C → RT

6
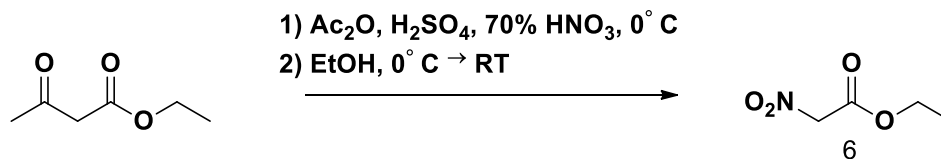
Reference: US Pat. 5,162,572

Acetic Anhydride (120 mL, 1.27 mol) and H$_2$SO$_4$ (0.3 mL, 18M, 5.6 mmol) were cooled

to 0° C before slow addition (weak exotherm) of ethyl acetoacetate (25.0 mL, 0.196 mol).

HNO$_3$ (70% wt/wt, 13.5 mL) was added **very slowly** (strong exotherm, must be kept below 5°C)

and stirred an additional 90 min, before dilution into ice-cold EtOH (250 mL) and stirred 10

minutes on an ice bath, then allowed to reach rt overnight. Na$_2$CO$_3$ (2.355g, powdered) was

added and the solution filtered through celite and concentrated. Crude product was distilled

under reduced pressure (80-85° C @ ~4 mm Hg) to yield 19.1897g (73%) of a colorless oil. [1]H

NMR spectrum in CDCl$_3$: **6**: δ5.18 (2H, 2), 4.33 (2H, q, *J* = 7.2), 1.34 (3H, t, *J* = 7.2)

^{1}H-NMR **6a**: 300MHz: δ4.48 (dq, 4H), 1.41 (dt, 6H)

*Isoxazoline **10***

ethyl 5-(((2,2,10,10-tetramethyl-4,8-dioxo-3,9-dioxa-5,7-diazaundecan-6-ylidene)amino)methyl)
-4,5-dihydroisoxazole-3-carboxylate: $C_{18}H_{30}N_4O_7$ 414.45g/mol

Abbreviation/code name: diBoc-guan isoxazoline ethyl ester
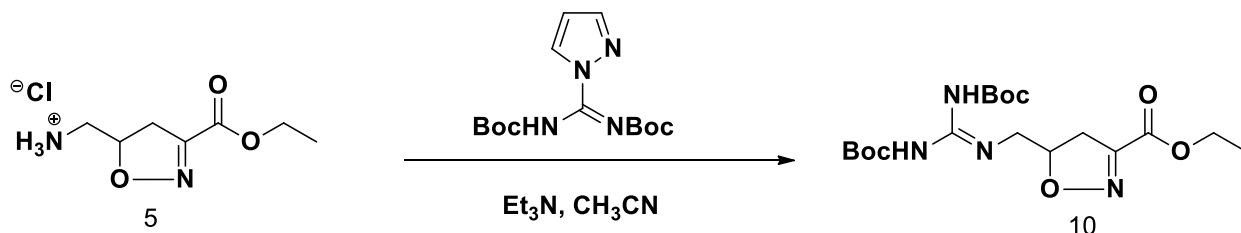
Diboc-guandinyl-pyrazole (2.245g, 7.23mmol) is dissolved in CH_3CN (15 mL), followed by

Isoxazoline **5** (1.509g, 7.23mmol) and 1.02mL (7.3mmol) Et_3N to form a slurry and stirred for

4h-16h. (Improper solution of the pyrazole will cause long reaction times or incomplete

reactions). The mixture was evaporated to dryness, dissolved in 30mL CH_2Cl_2, and washed with

3 x 25mL H_2O. The combined aqueous washes were back-extracted with 25mL CH_2Cl_2, and

combined organic extracts were dried over Na_2SO_4 and then evaporated to an estimated volume

of 5mL. Hexanes (50mL) are added until solution is translucent, and then the mixture is cooled

to encourage crystallization, affording 2.718g crystals (91% isolated yield) with MP: 98-100°C.

^{1}H NMR spectrum:
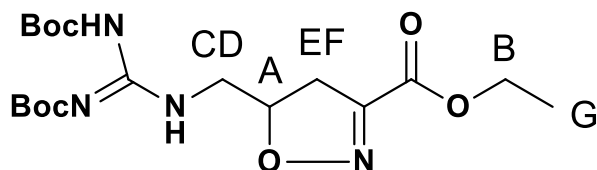
SAO-1-53c ^{1}H-NMR Assignments: 1H NMR Data: δ11.5 (1H, s, H-bonded BocNH), 8.65 (1H, t,

J = 5.4 Hz, NH), 4.998 (1H, 6tet, *J* = 3.9, A), 8.71 (2H, q, *J* = 7.2 Hz, B), 3.82, (1H, dq, *J* = 3.9,

14.4 Hz, C), 3.58 (1H, 5tet, *J* = 5.7, 6.0, 7.5 Hz, D), 3.29 (1H, dd, *J* = 11.1, 18 Hz, E), 2.97 (1H,

dd, *J* = 7.8, 18 Hz, F), 1.50 (9H, s, Boc), 1.495 (9H, s, Boc), 1.37 (3H, t, *J* = 7.2 Hz, G)

Carbon assignments are verified with HSQC (SAO-1-53f) correlation.
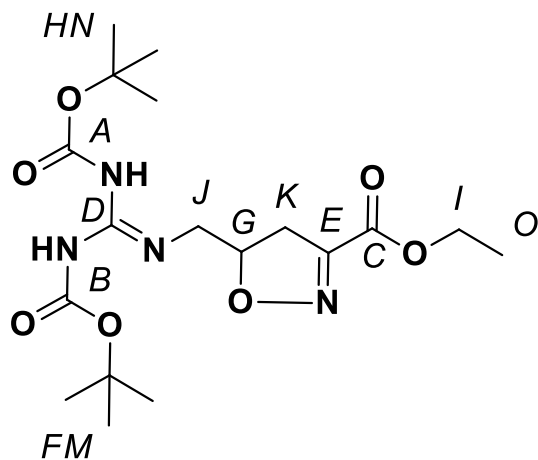
^{13}C NMR number: SAO-1-53e Solvent: CDCl$_3$ ^{13}C NMR 300 MHz: δ163.4 A, 160.4 B, 15.7 C, 152.9 D, 151.7 E, 83.5 F, 81.7 G, 79.6 H, 62.2 I, 43.4 J, 36.5 K, (weak signal at 31.6, L, likely impurity), 28.3 M, 28.0 N, 14.1 O

R$_f$ on TLC: 0.34 in 30%EtOAc/Hexane

Mass Spec: Exact mass 414.21, m/z = 415.5 [M+H]$^+$ ion.

Deprotection: Isoxazoline 11
amino(((3-carboxy-4,5-dihydroisoxazol-5-yl)methyl)amino)methaniminium chloride

10 (0.409g, 0.9mmol) is dissolved in 25mL 12M HCl, stirred at 75°C for 15 minutes and then evaporated to near dryness, a second portion of 25mL of 12M HCl is added and stirred while heating for 1 h. Then evaporated to constant mass. 96% Yield (0.210g). MP: 155-156°C.

*Isoxazoline **12***
5-(((2,2,10,10-tetramethyl-4,8-dioxo-3,9-dioxa-5,7-diazaundecan-6-ylidene)amino)methyl) -3-hydroxymethyl-4,5-dihydroisoxazole
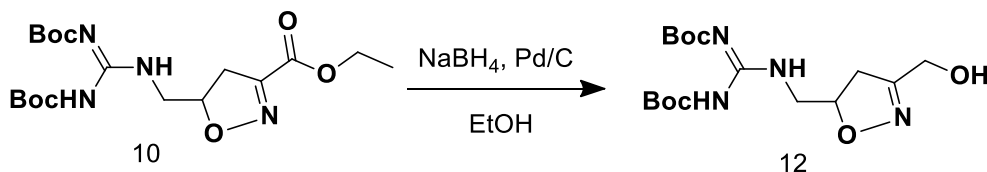
10 (24.1mg, 0.06mmol) is dissolved in 0.71mL EtOH then 2mg Pd/C and NaBH$_4$ (12mg, 6eq) was added. After 3h, the reaction was evaporated, dissolved in 5mL H$_2$O and extracted with 3 x 5 mL CH$_2$Cl$_2$. 15.7 mg of white solid was obtained, 70% yield.

1H NMR 300MHz δ11.477 (1H, s), 8.544 (1H, s), 4.827 (1H, m), 4.40 (2H, q, J=14.1Hz), 3.754 (1H, dq), 3.520 (1H, dq), 3.133 (1H, dd), 2.876 (1H, dd), 2.3 (2H, broad), 1.484 (18H, s), 1.269 (4H, d). MS: DUIS ionization, positive ion, 373.50 = [M+H]

*Boc-Amino Alcohol **14***
ethyl 5-(2,3-bis(tert-butoxycarbonyl)guanidino)-2-((tert-butoxycarbonyl)amino)-4-hydroxypentanoate
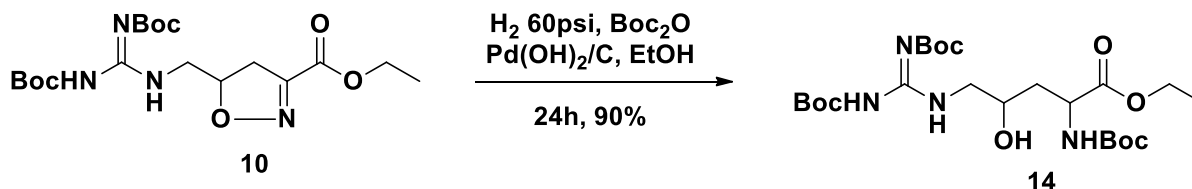
Isoxazoline **10** (0.8357 g, 2.016 mmol), 0.88g Boc$_2$O (2 eq), 0.08g 20% Pd(OH)$_2$/C (10% by mass), and 15mL of EtOH (0.133M limiting reagent) is mixed in a test tube with a glass bead to ensure good mixing, this is placed inside of a thick-walled bottle and reacted under 60psi H$_2$ using a Parr shaker apparatus for 24h. Complete consumption of **10** is visualized by TLC and mass spectrum shows high intensity base peak at +519, with no trace of **10.**

Chapter 3. Artificial β-Sheet for Inhibition of β-barrel Assembly Machine

3.1 Introduction to β-barrel Assembly Machine Inhibition

Two targets we have focused on are the Lipid II and the β-barrel Assembly Machine (BAM). With the exception of BAMa, which is itself a β-barrel protein,[42] all other known β-barrel proteins must be assembled by the BAM complex. Curiously, BAMa is able to fold spontaneously but also participates in the folding of subsequent BAM assemblies.[43]
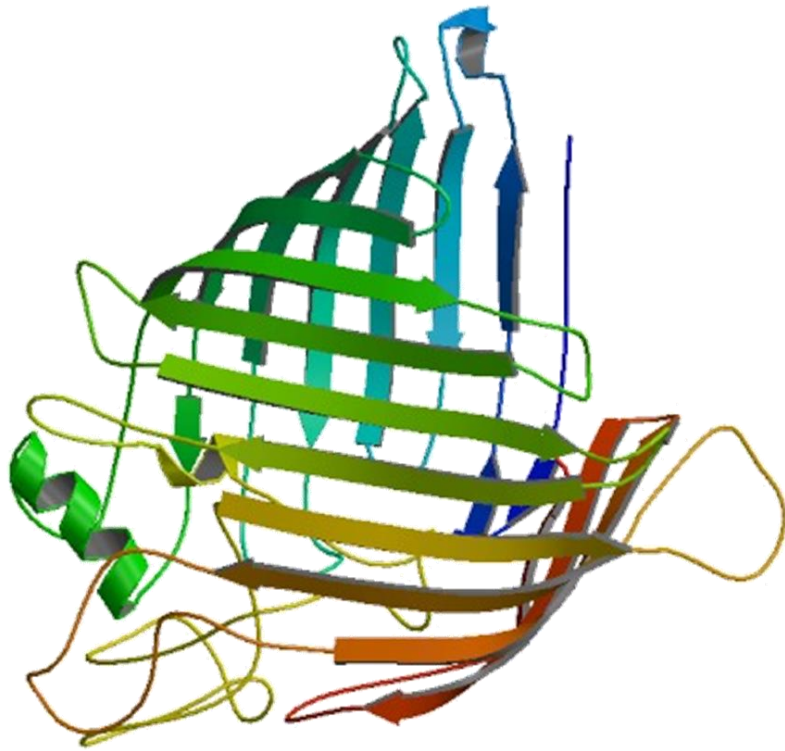
Figure 37. Crystal Structure of BAMa

The β-barrel fold (Figure 37) is common to porins, proteins that span the cellular exterior and act as pores for the transport of molecules, including antibiotic drugs. As shown in Figure 38, these outer membrane proteins (OMP) are synthesized in the cytoplasm and carried across the periplasm by a surrogate protein and folded into their final form by BAM.[44]

The β-signaling terminus of the nascent OMP is recognized by BAM, it is the recognition of this region that initiates protein folding (Figure 38).[43]
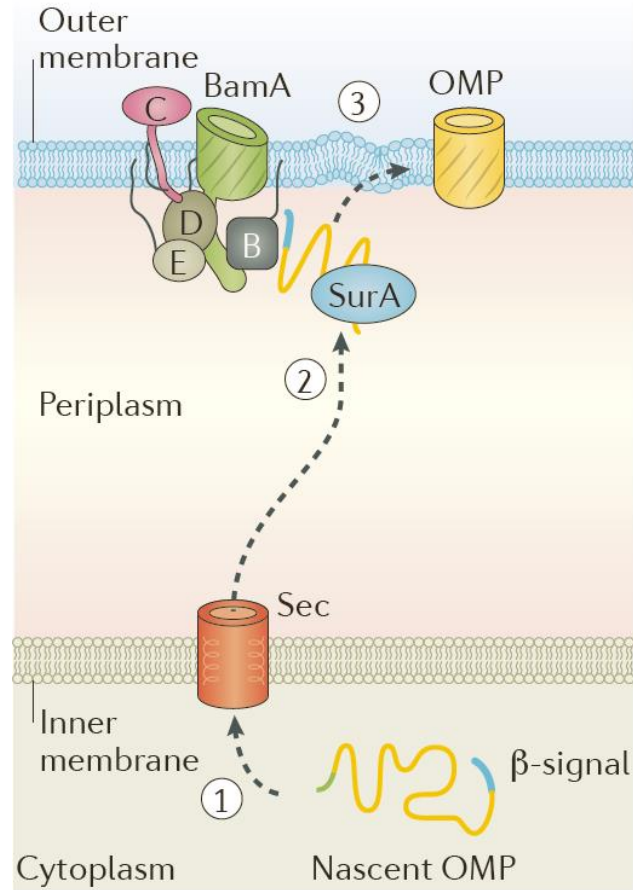
Figure 38. BAM Function

Intermolecular protein stability within the cell is influenced by a variety of factors. In the formation of β-sheets, extended polypeptide strands form hydrogen bonds with adjacent strands (β-strands); these are crucial factors in biomolecular recognition. β-sheet mimicking molecules have been used to study intermolecular hydrogen bonding to identify parameters that can be used to control the formation and specificity of protein-protein interactions.[45]

The study of protein β-sheet folding has been an important field in developing drugs to treat disease. The chief focus on drug development is concerned with binding specificity between the drug of interest and the target site of an enzyme. Although much knowledge has been gained in this field,[46] scientists are still faced with an enormous amount of complexity within subcellular environments that often forces re-evaluation of drug design due to the formation of undesired structures. By synthesizing small molecules that form intermolecular hydrogen bonds, we hope to be able to elucidate key factors that affect formation of β-sheets.

James Nowick synthesized a small peptide template which recognizes hydrogen bonds and has sticky edges with self-recognition, forming dimeric pairs resembling the binding in β-sheets.[47] His work on small chemical model systems has led to the exploration of biological systems through simple, easy to manipulate synthetic molecules.[48] His artificial β-sheets mimic the structures and binding behavior found in natural proteins. We propose a new small molecule template which we wish to incorporate into a β-signaling peptide sequence.

We are developing a functionalized peptide derivative of quinolone, with hydrogen bonding capability for self-recognition. Our model is different from Nowick's templates in the following three ways: quinolone contains two aromatic rings, there is a phenol (allowing further alkylation) instead of a methoxy group, and the quinolone has an additional carbonyl that allows even further derivatization. Our quinolone has the length of three α-aminopeptides and could replace three residues of a peptide sequence with a rigid scaffold that is conformationally restricted, holding hydrogen bond donors and acceptors in β-sheet binding geometry without free rotation. Incorporating the quinolone into an inhibitory peptide sequence that recognizes and binds the β-barrel assembly machine may provide a new antibiotic with a new mechanism of

action that may be antimicrobial itself, or block drug efflux and may allow known antibiotics to overcome a former mode of drug resistance.

Nowick's β-sheet inducer
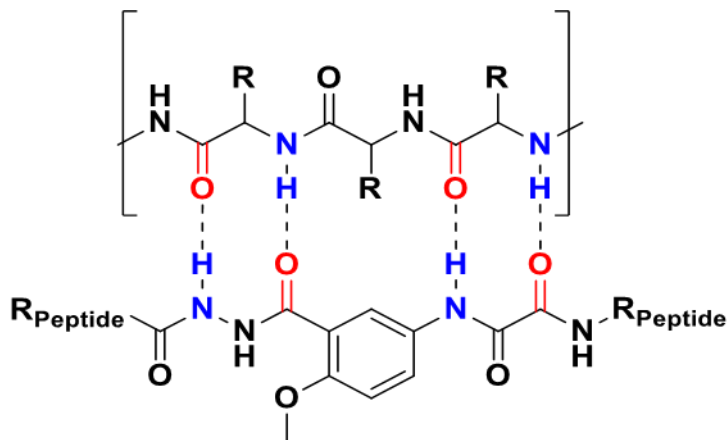
Our Proposed Quinolone
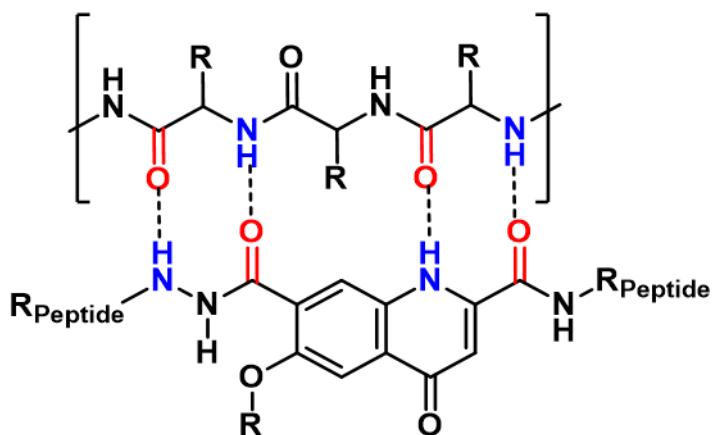
20

Figure 39. Structure and Hydrogen Bonding of Mimics

Inhibition of the β-barrel assembly machine with modified substrate peptides has been shown to be bactericidal *in vivo*.[49] However, these peptides make poor drug candidates due to

digestion by proteases. Therefore, we propose inhibition of the β-barrel assembly machine by our synthetic molecule, which we expect to resist hydrolysis by protease, while mimicking the interactions of similar peptide sequences.

3.2 Proposed β-Sheet Mimic

The quinolone scaffold **20** (Figure 39) is being pursued through a condensation reaction (Figure 40) of dimethyl succinyl succinate (**DMSS**) and L-serine ethyl ester **15** to give enamine **16a**, which has been oxidized to its terephthalate derivative **17**, and isolated by column chromatography. In our lab, new enamines and bisenamines derived from **DMSS** have been of great interest towards interesting biological mimics; these are readily aromatized and form stable, colorful compounds. We have isolated and characterized the mono- and bis-substituted L-serine ethyl esters of the aromatized dimethyl succinyl succinate **17a** and **17b**, respectively. We have demonstrated model reactions on L-serine ethyl ester to tosylate and eliminate the β-hydroxyl to give an olefin that, in our terephthalates can be cyclized via Dieckmann condensation to yield the desired quinolone with functional groups at positions 2, 6, and 7 for further derivatization.
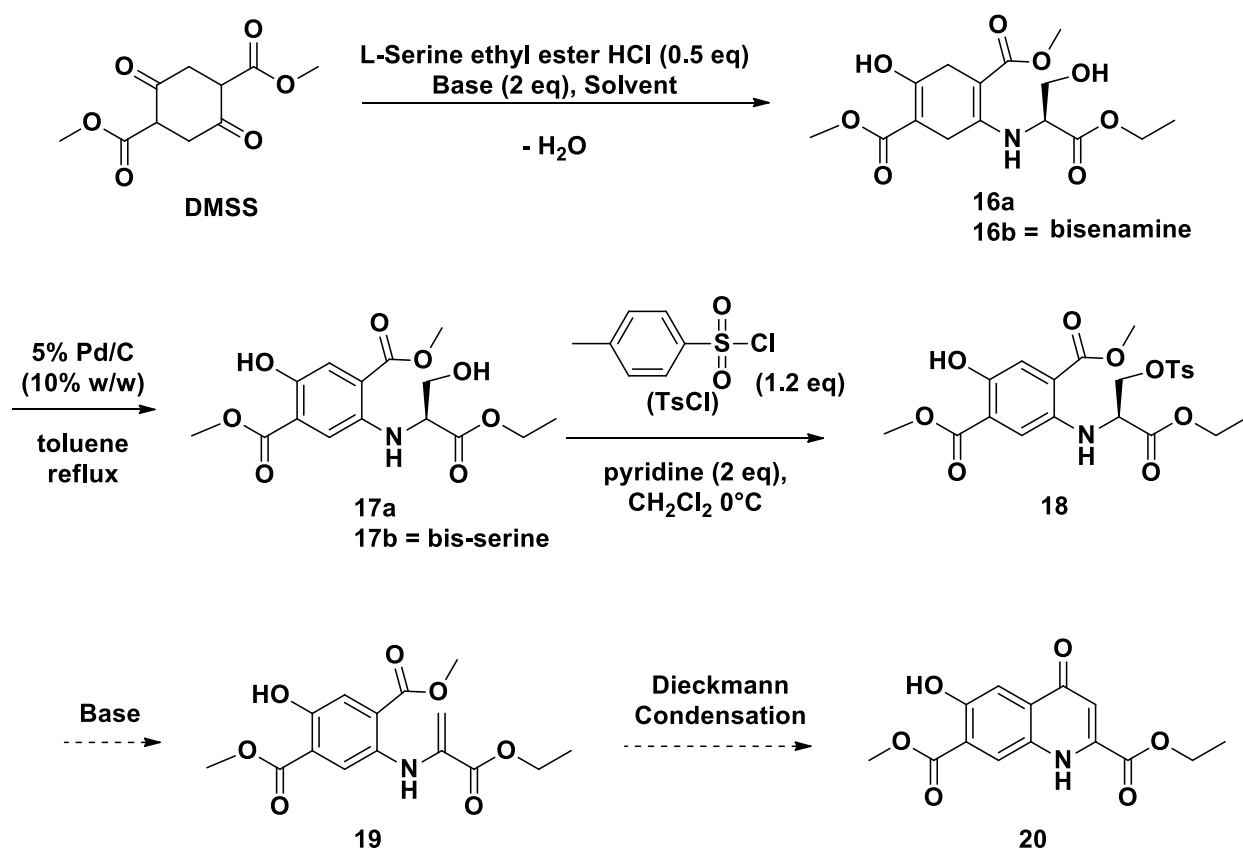
Figure 40. Proposed Synthesis of Quinolone

3.3 Results and Discussion

Our group has made enamines and bisenamines derived from DMSS for a host of

applications. The condensation of L-serine ethyl ester and DMSS has been pursued by several

undergraduates under my mentorship. The selectivity for mono-serine enamine is difficult to

control by stoichiometry alone and requires chromatographic separation from the bis-serine

enamine. Several attempts in recrystallization have proven it is much more convenient to

separate the mono and bis enamines by column chromatography, and both of these products are

interesting substrates for cyclization to the quinolones.

Complete transamination of both ketones of DMSS presents a challenge in overcoming equilibrium. We've found that the enamine forms quickly, but that complete reaction is limited by reversible equilibrium (Figure 41).
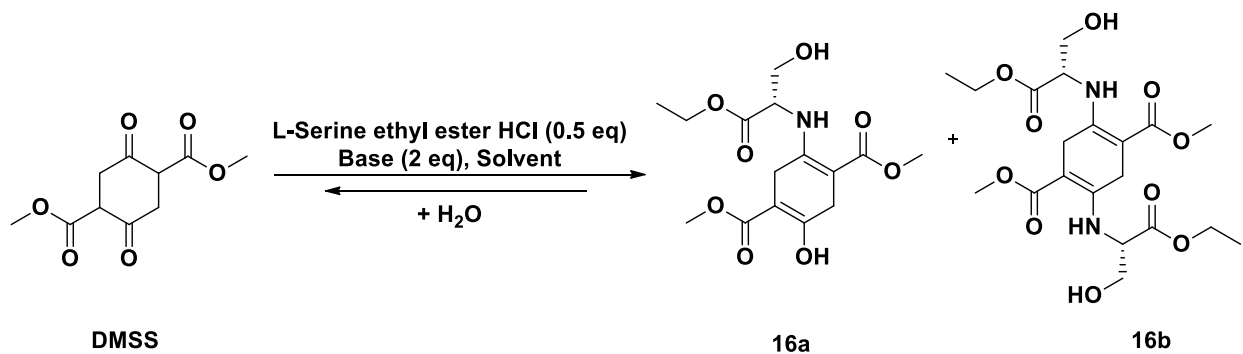
Figure 41. Reversible Enamine Condensation

To drive the enamine reaction to completion we have explored various methods for the removal of water. We have tried chemical methods, such as adding tetraethoxysilane to the reaction mixture to react with H_2O as it is formed. We have tried physical methods to remove water, via the use of a Soxhlet extractor filled with molecular sieves or a Dean-Stark trap. Putting molecular sieves directly into the reaction mixture was not a good idea, the mechanical wear on the sieves created a very fine particulate that made the reaction mixture into clay. The molecular sieves in the Soxhlet extractor were less effective than the Dean-Stark trap, due to low capacity.

The oxidation of enamine and bis-enamine with Pd/C in refluxing toluene is best performed on the crude reaction mixture and chromatographed once everything has been aromatized. We have tried adding Pd/C to the reaction mixture during the transamination as a way to overcome the reversibility of the reaction, but DMSS oxidizes more readily than the enamines and won't undergo substitution once aromatized. The aromatized DMSS, mono enamine, and bis-enamine are each highly fluorescent and can be identified by their

52

characteristic colors. The aromatized DMSS fluoresces a brilliant blue, the mono-enamine is fluorescent chartreuse yellow-green, and the bis-enamine is a bright orange. Following chromatography, fractions can be identified by placing under long-wave UV light; TLC used to verify the purity.

The dehydration to form olefin **19** (Figure 40) has been probed by undergraduates Tye Seideman and Dan Murphy mentored by Tyler Fenske and myself; Dan Murphy describes his work in his Senior Thesis under my supervision, and his findings are summarized here.

We currently do not have a standard procedure for the transformation of **18** to **19** but have tried activation of primary alcohol by carbonyl diimidazole (CDI), phosphoryl chloride, and tosylation followed by elimination.

Conclusion

Thus far, our most promising route has been demonstrated by model reactions (Figure 42) performed by Dan Murphy. The L-serine is esterified following our standard method using SOCl$_2$ in cold EtOH to yield ester **15**, Figure 42. This is converted to free amine with NaHCO$_3$ and Boc-protected in EtOH to give **17'** in 68% yield after chromatography. This reaction was straight forward and provided ample material to serve as a model compound in our elimination studies, so the reaction was not repeated or optimized for yield.
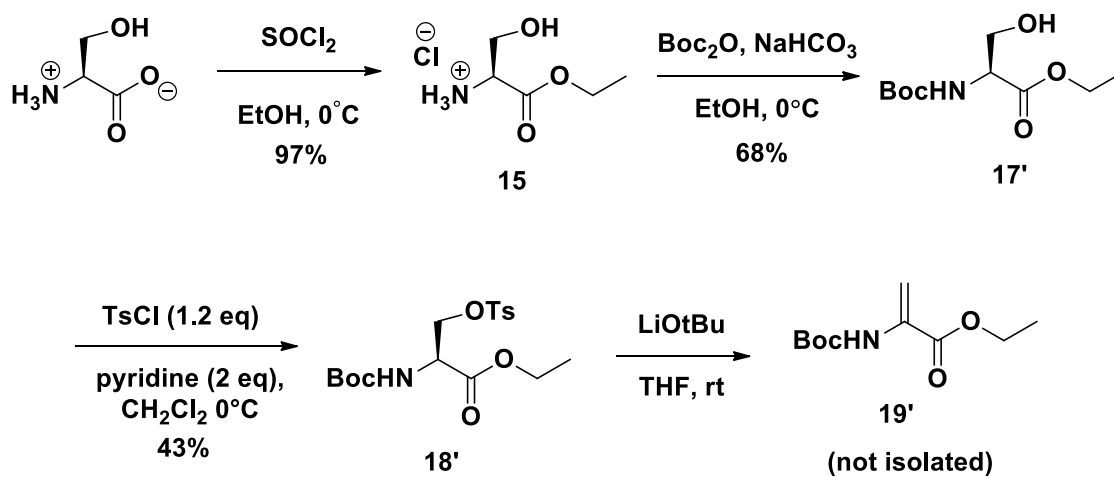
Figure 42. Dehydration of L-Serine

Tosyl chloride and pyridine is used in ice cold CH$_2$Cl$_2$ to activate the hydroxyl for elimination in THF by base. Tosylation was achieved in 43% yield. Reaction conditions and work up were not optimized in the case of **18'** as tosylation of serine enamine terephthalates has been demonstrated by multiple students in our lab.

The first attempt at olefin **19'** was with Et$_3$N and CH$_2$Cl$_2$ were tried for the elimination reaction. Bulky bases were screened to favor elimination over acyl substitution, but none of the desired olefin product was identified with triethyl amine. Next lithium t-butoxide in THF was

screened in elimination of **18'** and these conditions gave **19'** in a crude mixture, the methylene

proton signals were identified in ^{1}H-NMR as evidence of this transformation. This sequence has

been carried out without isolation of the final olefin. Further work on this project has been the

focus of Tyler Fenske and Alex Vincent.

3.4 Experimental: 15, 17a, 17', 18', 19'

Synthesis of L-Serine Ethyl Ester Hydrochloride 15
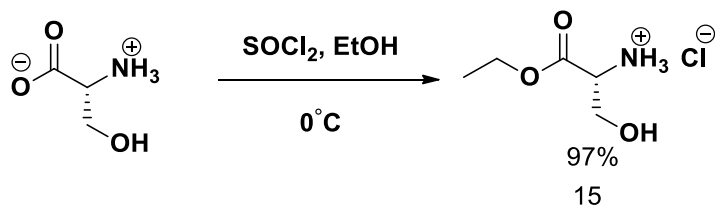
Anhydrous ethanol (85mL) is poured into a 250-mL round bottom flask and chilled in an ice bath to 0°C. Thionyl chloride (18 mL, 0.248 mol, 5.2 eq) is added dropwise to the ethanol, followed by 5.0070g L-serine (0.0476 mol, limiting reagent). The flask is fitted with rubber septum and wired on. The reaction is allowed to stir overnight and gradually come to room temperature. TLC developed with 4:1:1 n-BuOH: AcOH: H_2O and visualized by ninhydrin stain showed consumption of L-serine was complete. The reaction was concentrated (<10mL) and product crystallized by addition of ethyl ether (~50mL). The solid was collected by filtration for 97% isolated yield. The compound gave a clean NMR proton spectrum in D_2O and MP = 130-131°C.

15: ¹H NMR 300 MHz: δ4.29 (2H, q), 4.03 (2H, m), 3.93 (1H, m), 1.29 (3H, t)

SAO-1-57a   1   1   Z:\u\data\saoehm\nmr
Proton Spectrum
L-serine Et ester HCl White xtals in D2O
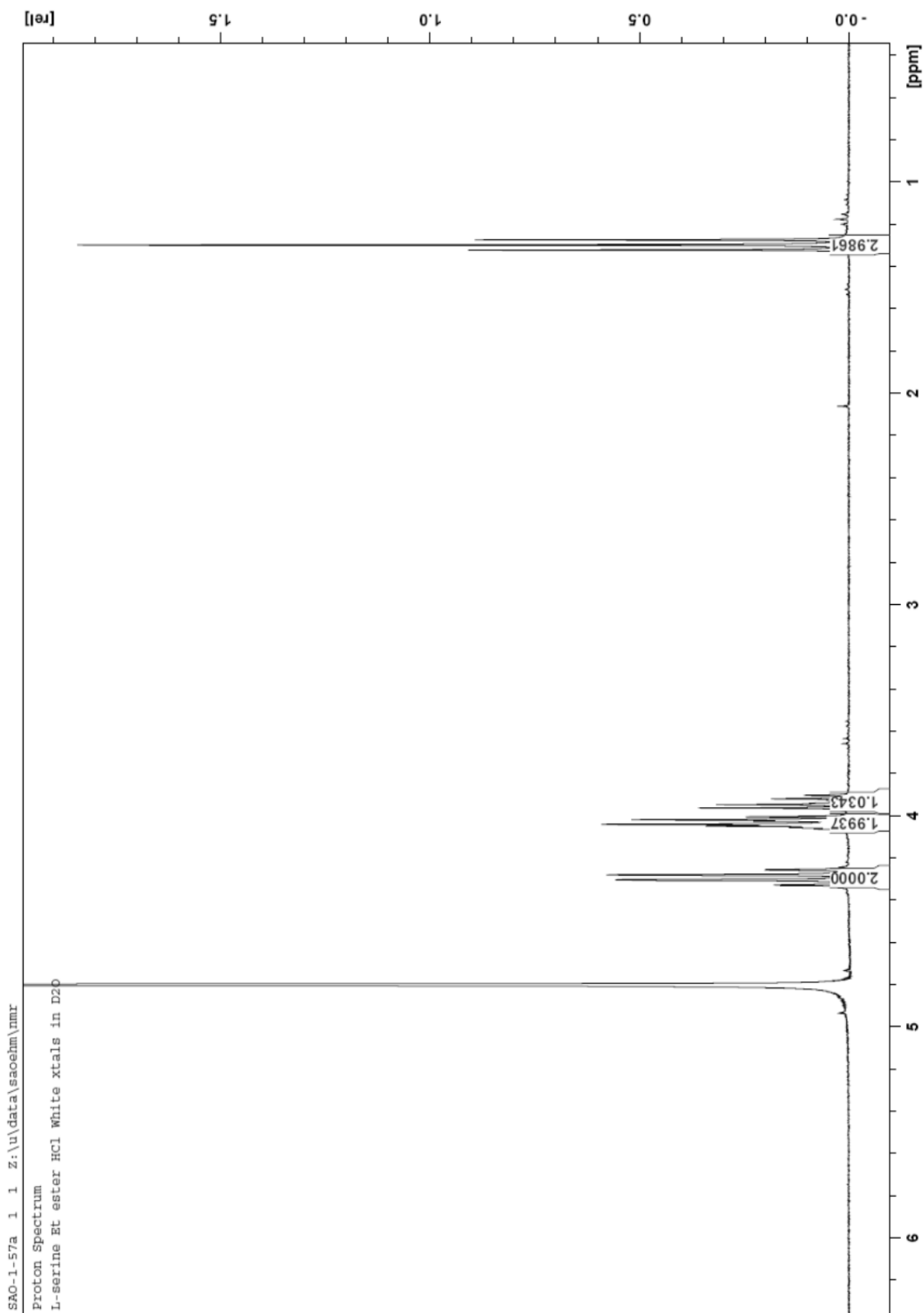
Compound **16a** and **17a**

name: dimethyl 2-[(1-ethoxy-3-hydroxy-1-oxopropan-2-yl)amino]-5-hydroxy-terephthalate
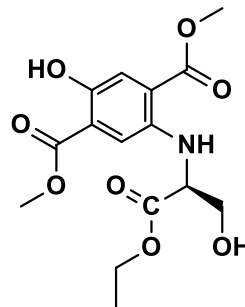
Notebook page reference: SAO-1-34   Structure:

Formula: C$_{15}$H$_{19}$NO$_8$

Equation for preparation:
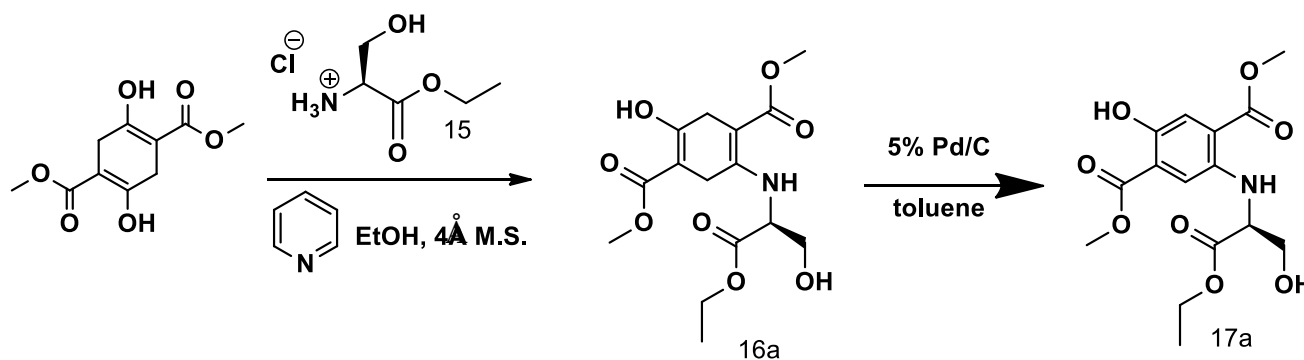
A solution of **DMSS** (0.9990g, 4.3mmol), 0.7432g **15**, 0.7mL pyridine in 100mL EtOH is

brought to reflux with a Soxhlet extractor filled with molecular sieves to remove water. After

refluxing 1h, 92mg 5% Pd/C is added with 100mL toluene. After 12 hours, the reaction was

evaporated and dissolved in CH$_2$Cl$_2$ and purified by flash chromatography using 10%

CH$_3$CN/CH$_2$Cl$_2$. Isolated yield of 2% afforded enough **17a** for its full characterization.
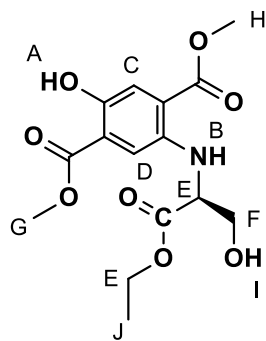
SAO-1-34 ^{1}H NMR spectrum CDCl$_3$: (Assigned using HSQC data SAO-1-34c) 300 MHz: δ9.864 (1H, s, A), 7.79 (1H, d, B), 7.609 (1H, s, C), 7.154 (1H, s, D), 4.25 (2H, q, overlaps with 1H, m, E), 4.00 (2H, m, F), 3.96 (3H, s, G), 3.911 (3H, s, H), 2.191 (1H, t, I), 1.279 (3H, t, J)

SAO-1-34a ^{13}C NMR spectrum CDCl$_3$: 300MHz: δ171.59, 169.59, 167.62, 151.54, 141.96, 120.20, 118.95, 117.22, 112.28, 62.96, 61.70, 58.53, 52.66, 52.28, 14.18

Mass Spectrum: DUIS:

M+ peak: 342.2 m/z, intensity: 800000

M+1 peak: 343.2 m/z, intensity: 200000

M+22 peak: 364.2 m/z, intensity: 300000

Rf on TLC :Silica TLC plates, Eluent: 10% acetonitrile in dichloromethane Rf = 0.48.

Fluorescent green under long-wave UV.

Yellow-orange solid, MP: 100-101°C

17': Boc Protection of L-Serine Ethyl Ester Hydrochloride
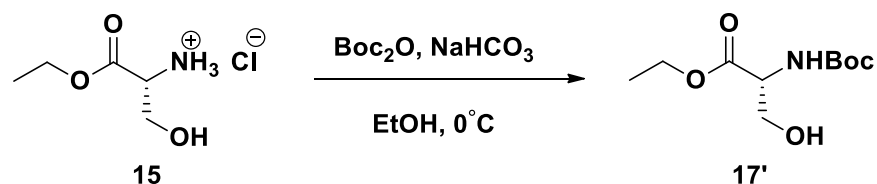
L-serine ethyl ester hydrochloride (2.005g, 0.0102 mol) is dissolved in anhydrous EtOH (20mL) and cooled to 0°C, followed by addition of 4.297g NaHCO$_3$ (0.0512 mol, 2.5 eq). Boc anhydride (6.21g, 0.247 mol) is dissolved in 15 mL anhydrous EtOH and added via addition funnel. This is allowed to stir overnight and gradually come to room temperature. The reaction was monitored via TLC using 4:1:1 n-BuOH: AcOH: H$_2$O and visualized with acidic ninhydrin stain. The boc protected product reacts with acidic ninhydrin stain and shows a spot with an Rf very near the solvent front. The reaction mixture was concentrated via rotary evaporator. The crude product was dissolved in acetonitrile and washed with hexanes, then concentrated and redissolved in 25mL sat. NaCl (aq) and 25mL ether, the aqueous layer was extracted twice more with 25mL portions of ether. The organic extracts were combined and dried with Na$_2$SO$_4$, the product was found to be 81% pure, contaminated with excess Boc anhydride, with 68% yield was calculated from the ^{1}H-NMR spectrum. As this was desired for model reactions for a later elimination step, the material was used as is.

18': Tosylation of N-Boc-L-Serine Ethyl Ester
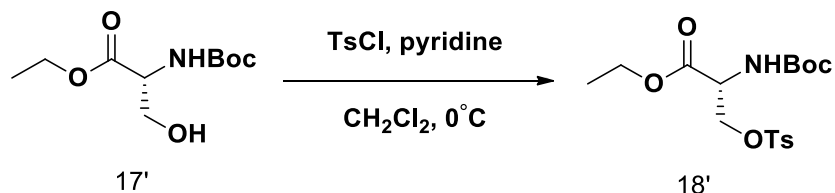
Crude N-Boc-L-serine ethyl ester (81% pure, 3.31g, 11.5mmol) and TsCl (2.31g, 12,1mmol, 1.05 eq) are mixed together and dissolved in CH_2Cl_2 (20mL) and cooled in an ice bath. Pyridine (1.85mL, 23mmol, 2 eq) was added dropwise via syringe. Reaction was monitored via TLC with CH_2Cl_2 as the eluent and visualized under short-wave UV. After 24h, the reaction mixture was worked up by washing with 2-20mL portions of pH 5 AcOH(aq), 20mL saturated $NaHCO_3$, and 20mL of brine, and then dried with Na_2SO_4. This was concentrated to a viscous yellow oil and crystallized by allowing stand in the refrigerator for one week. Pale yellow crystals were collected by filtration and washed with cold hexanes. Crystals had mass 1.924g, 43% yield with MP = 80-105°C. This material was used in subsequent reactions as a model substrate and yield and purity were not optimized.

19': Elimination of ethyl 2-((tert-butoxycarbonyl)amino)-3-(tosyloxy)propanoate

18' → **19'**
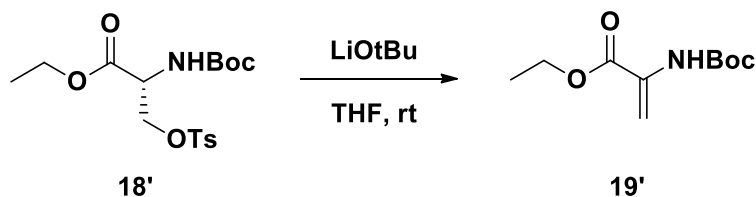
Ethyl 2-((tert-butoxycarbonyl)amino)-3-(tosyloxy)propanoate (1.5162g, 3.9 mmol) and solid

lithium t-butoxide (97%, 1.525g, 19mmol) were combined and dissolved in 10mL THF. This

was quickly fitted with a rubber septum and N_2 (g) balloon. The reaction was exothermic

and the solution quickly turned brown. (If repeated I would suggest dissolving the ester in

THF and cooling in an ice bath with slow addition of base as a solution.) The reaction was

allowed to stir over the weekend, after which time it was partitioned between ethyl acetate

and water. The organic layer was dried with Na_2SO_4 and concentrated. The crude ^{1}H-NMR

spectrum showed alkene formation, new signals at δ6.1, 1H, $J = 23$ Hz and δ5.7, 1H, $J = 28$

Hz. Note: This reaction was attempted first with Et_3N in CH_2Cl_2 and no product was

observed.
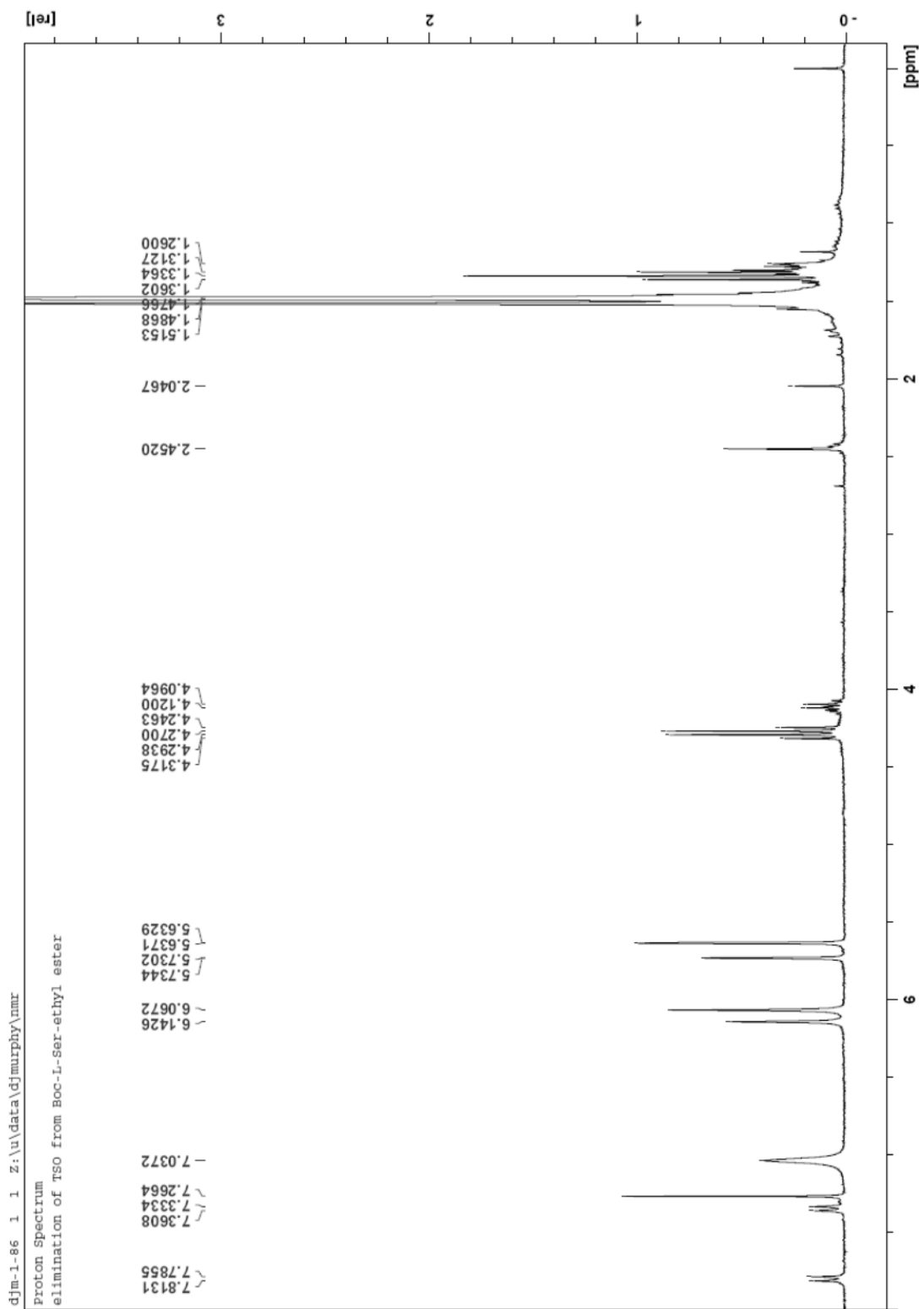
^{1}H-NMR: DJM-1-86 Model reaction, evidence of Olefin 19'

Chapter 4. Recognition and Reporting of Metal Ions

4.1 Introduction to Metal Sensing

Sensitive detection of metal ions has become an area of intense focus due to the adverse effect of metal pollutants in the environment and on human health.[50] Trace amounts of iron, copper, manganese, and zinc are essential nutrients; however, metals can form complexes with biological molecules containing ligating atoms such as nitrogen, sulfur and oxygen. As a result, enzyme inhibition or changes in protein folding may occur through disruption of hydrogen bonding or disulfide bonds leading to dramatic consequences.[51] Lead contamination in drinking water is a concern in several American cities, as lead disrupts protein and peptide secondary structures and leads to developmental disorders in children.[52] Accumulation of Zn^{2+} in the brain induces amyloid plaque formation seen in Alzheimer's disease.[53] Heavy metals in soil can accumulate in food, or enter humans directly through contaminated water.

We have focused our efforts in the determination of metal ions in aqueous solution, with an application for monitoring wastewater. Our general idea has led to patented technology[54,55] for continuous measurement of metal ions with a sensor array. This technology has been licensed by Advanced Chemical Systems (now AquaMetals LLC.) who are interested in Zn^{2+} remediation, as the Environmental Protection Agency (EPA) has limited Zn^{2+} to 5ppm (76.5μM) in water effluent, which defines the sensitivity of sensor needed.

Methods for Metal Quantitation

Complexometric titration, or chelatometry, is an established method of metal quantitation but it is not suitable for identifying unknown metal ions. In complexation methods, a chelating agent, such as EDTA, is used in an alkaline buffered solution with a colorimetric indicator.[56]

Atomic absorption spectroscopy (AAS) is the standard method for quantitation of free metal ions in aqueous solution.[57] This method requires expensive instrumentation and a specific hollow cathode lamp (HCL) source for each analyte of interest. Requiring an active human technician, the AAS method is slow and cannot be used to monitor multiple analytes continuously in real-time.

Complexation with colorimetric indicators such as fluorescent chemosensors or visible absorbing chemosensors has been investigated for a large number of applications in metal quantitation.[58,59] For biological purposes, high affinity sensors are needed due to low concentration and limited sample size of analyte, and fluorosensors have been favored for these reasons. For biological probing, sensors must be compatible with physiological conditions. Azo dyes can be bioreduced under physiological conditions,[60,61] and have largely been ignored in recent metal sensing. Azo dyes are less appropriate as intracellular metal ion probes than fluorosensors, due to the reduction potential of the nitrogen double bond.[61] However, photobleaching, particularly under aerobic conditions, makes oxidation-prone fluorosensors less robust than azo dyes for our purposes.[62]

4.2 Sensor Design

The design and synthesis of a sensor array for metal ion identification and quantitation has been our goal in this long-time collaborative effort. We began our pursuit using arrays of fluorescent sensors covalenty bound along an optical fiber, distinguishing the output of individual sensors by optical time of flight.[63] However, as we investigated the wastewater application of interest to our industrial collaborator, we decided the nanosecond timescale and spatially distributed special features of our patented[54] method were not needed, and that oxidation and photobleaching of fluorescent sensors limits their useful lifetime. In wastewater,

65

there is an abundance of analyte and the high degree of sensitivity is not needed, as we are not limited in sample size. For simplicity and longevity, our focus has moved from fluorescence to absorbance-reporting chemosensors. Consequently, we chose to investigate UV-VIS absorbance reporting chemosensors, retaining the covalently bound dyes of the previous scheme.

Several azo dyes are known to chelate metal ions such that they generate a distinct response in their absorbance profile, typically in the visible range.[64] The goal of the research herein is to develop an array of chemosensors based on the general azo dye structure to allow highly specific metal ion quantitation from the combined response of many **semi-selective** azo dyes. Giving more detailed information in an aggregate response, a complementary array of sensors allows detailed information to be obtained without necessitating perfect selectivity for only one specific analyte. Highly selective sensors for such specific identification of metal-ions are quite expensive due to the need for complex structures. On the other hand, metal-binding azo dyes have only three primary components and each contributes in the ligation of metal ions; an electron rich phenol or naphthol variant and an electron poor heterocycle linked by an azo bond (Figure 42). These highly conjugated sensors absorb light wavelengths in the visible range and their affinities to metal ions are ideal properties for use in continuous-monitoring system. In a flow system, very high affinity is a problem for continuous measurement, as the binding event must be reversible at a reasonable rate. We have pursued azo dyes for access to diverse responsive structures with elegance in their simple design.[65]
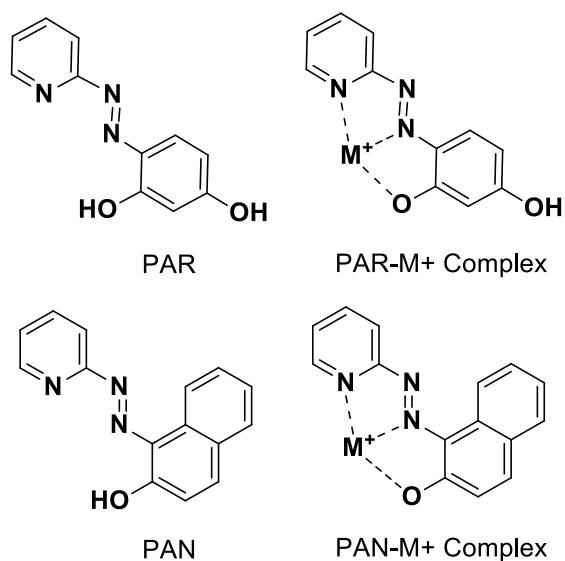
Figure 43. Commercial Azo Dyes and Metal Chelation

PAR and PAN are reported metal indicators[66,67] and commercially-available. These azo

dyes are reported to coordinate with Zn^{2+} and other metal ions to form complexes in 1:1 and 2:1

[host:guest] ratios. These two sensors have remarkably similar design and yet they respond with

distinctly different absorbance profiles in the presence of metals. These two dyes are similar in

their selectivity to several metals, and we set out to explore the brilliantly colored world of azo

dyes by experimenting with the chelation geometry of the binding atoms. The three ligating

atoms of PAR and PAN bind metal through two five-membered metallacycles. We sought

binding geometries involving six-membered rings by extending the length of heterocycle,

replacing pyridine-derived structures with quinoline-azo dyes.

Quinoline-Azo-Resorcinol

The primary method for synthesizing azo dyes involves the formation of an electrophilic

diazonium salt followed by coupling to an electron rich phenol in base (Figure 44). The

formation of the diazonium salt is dependent on the nucleophilicity of the heterocyclic aromatic

amine and its ability to attack the generated nitronium ion and dehydrate to form the diazonium. The diazonium electrophile attacks electron-rich phenol under basic conditions to produce a spectacularly colored conjugated system.
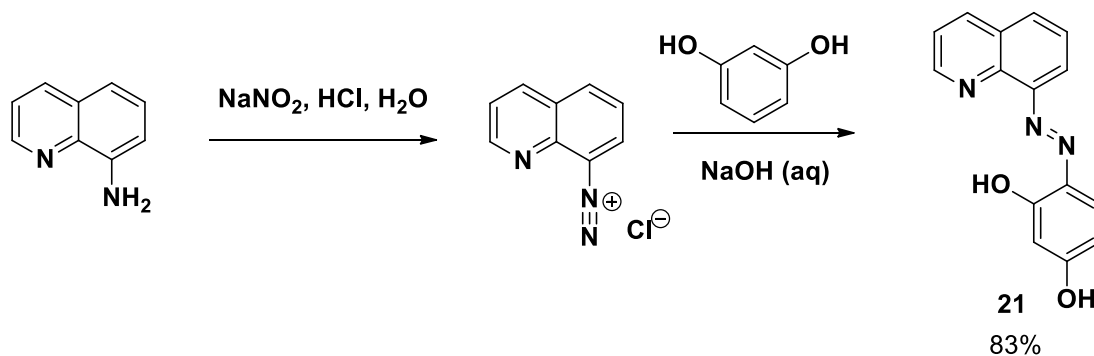

Figure 44. Preparation of QAR

Our interest in quinoline-azo-resorcinol (QAR **21**) was influenced by the structures of PAR and PAN. The heterocyclic moiety in QAR affords a new geometry to the metal-cation ligating site, as the quinoline-nitrogen is further from the azo bond compared to the pyridyl-nitrogen in the other examples. Quinoline-azo dye is a longer "particle in a box[68]" than pyridine-azo dye and with that we expected longer wave absorption and bathochromic shifts when complexed to metals; with absorbance profiles that differed from their smaller pyridine based cousins, and a binding site offering a 6-membered metallacycle, QAR revealed information complementary to PAR and PAN when bonded to metal ions in solution. There is very little literature describing QAR; it was first reported in 1969 as a Co^{2+}-indicating dye[69] and then briefly mentioned as part of a combinatorial library in the year 2000[58] without any further characterization or analytical data.
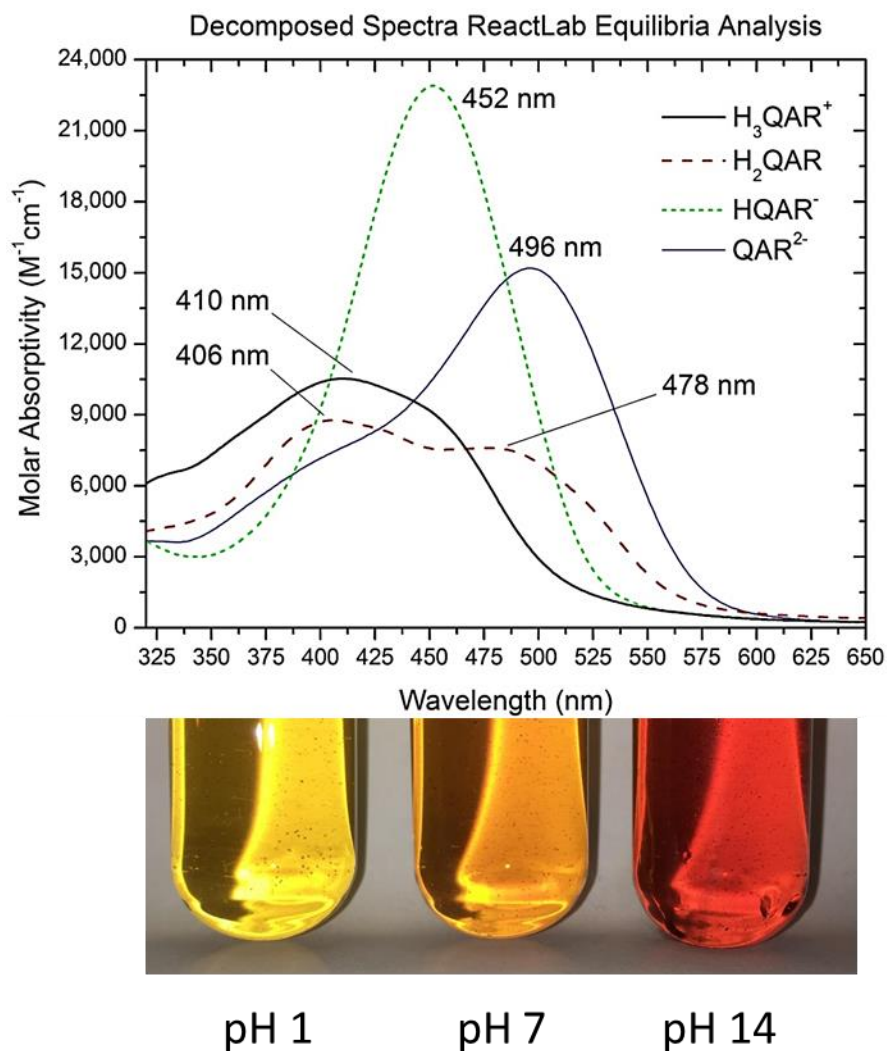
Figure 45. QAR as a pH Indicator

QAR behaves as a pH indicator (Figure 45), like many other azo dyes.[70] As such, understanding its spectral response of various protonation states and its acid-dissociation constants is important to the application of an absorbance-reporting chemosensor, as any spectral shifts interpreted as metal-ion binding must not be false positives due to changes in pH. We were fortunate with QAR, that its three pKa's (2.4, 6.5, 12.9) do not further complicate our

spectral analysis, as the pKa's are far enough away from the pH of the analyte so as not to cause any spectral interference.

We are interested in the spectral response of QAR to metal cations. In comparison to the spectral shift observed when PAR binds Zn^{2+}, QAR does not exhibit such a dramatic bathochromic shift (Figure 46). However, there is a dramatic change in the shape of its spectrum, which allows measurement of a difference plot, where we can subtract one spectrum from the other and relate the change in the spectrum to concentration.
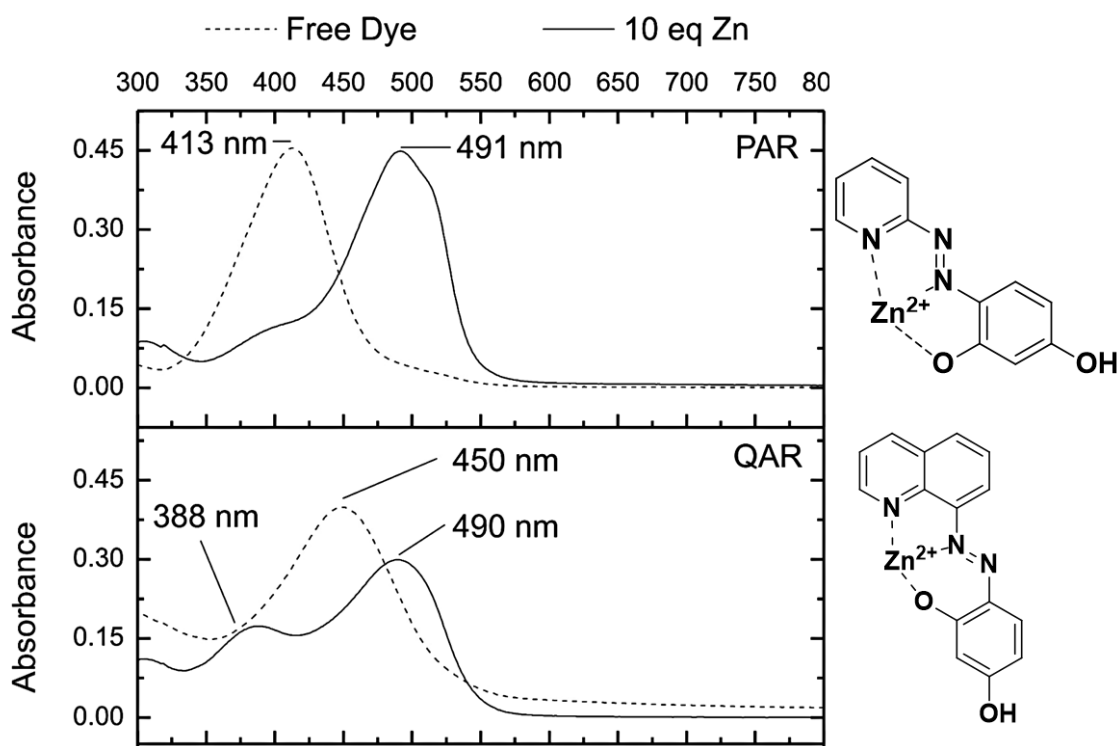

Figure 46. PAR and QAR Respond to Zinc

QAR was further characterized by titration with Zn^{2+} to determine its dissociation constant. In Figure 46, we observe the spectral shift of the azo dyes with a large excess of Zn^{2+}, with this abundance of Zn^{2+} the spectrum is likely of the 1:1 [host:guest] complex.

70

Titration of dilute QAR with Zn^{2+} (Figure 47) found the sensor to bind zinc with in a 2:1 QAR:Zn ratio, with an estimated K_D of 0.6μM in solution, calculated by taking the square root of measured the K_{eq} of a second-order process. Since the EPA limit of Zn^{2+} is 5ppm, and 1ppm Zn = 15.3 μM, we can make meaningful measurements within the range of interest.

Binding Curve at pH 8.8
$$Zn^{2+} + 2HQAR^- \longrightarrow Zn\text{-}QAR_2$$

HQAR⁻ $\log K_F$ = 12.490 ± 0.007 M⁻²
Zn-QAR₂ K_F = (3.09 ± 0.05) ×10¹² M⁻²
    K_{eq} = (3.24 ± 0.05) ×10⁻¹³ M²
    K_D = [(5.69 ± 0.72) ×10⁻⁷ M]

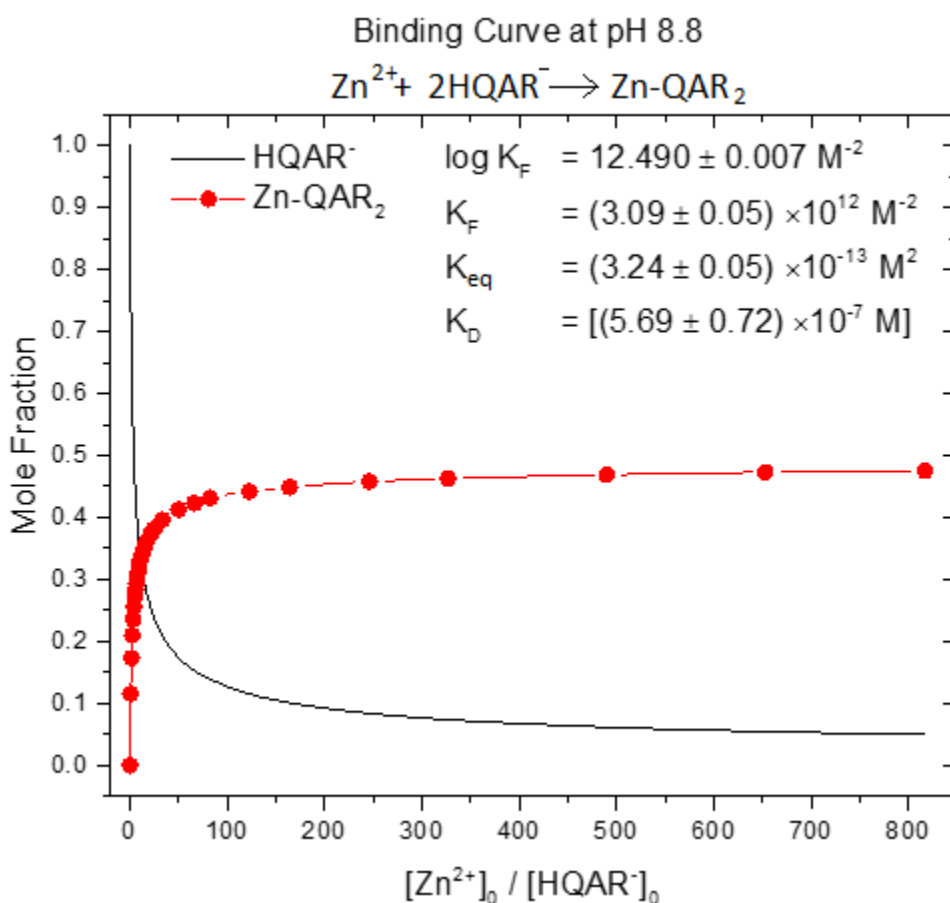*Figure 47. QAR-Zn Binding Titration*

We investigated the spectral response of QAR with other metal cations in a 2:1 [QAR:M+] ratio (Figure 48). Each of the metals elicits a unique response, and while the λ_{max} for each spectrum may not vary drastically, the shape of the spectrum allows for decomposition of the aggregate response, by looking at the difference in response at every wavelength.
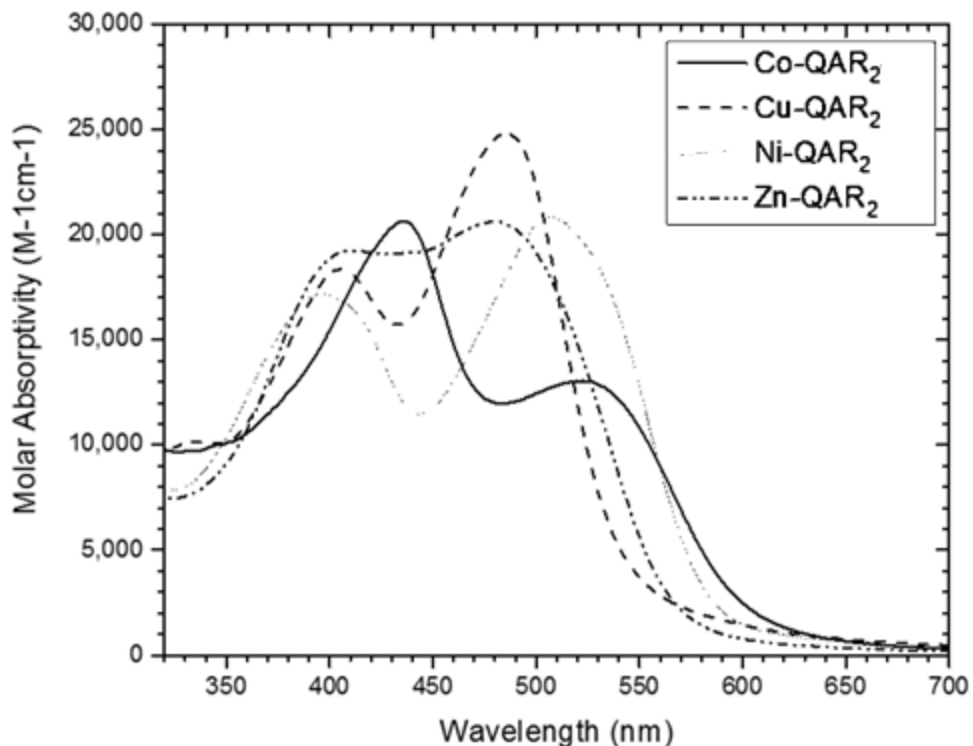
Figure 48. QAR Response to Various Metal Cations

Sensor Array

PAR, QAR, and PAN each give varied spectra with metal cations in solution. None of these chemosensors is especially specific to any analyte, and this is by design. By using a combination of semi-selective sensors, we can get more information about a mixture of metals from any given sensor than what can be learned from a single very selective sensor about more than one metal. The cumulative response of an array of sensors allows determination of several analytes from a limited number of sensors. We have demonstrated simultaneous determination of up to 7 metals in solution, using only four azo dye chemosensors.

4.3 Results and Discussion of Sensors
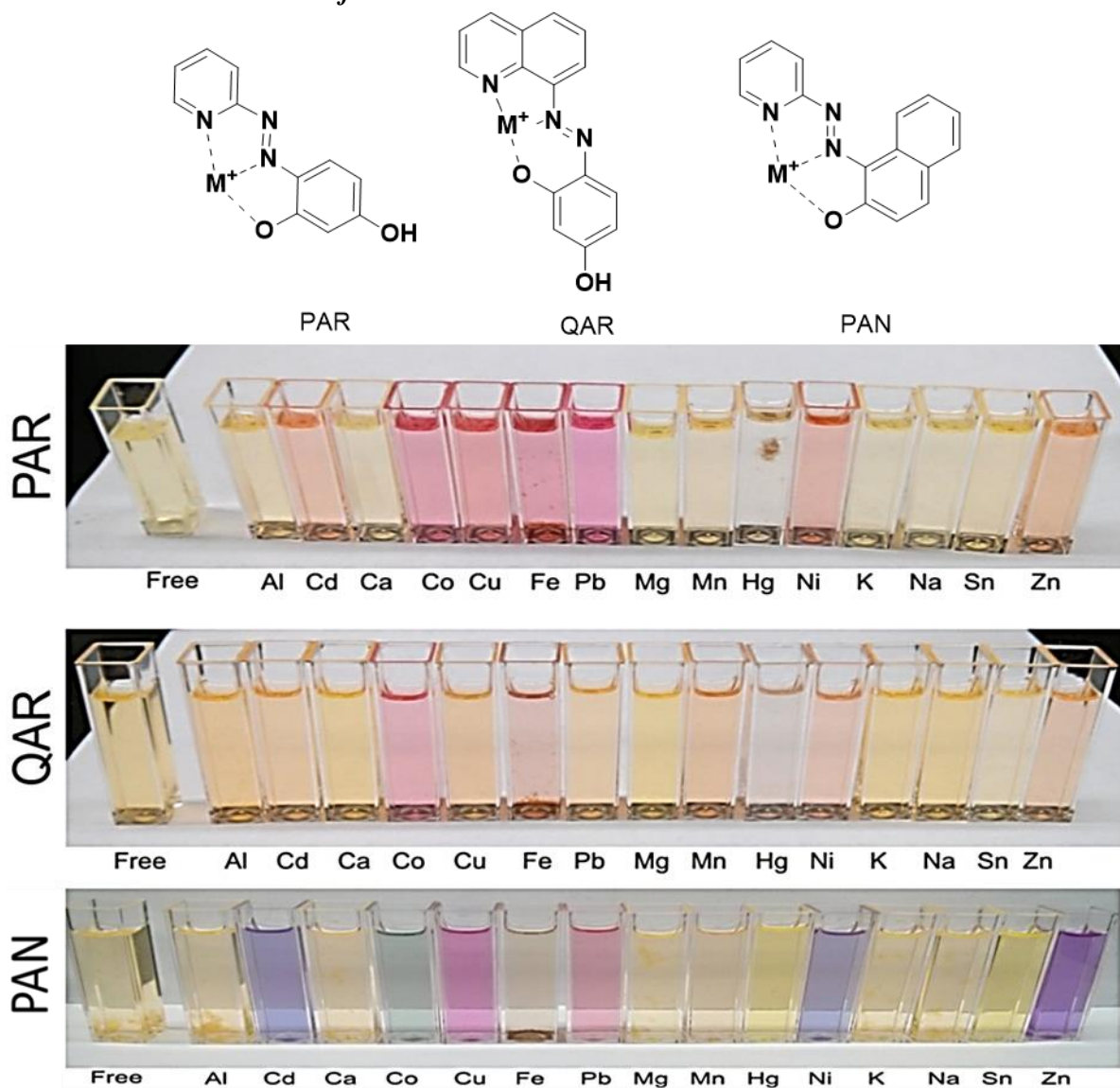
Figure 49. Sensor Array

The identification of metals can be achieved visually using Figure 49. Note that each of these substances has one ligating phenolic oxygen and two coordinating nitrogen atoms, positioned to interact with a metal cation: that interaction is shown with dashed lines.

Solution studies in Figure 49 show that we can discriminate among many transition metals simply by visual inspection, on exposure of each to these and related sensor molecules.

For example, PAR responds positively to Co^{2+}, Cu^{2+}, Fe^{2+}, and Pb^{2+} in a way that is difficult to tell apart, but when the information from QAR and PAN are combined, an unknown solution that is pink with PAR and QAR but green with PAN can be identified as Co^{2+}. Cu^{2+} elicits a bathochromic shift in PAR and PAN, but not QAR, allowing similar determination.

Each sensor is different: even PAR and QAR, nominally having the same types of coordinating atoms, are distinct in the aromatic systems that comprise length of "the box" as the size of their phenol system differs by the length of a benzene ring. Differences in π-π interactions with the longer naphthol may involve discernment of analytes through selection for preferred ionic radii or in how their colorimetric response is affected by strange binding conformations; these differences result in distinct metal binding and reporting preferences. Variance of the phenolic portion of the azo dye would be expected to primarily change spectral response rather than radical differences in Kd, as long as the metal-binding phenol group is retained.

The small combinatorial library is the first screening of an array of azo dye (Figure 50). The heterocylces and phenols were chosen to include what look like unusual ligand geometries, in the hope that distinctions among metals would be present in the binding behaviors and differences of colorimetric response to metal ions. In this way, this array differs from the library of azo dyes reported by Walt[58] which has sensors with relatively conservative changes to coordination geometries.

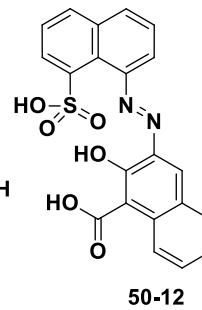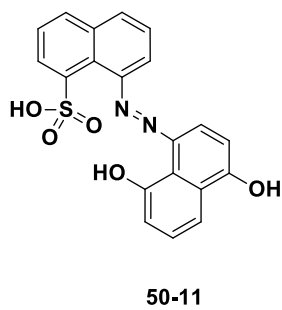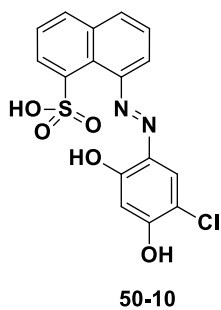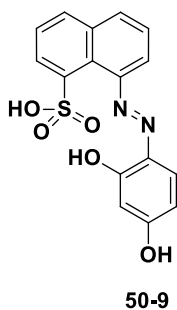The library **50: 1-12** was prepared using the scheme in Figure 50:
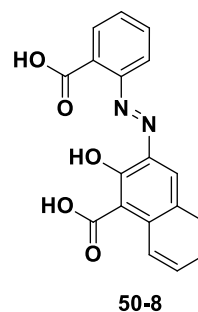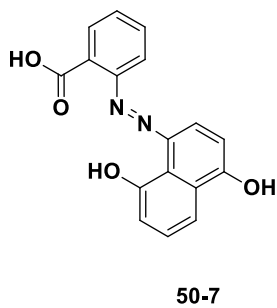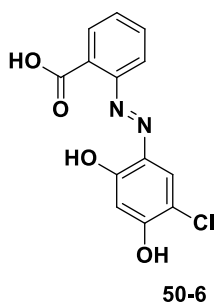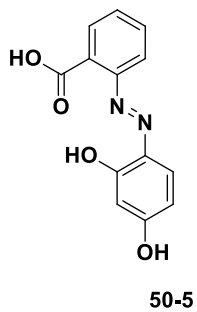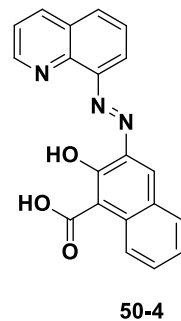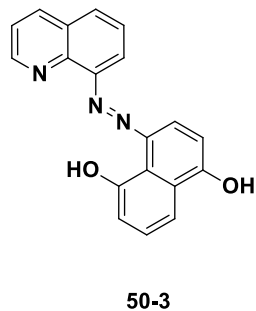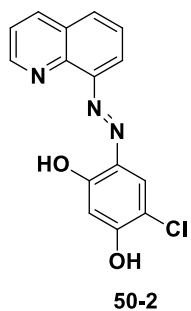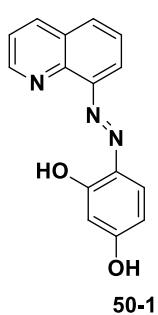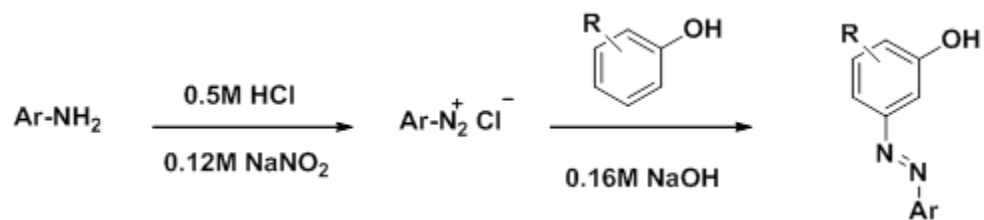
Figure 50. Small Combinatorial Library of Azo Dyes

75

We claim here a practical approach. The key idea is that a small number of chemosensors somewhat selective for various ions provide much more specific data in combination than individually. Rather than simply screening large numbers of substances whose properties may not vary in significant ways,[58] we chose our sensor molecules in terms of metal-ligating atoms whose nature and geometry affect metal-binding affinity and selectivity. Other portions of the molecule may be indirectly responsible for metal binding, for example by geometrically precluding metal ligating atoms from attaining certain positions (steric interference). The major influence on sensor behavior of non-metal-interactive molecular regions is on spectroscopic response to that binding. However, as both libraries were made by the standard acidic diazotization approach, the pyridyl diazonium that would lead to PAR and PAN was not included.
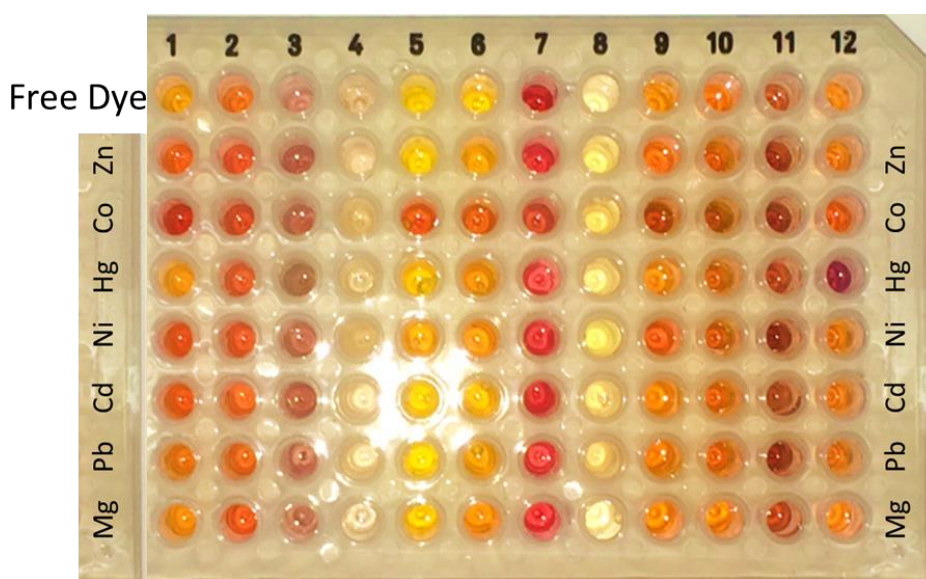
Figure 51. Screening for Metal Response

The 12 crude dyes were screened for sensor activity with 7 metals: Zn, Co, Hg, Ni, Cd, Pb, and Mg (Figure 51). The assigned numbers of compounds **50 1-12**, correspond to the lanes of the 96-well plate: Figure **51 1-12.** This screening allows discrimination of compounds that

76

cannot be prepared by this general method, and allows a quick visual inspection of the behavior of those azo dyes which were formed successfully by this method. The method is versatile, but limited in scope, and Trevor Hagemann pursued alternative syntheses to pursue compounds of interest.

Compound **50-3** did not respond distinctly to metals in the metal screen shown in Figure 51, but was found to be solvatochromic when rinsing out glassware with organic solvent. The tautomers proposed in Figure 52 may explain the extreme solvatochromic behavior of **50-3**, which at the time of writing this dissertation, was lovingly referred to as QAN-1,5OH (Figure 53).

QAN-1,5-OH (**50-3**) sensor is solvatochromic: its color in solution varies across the visible spectrum depending on solvent. More polar solvents tend to blue shift the absorbance of the dye while the less polar solvents appear to red shift the absorbance of the dye, however this correlation is not absolute by any means. The ^{1}H NMR spectra of **50-3** for QAN-1,5-OH shows two singlets in the range one would expect to see a hydrogen bond, thus the red color observed in CDCl$_3$ is likely the keto-tautomer of QAN-1,5-OH. Compared to its ^{1}H NMR spectrum in a strongly hydrogen-bonding solvent like DMSO-d$_6$, from the same sample, all of the aromatic peaks are broadened and no hydrogen bonds are observed. This seems to infer that in polar solvents, the dye is present in both the enol and keto tautomers at some equilibrium.

50-3
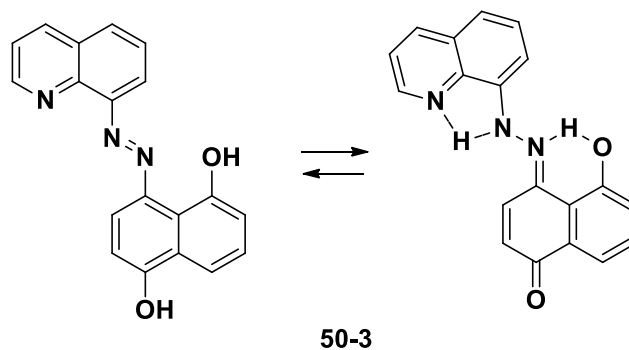
Figure 52. Tautomers of QAN-1,5OH
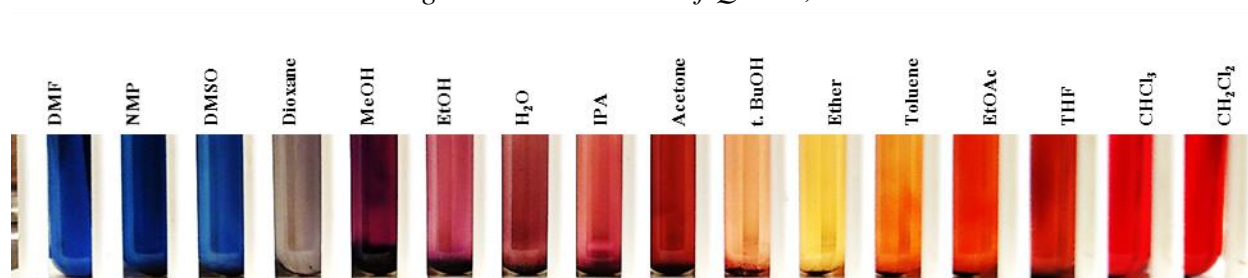
Figure 53. Solvatochromism of QAN-1,5,-OH

Our chemosensing application depends on covalent linkage of metal sensor molecules to a stable matrix. The reason for this is two-fold, we are designing a flow cell sensor with direct contact to moving water and the sensor must not be washed away to prevent loss of signal over time and ensuring minimal leaching of dye to the environment. Furthermore, attachment of the sensor through the distal phenols enhances longevity by eliminating a common mechanism of oxidation. A schematic representation for an instrumental prototype is shown in Figure 54.
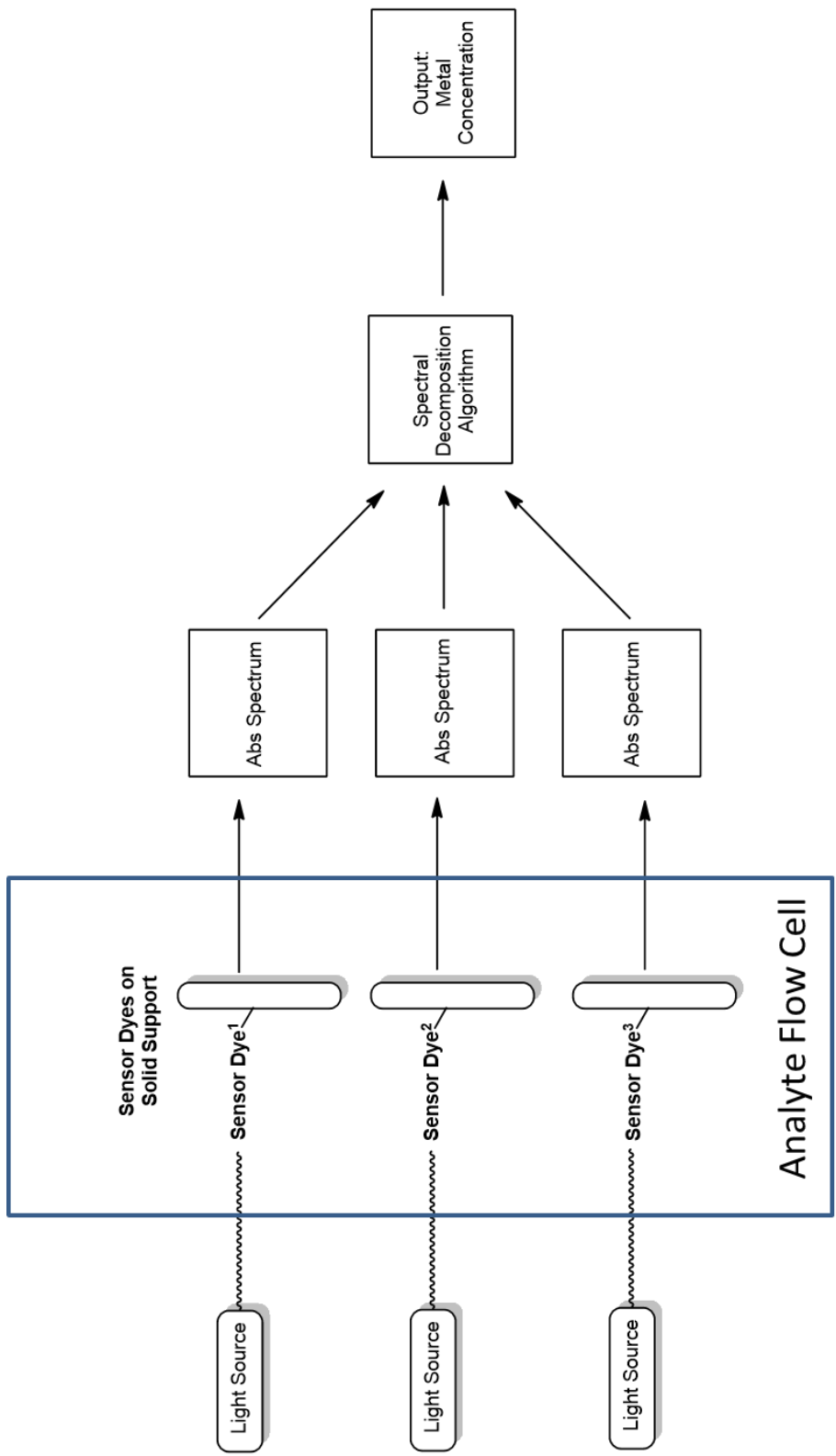
Figure 54. Schematic of Flow Cell Concept

Covalent Attachment to Solid Support

Two general methods for covalent attachment to solid supports are described here, these two methods allow attachment to a variety of solid supports through alkylation and acylation. Methods were developed on cellulose. Cellulose was chosen for its transparency and expectation to give fair optical transparency as well as its chemical structure. Cellulose is a natural polymer of D-glucose linked by β(1→4)-glycosidic bonds. By nature, cellulose is durable and contains several primary alcohols ready for chemical functionalization.

Functionalization of cellulose was thought to require extensive drying steps for removal of water from its hydrophilic network. Carbonyldiimidazole (CDI) was to be used for activation of primary alcohol for further acyl substitution yielding stable carbamates. CDI is destroyed by water, and to reduce wasted starting materials and give more efficient procedures, water was removed from the cellulose by dehydration in a Soxhlet extractor. The cellulose was placed inside a solvent-permeable thimble and cycled several times with CH_3CN refluxed over CaH_2. Dehydration by Soxhlet extraction was found to be no better than simply soaking and rinsing the cellulose in three portions of N-methyl pyrrolidinone (NMP), requiring only as much NMP as necessary to submerge the cellulose. NMP rinses were much more convenient as they could be carried out in a centrifuge tube quickly and did not require a complicated glass apparatus or long reflux times.

CDI was employed to yield an imidazole carbamate receptive to acyl substitution by (polyethylene)glycol diamines. Carbamates are well-known as stable functional groups and often employed as protecting groups (Fmoc, Boc, Cbz). The nucleofugality of imidazole facilities acyl substitution from an activated carbamate to form a very robust covalent linkage to a hydrophilic polyethylene glycol tether.

The utility of hydrophilic polyethylene glycol tethers allows for sensors to be attached to a durable support and extends them away from the surface of the support and into the bulk solution. Flexible water-soluble polyethers are stable and allow free movement of sensors so that even when covalently attached to a support, their spectral response to metal ions is comparable to that in free solution. The polyethylene glycol tethers are derivatized with an amine terminus for acylation with appropriate function group for sensor attachment.

Acylation by sensors with carboxylic acid moieties are readily attached to the amine terminus, while acylation by bromoacetic acid provides a route for alkylation of phenolic sensors by substitution of bromide.

QAR-cellulose is pictured in Figure 55. This sample was prepared from cellulose dialysis tubing with QAR *via* the alkylation method from bromoacetylated cellulose. The spectral data obtained in solution (bottom left spectrum) corresponds nicely to the difference plot shown above it. The response of QAR-cellulose is clearly visible without a spectrophotometer as shown in the photo on the top right, but these films scatter light too much to give usable spectra.

QAR Alkylated Cellulose vs QAR solution

Difference Plot QAR-dialysis film

QAR

no Zn²⁺   with Zn²⁺

QAR solution
388 nm
450 nm
490 nm
QAR Zn solution

QAR film with Zinc similar to solution phase QAR-Zn complex

λ_{max} shifted from 490nm to 497nm
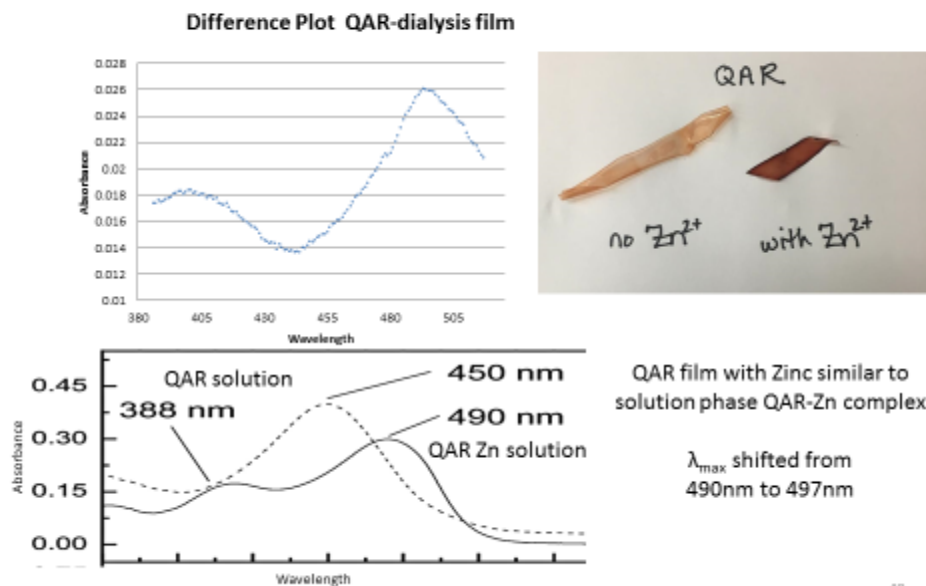
Figure 55: QAR-Cellulose

The covalent attachment of an azo dye chemosensor was achieved via both alkylation and acylation (Figure 56). The scheme shown in Figure 56 shows how the cellulose has been functionalized for sensor attachment through complementary methods of acylation and alkylation. In the alkylation, QAR$_2$Zn **22** is used to protect the metal-ligating oxygen from alkylation, the Zn^{2+} can be removed with EDTA, and the derivatized films will become a light orange color, similar to the color of QAR solutions in the absence of metal ions.
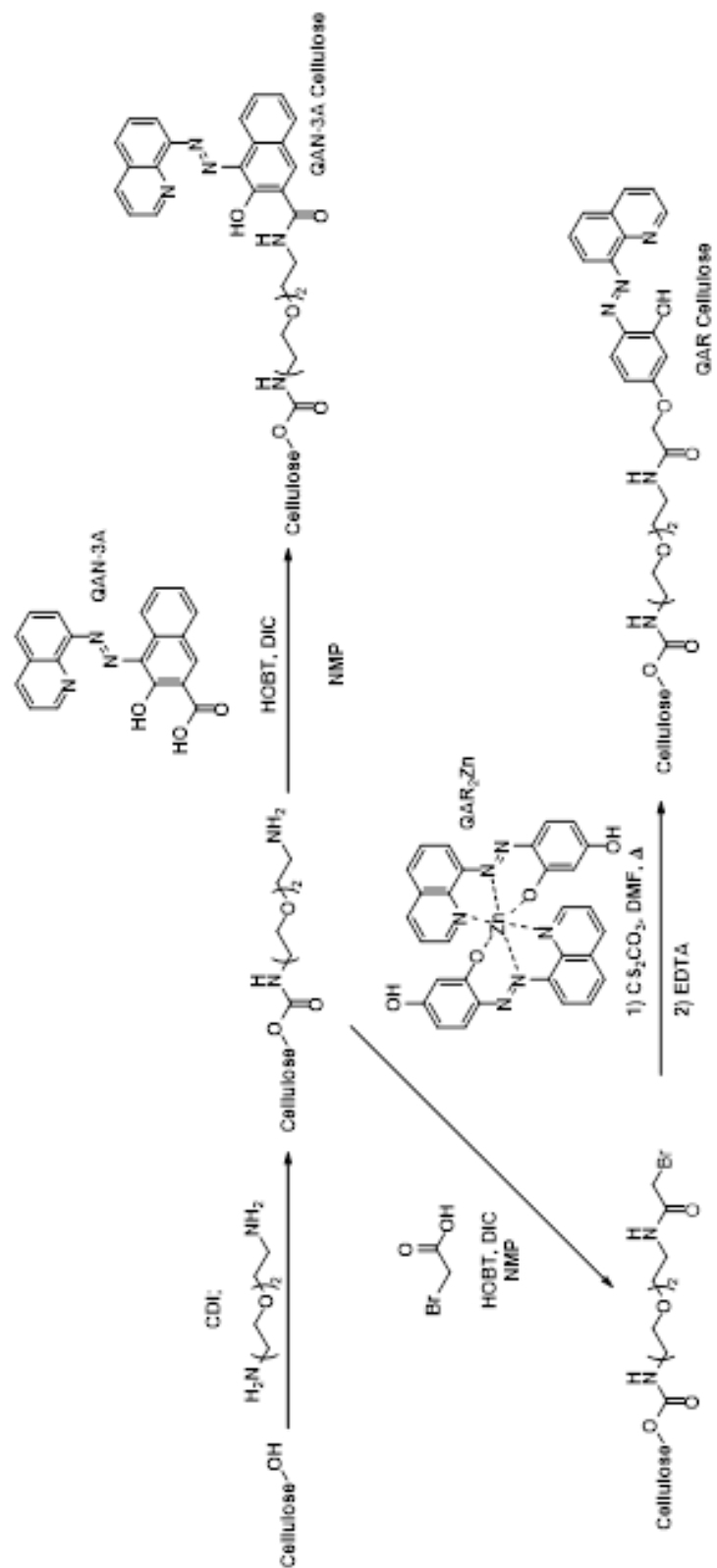
Figure 56: Preparation of QAN-3A and QAR celluloses
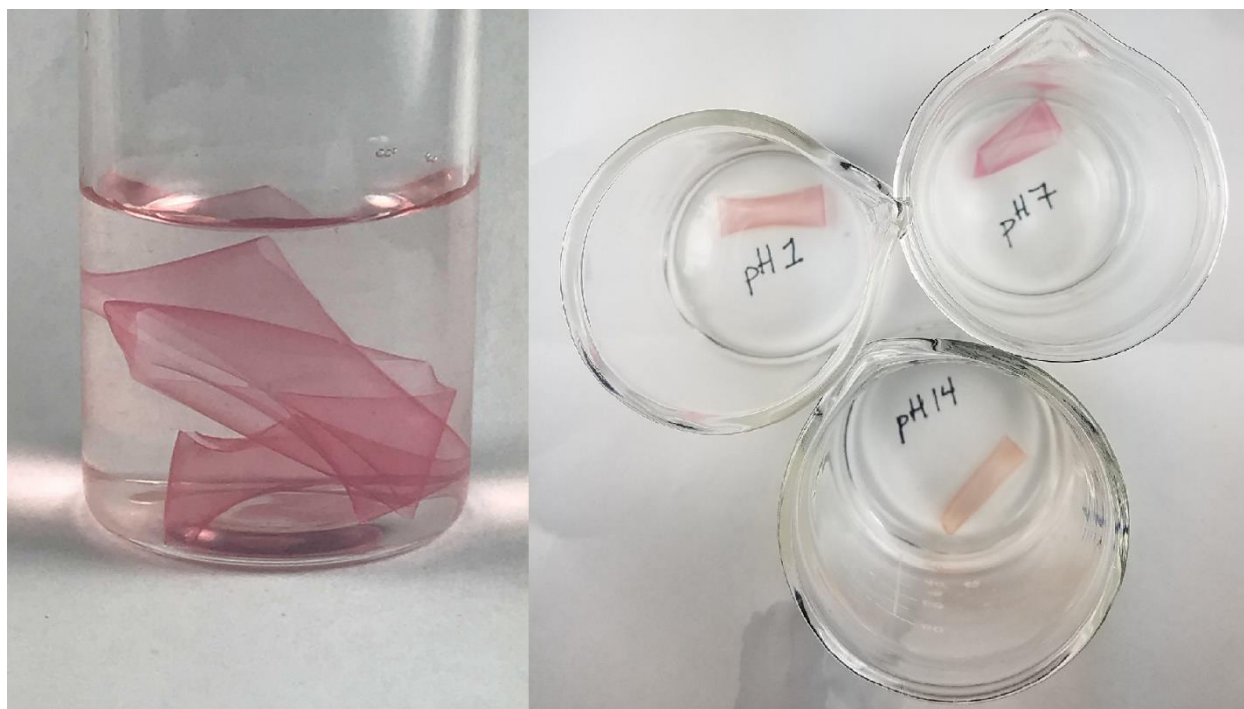
Figure 57. QAN3A-Cellulose

Covalent-linked cellulose films retain absorbance properties over several months even when exposed to water, air, and light, they retain intense color. Figure 57 shows QAN3A-cellulose strips that have been stored in aqueous solution for nearly 3 years, without loss of dye or leeching into solution (left). These strips respond to pH and give colorimetric response visible to the naked eye.

The procedures described on cellulose will allow covalent linkage of any of the azo dyes that bears a nucleophilic group not involved in metal binding. A somewhat lower metal affinity, with lesser pH response, would result from the same procedure in the absence of the preformation of zinc complex: alkylation of phenolic groups in this case is not selective.

For incorporation into other materials and surfaces, another covalent linkage method involves alkylation of the zinc ion complex of sensor by 4-vinylbenzyl chloride. The product of

this reaction can be incorporated by free radical polymerization into a wide range of materials, exemplified here by (polyethylene)glycol diacrylate. The resulting hydrophilic gel, after removal of zinc ion by treatment with EDTA, is similarly stable and responsive to metals as the cellulose membrane.
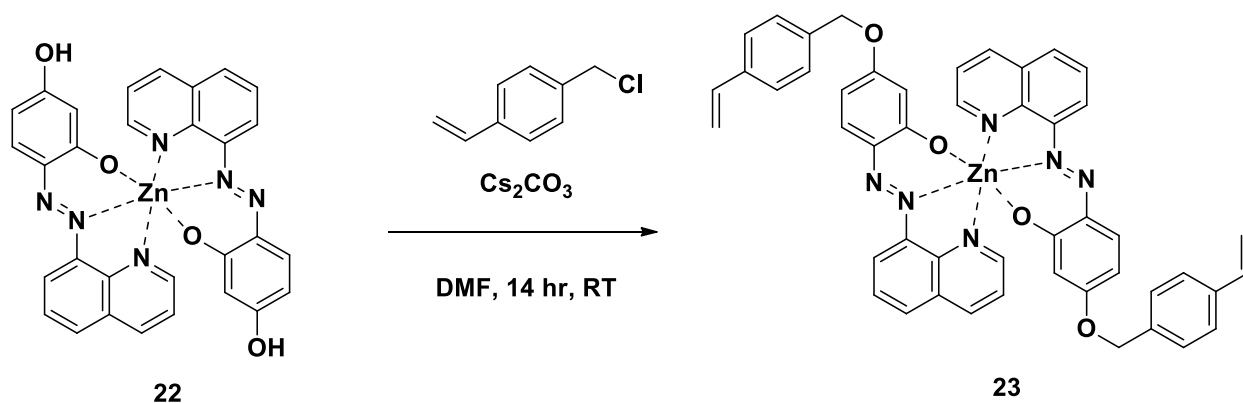
Figure 58. Alkylation of QAR₂Zn

Alkylation of QAR to give a functional monomer **23** for polymerization is done using zinc-complex **22** (Figure 58). The advantage of zinc is two-fold. The Zn^{2+} functions as a protecting group for the metal-binding site, so that only the distal phenol is alkylated. The Zn-complex **23** also may serve as a metal template in polymers, holding two sensors in proximity and with good geometry for binding. This is expected to enhance affinity and could produce selectivity through size-exclusion favoring the metal-cation used in templating.

Attempts at alkylation of QAR without using the metal-complex were unsuccessful. Reactions were performed with QAR and K_2CO_3 or a prepared mono-anionic QAR salt, using either 4-vinylbenzyl chloride and NaI or a separately prepared and isolated 4-vinylbenzyl iodide, solvents such as MeCN or DMF (dimethylformamide) had been screened. These reactions proceeded slowly and gave complicated mixtures by TLC.

Iodine/iodide appears incompatible with the azo dye, as significant loss of color occurred, which I propose could be due to reduction of the azo bond (Figure 59). It is speculated that iodide and iodine may be having an effect on the QAR, possibly through reduction of the N-N double bond. Also, a red spot that has been present in all alkylation attempts has spontaneously appeared in the TLC standard of QAR. We hypothesize that this spot is the product of reducing the QAR.
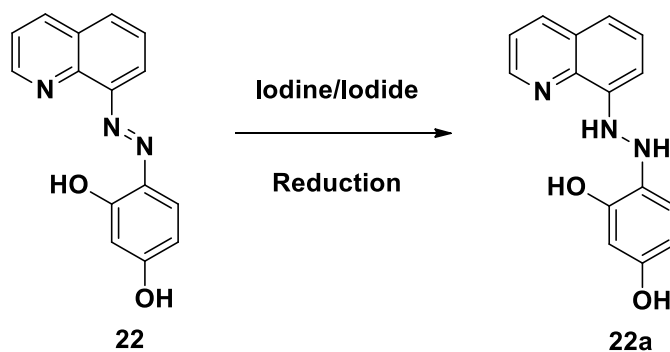
Figure 59. Proposed Azo Reduction by Iodine

Those reactions which were successful in forming the alkylated product were not selective for the distal end of the molecule and purification by crystallization and chromatography were problematic due to poor solubility of the product mixtures. (It has since been found that very pure QAR may be isolated by simple trituration in boiling MeOH, and subsequent alkylations will be performed using better quality QAR). However, recently the dianionic salt of QAR was prepared by mixing QAR with two equivalents KOtBu in MeCN. This salt was then dried by rotary evaporation and heated and stirred under high vacuum pump.

Post-polymerization alkylation was achieved on our simple polymers by meslaytion followed by alkylation. The sensor dye were first formed as a zinc complex to protect the binding site from modification and then allowed to alkylate with the mesylated hydrogel:

In situ alkylation was achieved by using 4-vinylbenzyl chloride as a monomer and by replacing a portion of the co-solvent with a previously prepared alkylation solution that contained the protect sensor dye complex and a base to allow for alkylation on the distal phenols of the dye molecule (Figure 60).
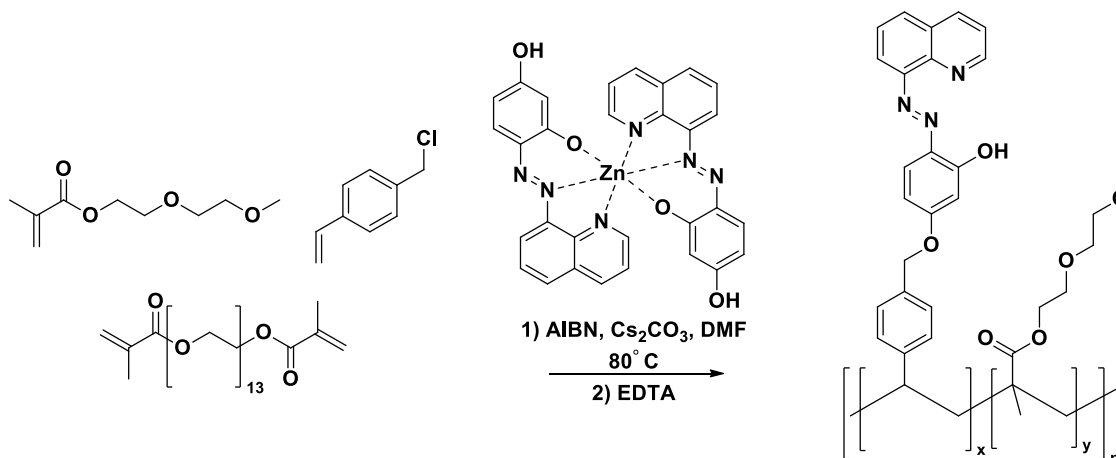
Figure 60. In Situ Polymer Alkylation of QAR

The more difficult method involves alkylating the sensor dye first to create a functional monomer (Figure 61). This method is advantageous because it allows for a more controlled loading of the sensor dye and there will be no additional crosslinking of the polymer. In comparison to the other methods described, the pre-polymerization alkylation method does not template the polymer in the 2:1 sensor to analyte ratio. This has a potential effect on the kinetics of the analyte binding.
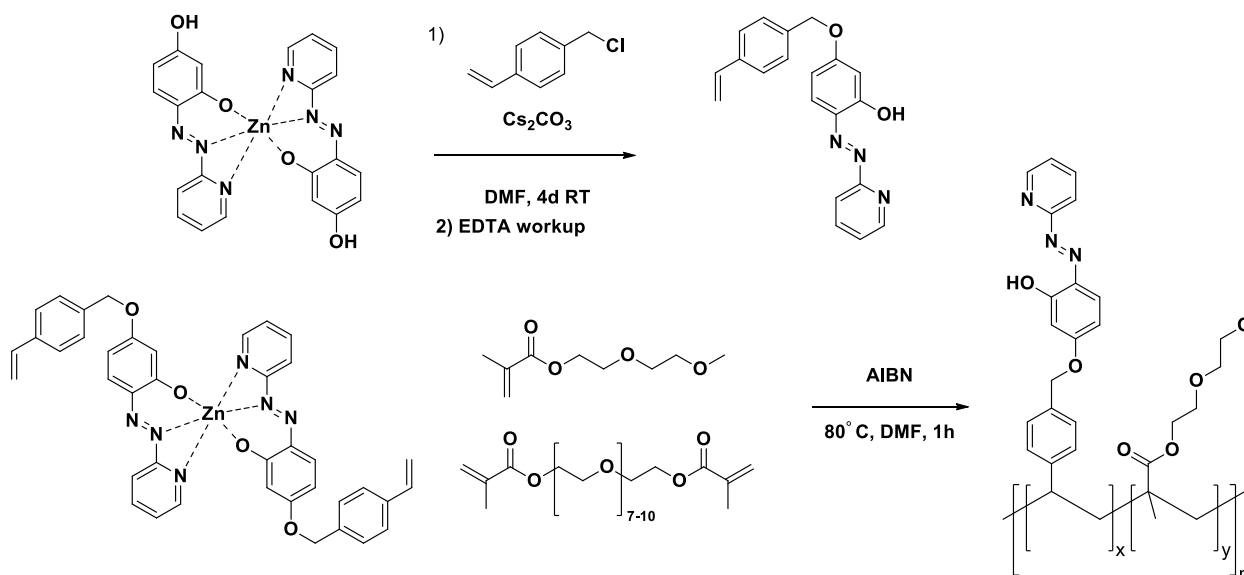
Figure 61. QAR Polymer from a Functional Monomer

Conclusion

A sensor array for the continuous monitoring of metal ions in aqueous solution has been studied in solution and when covalently attached to solid supports. A generic approach to the covalent attachment of azo dyes to solid supports has been achieved and implemented in polymers that are compatible for optic instruments. A prototype flow cell sensor has provided reproducible response to metals and consistency in cycling with excellent sensor lifetime; several month.

4.4 Experimental: 21, 22, 23, Derivatized Cellulose

21: preparation of 4-(quinolin-8-yldiazenyl)benzene-1,3-diol (QAR)

Chemical Formula: $C_9H_8N_2$
Molecular Weight: 144.17

Chemical Formula: $C_{15}H_{11}N_3O_2$
Molecular Weight: 265.27
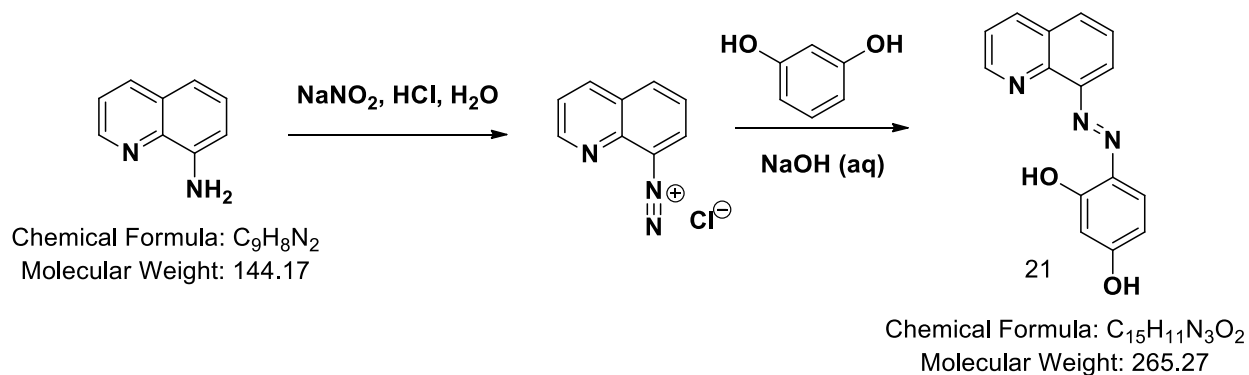
To a stirring solution of 8-aminoquinoline (2.0284g, 14.07mmol) in HCl (40mL 6M) at 5°C on an ice bath was added $NaNO_2$ (1.0733g in 2mL cold H_2O) dropwise until the reaction mixture gave a positive test on KI-starch paper. The resulting mixture was added dropwise to a solution of 0.492g resorcinol in 78.5mL of 1M NaOH stirring on an ice bath. After standing overnight, the solid was isolated by filtration, rinsed thoroughly with cold water, and dried *in vacuo.* Extraction of solid in *ca.* 100 mL boiling methanol, filtration and evaporation gave 0.984g (83% yield) QAR, MP > 320°C.

^{1}H NMR (CD$_3$OD): δ 8.866 (dd, j=1.8, 4.2; 1H) δ 8.250 (dd, j=1.8, 8.4, 1 H) δ 7.989 (dd, 2.1, 6.6, 1H) δ 7.613 (m, 1H) δ 7.562 (m, 1H) δ 7.506 (dd, j=8.4, 4.2, 1 H) δ 6.982 (d, j=9.6, 1 H) δ 6.215 (d, j=9.6, 1 H) δ 5.682 (d, j=2.1, 1H)

^{13}C NMR (CD$_3$OD): δ 148.72, 135.56, 134.83, 128.8, 126.91, 123.90, 121.62, 121.32, 116.72, 110.60, 106.

R_f on TLC: 0.43, in 10% MeOH/CH$_2$Cl$_2$ MS: DUIS m/z 266.15[M+H]+; 264.05[M-H]-

22 QAR$_2$Zn and 23 QAR$_2$Zn-Functional Monomer:

Chemical Formula:
C₁₅H₁₁N₃O₂
Molecular Weight:
265.27

21

Chemical Formula: C₃₀H₂₀N₆O₄Zn
Molecular Weight: 593.90

22

23

Chemical Formula: C₄₉H₃₉N₆O₄Zn
Molecular Weight: 841.25
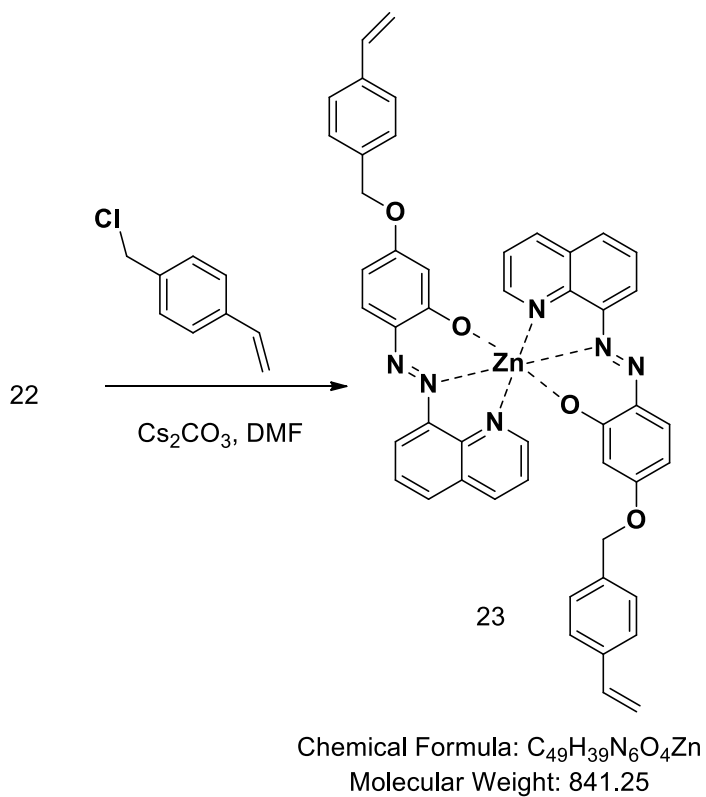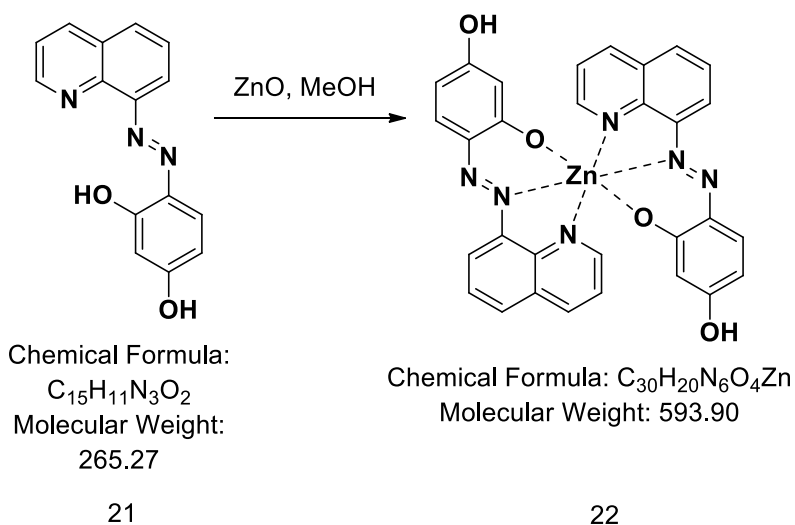
A suspension of QAR (239.3mg) and Zn(OH)$_2$ (36.7mg) in 25mL acetonitrile was heated at reflux for 24hand then solvent removed by rotary evaporation. To the solid, 0.2968g Cs$_2$CO$_3$ is added followed by 11mL dimethylformamide (DMF) and 0.14mL 4-vinyl benzylchloride. This is stirred under nitrogen at room temperature. After 3 hours a fine pale color precipitate is

90

observed. The mixture was filtered and most of the solvent was removed by rotary evaporation followed by vacuum pump. The reaction mixture was dissolved in 50mL CH$_3$CN and washed with 25mL hexanes. The bright orange CH$_3$CN solution was rotary evaporated to dryness to yield polymerizable sensor 4-(quinolin-8-yldiazenyl)benzene-3-ol-1-styrene-zinc complex.

Preparation of QAR2-Zn Salt and Alkylation

A separate solution of 85mg QAR and 13mg Zn(OH)$_2$ (0.5 mol eq) was refluxed in 50mL DMF. A short-path distillation apparatus was used to remove about half the volume of DMF. Cs2CO3 (100mg) was added to the remaining solution and the prepared films were then submerged in vials containing the QAR solution. These were vortexed and allowed to stand overnight. The strips were removed from the QAR solution and rinsed with several portions of nanopure water. (Control strips of untreated tubing were placed in the QAR solution and did not take on the color of the dye).   The treated strips were further treated with ethylenediaminetetraacetic acid (EDTA) to remove Zn2+ from the final template.

Preparation of: 4-(quinolin-8-yldiazenyl)benzene-3-ol-1-styrene-zinc complex

Notebook page reference: SAO-4-88   Formula: C49H39N6O4Zn

Abbreviation/code name: QAR2Zn-Sty2

FW: 841.25 g/mol

The mixture was filtered and evaporated by rotary evaporator and vacuum pump, some DMF remained. The reaction mixture was dissolved in 50mL CH3CN and washed with 25mL hexanes. The CH3CN is brightly orange colored, and was decanted away from a black tar stayed stuck to the glass. This was then evaporated to dryness.

NMR sample was prepared by dissolving a small quantity in CDCl3 and filtering. The spectrum

obtained was very messy and appeared to contain self-polymerized product. The TLC plate

(mobile phase: 10%MeOH/CH2Cl2, stationary phase: Agela technologies TLC silica, non-

fluorescent, pH 5) showed 2 spots: an orange spot with Rf= 0.93, and a yellow spot Rf= 0.83.

The TLC plate (mobile phase: 10%MeOH/CH2Cl2, stationary phase: Silica gel 60 F254) showed

4 spots: a yellow spot Rf= 0.99, a pink spot Rf = 0.92, an orange spot with Rf= 0.88, and a long

orange streak centered at Rf= 0.39.
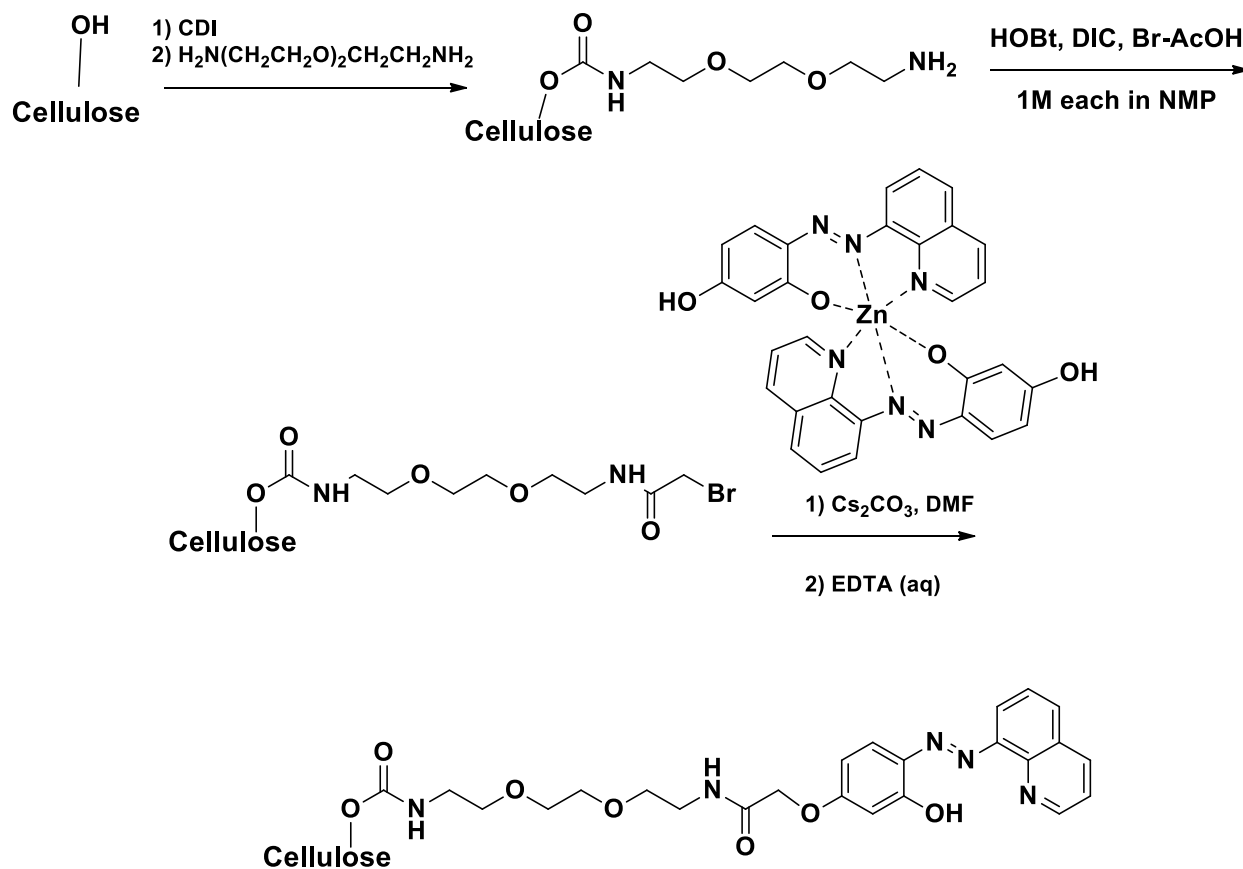
Cellulose for Method Development

Figure 62. Alkylation of sensor to cellulose

Preparation of: QAR-functionalized dialysis tube

Preparation of Dialysis Tube:

Dialysis tubing was cut to a width of 1cm and rinsed 3 times with 25mL NMP. The tubing was placed into a dry centrifuge tube containing carbonyldiimidazole (CDI, 1M in NMP). After 24h, the tubing was rinsed thoroughly with fresh NMP and then placed in a new centrifuge tube filled with 25% triethylene glycolamine. Then the tubing was washed thoroughly with dioxane, glacial acetic acid, and again with dioxane.

The remaining tubing was stored in methyl-2-pyrrolidinone (NMP). The tubing was cut into 1cm slices and each slice was added to 1.5ml solution of hydroxybenzotriazole/N,N-dicyclohexylcarbodiimide/ bromoacetic acid (1M in each in NMP). These films were washed 5x with dimethylformamide (DMF) and stored in DMF for further use.

Experimental: Alkylation Method on Cellulose

Cellulose dialysis membrane was dried in a Soxhlet extractor with CH_3CN refluxing under N_2 over CaH_2 for several days. The dried membrane was soaked in a solution of 1g carbonyldiimidazole (CDI) 14mL CH_3CN for 48h, rinsed thoroughly with CH_3CN, and allowed to stand in 14 mL 1,5-diamino-3,5-dioxaoctane for 24 h. After thorough rinsing, the membrane was exposed to 1.5ml solution of hydroxybenzotriazole/N,N-dicyclohexylcarbodiimide/ bromoacetic acid (1M each in N-methyl-2-pyrrolidinone (NMP)). These films were washed 5x with dimethylformamide (DMF) and stored in DMF for further use.

A mixture of 85mg QAR and 13mg ZnO (0.5 mol eq) was heated at reflux in 50mL DMF, then distilled to remove about half the solvent volume. Cs_2CO_3 (100mg) was added to the remaining

solution and the prepared films were then submerged in vials containing the QAR solution. These were agitated with a vortex-genie and allowed to stand overnight. The intensely colored strips were removed from the QAR solution and rinsed with several portions of nanopure water. (Control strips of untreated tubing were placed in the QAR solution and did not take on the color of the dye). The treated strips were further treated with ethylenediaminetetraacetic acid (EDTA) to remove Zn^{2+} from the final template.

QAN-3A-Cellulose

Acylation procedure: Cellulose dialysis membrane was dehydrated by rinsing with N-methyl-pyrrolidinone (NMP). The dried membrane was soaked in a solution of 1g carbonyldiimidazole (CDI) 14 mL CH3CN for 4 hours, rinsed thoroughly with CH3CN, and allowed to stand in 10% (v/v) triethyleneglycol diamine CH3CN for 24 hours. Azo dye with a carboxylic acid functionality can be acylated to amine-terminated cellulose, in this example QAN-3A was used. A solution of QAN-3A with diisopropylcarbodiimide and hydroxybenzotriazole was combined in a 1:1:1 molar ratio in N-methyl-pyrrolidinone so that the final solution is 0.5 M in each reactant and adding the solution to the amine-terminated cellulose. QAN-3A was used to acylate amine-terminated cellulose by making a solution of QAN-3A (0.0082 g, 0.024 mmol) dissolved in 0.48 mL N-methyl-pyrrolidinone (NMP), this was charged with diisopropylcarbodiimide (0.024 mmol) and hydroxybenzotriazole (0.024 mmol). The solution was applied to the amine-terminated cellulose and allowed to react for 5 minutes before washing with NMP and several portions of nanopure water.

References

(1)   Szejtli, J. Introduction and General Overview of Cyclodextrin Chemistry. *Chem. Rev.*
        1998, *98* (5), 1743–1754.

(2)   Pedersen, C. J. Cyclic Polyethers and Their Complexes with Metal Salts. *J. Am. Chem.
        Soc.* **1967**, *89* (26), 7017–7036.

(3)   Breslow, R. Biomimetic Control of Chemical Selectivity. *Acc. Chem. Res* **1980**, *13*, 170–
        177.

(4)   Breslow, R. Hydrophobic Effects on Simple Organic Reactions in Water The Diels-Alder
        Reaction in Water. *Acc. Chem. Res.* **1991**, *24* (6), 159–163.

(5)   Ngola, S. M.; Dougherty, D. A. Evidence for the Importance of Polarizability in
        Biomimetic Catalysis Involving Cyclophane Receptors. *J. Org. Chem.* **1996**, *61*, 4355–
        4360.

(6)   Kawakami, M.; Nagai, Y.; Fujii, T.; Mitsuhashi, S. Anti-Microbial Activities of
        Enduracidin (Enramycin) in Vitro and in Vivo. *J. Antibiot. (Tokyo).* **1971**, *24* (9), 583–
        586.

(7)   Matias, V. R. F.; Beveridge, T. J. Native Cell Wall Organization Shown by Cryo-Electron
        Microscopy Confirms the Existence of a Periplasmic Space in Staphylococcus Aureus. *J.
        Bacteriol.* **2006**, *188* (3), 1011–1021.

(8)   Reynolds, P. E. Structure, Biochemistry and Mechanism of Action of Glycopeptide
        Antibiotics. *Eur. J. Clin. Microbiol. Infect. Dis.* **1989**, *8* (11), 943–950.

(9)   Knowles, J. R. Penicillin Resistance: The Chemistry of ß-Lactamase Inhibition. *Acc.*

Chem. Res **1985**, *18*, 97–104.

(10) Klevens, R. M.; Edwards, J. R.; Richards, C. L.; Horan, T. C.; Gaynes, R. P.; Pollock, D.
A.; Cardo, D. M. Estimating Health Care-Associated Infections and Deaths in U.S.
Hospitals, 2002. *Public Health Rep.* **2007**, *122*, 160–166.

(11) Wright, G. D.; Walsh, C. T. D-Alanyl-D-Alanine Ligases and the Molecular Mechanism
of Vancomycin Resistance. *Acc. Chem. Res* **1992**, *25*, 468–473.

(12) Pratt J. S., R. F. . K. Different Modes of Vancomycin and D-Alanyl-D-Alanine
Peptidase\rBinding to Cell Wall Peptide and a Possible Role for The\rVancomycin
Resistance Protein. *Antimicrob. Agents Chemother.* **1990**, *34* (7), 1342–1347.

(13) Münch, D.; Sahl, H.-G. Structural Variations of the Cell Wall Precursor Lipid II in Gram-
Positive Bacteria — Impact on Binding and Efficacy of Antimicrobial Peptides ☆. *BBA -
Biomembr.* **2015**, *1848*, 3062–3071.

(14) Ng, V.; Chan, W. C. New Found Hope for Antibiotic Discovery: Lipid II Inhibitors.
Chem. - A Eur. J. **2016**, *22* (36), 12606–12616.

(15) Tsuchiya, K.; Takeuchi, Y. Enduracidin, An Inhibitor of Cell Wall Synthesis. *J. Antibiot.
(Tokyo).* **1968**, *21* (6), 426–428.

(16) Yin, X.; Zabriskie, T. M. The Enduracidin Biosynthetic Gene Cluster from Streptomyces
Fungicidicus. *Microbiology* **2006**, *152*, 2969–2983.

(17) Singh, M. P.; Petersen, P. J.; Weiss, W. J.; Janso, J. E.; Luckman, S. W.; Lenoy, E. B.;
Bradford, P. A.; Testa, R. T.; Greenstein, M. Mannopeptimycins, New Cyclic
Glycopeptide Antibiotics Produced by Streptomyces Hygroscopicus LL-AC98:

Antibacterial and Mechanistic Activities. *Antimicrob. Agents Chemother.* **2003**, *47* (1), 62–69.

(18)   Magarvey, N. A.; Haltli, B.; He, M.; Greenstein, M.; Hucul, J. A. Biosynthetic Pathway for Mannopeptimycins, Lipoglycopeptide Antibiotics Active against Drug-Resistant Gram-Positive Pathogens. *Antimicrob. Agents Chemother.* **2006**, *50* (6), 2167–2177.

(19)   Wang, B.; Liu, Y.; Jiao, R.; Feng, Y.; Li, Q.; Chen, C.; Liu, L.; He, G.; Chen, G. Total Synthesis of Mannopeptimycins α and β. *J. Am. Chem. Soc.* **2016**, *138* (11), 3926–3932.

(20)   Ling, L. L.; Schneider, T.; Peoples, A. J.; Spoering, A. L.; Engels, I.; Conlon, B. P.; Mueller, A.; Schäberle, T. F.; Hughes, D. E.; Epstein, S.; et al. A New Antibiotic Kills Pathogens without Detectable Resistance. *Nature* **2015**, *517* (7535), 455–459.

(21)   Giltrap, A. M.; Dowman, L. J.; Nagalingam, G.; Ochoa, J. L.; Linington, R. G.; Britton, W. J.; Payne, R. J. Total Synthesis of Teixobactin. *Org. Lett.* **2016**, *18* (11), 2788–2791.

(22)   Jad, Y. E.; Acosta, G. A.; Naicker, T.; Ramtahal, M.; El-Faham, A.; Govender, T.; Kruger, H. G.; Torre, B. G. de la; Albericio, F. Synthesis and Biological Evaluation of a Teixobactin Analogue. *Org. Lett.* **2015**, *17* (24), 6182–6185.

(23)   Tsuji, S.; Shoichi, K.; Shiba, T. Synthesis of Enduracididine, a Component Amino Acid of Antibiotic Enduracidin. *Chem. Lett.* **1975**, 1281–1284.

(24)   Craig, W.; Chen, J.; Richardson, D.; Thorpe, R.; Yuan, Y. A Highly Stereoselective and Scalable Synthesis of L-Allo-Enduracididine. *Org. Lett.* **2015**, *17*, 4620–4623.

(25)   Han, L.; Vuksanovic, N.; Oehm, S. A.; Fenske, T. G.; Schwabacher, A. W.; Silvaggi, N. Streptomyces Wadayamensis MppP Is a PLP-Dependent Oxidase, Not an Oxygenase.

2018.

(26)   Yoon, G.; Zabriskie, T. M.; Seung, H. C. Synthesis of [Guanido-13C]-γ-Hydroxyarginine. *J. Label. Compd. Radiopharm.* **2009**, *52* (2), 53–55.

(27)   Burroughs, A. M.; Hoppe, R. W.; Goebel, N. C.; Sayyed, B. H.; Voegtline, T. J.; Schwabacher, A. W.; Zabriskie, T. M.; Silvaggi, N. R. Structural and Functional Characterization of MppR, an Enduracididine Biosynthetic Enzyme from Streptomyces Hygroscopicus: Functional Diversity in the Acetoacetate Decarboxylase-like Superfamily. *Biochemistry* **2013**, *52* (26), 4492–4506.

(28)   Burroughs, A. M.; Hoppe, R. W.; Goebel, N. C.; Sayyed, B. H.; Voegtline, T. J.; Schwabacher, A. W.; Zabriskie, T. M.; Silvaggi, N. R. Structural and Functional Characterization of MppR, an Enduracididine Biosynthetic Enzyme from Streptomyces Hygroscopicus: Functional Diversity in the Acetoacetate Decarboxylase-like Superfamily. *Biochemistry* **2013**, *52*, 4492–4506.

(29)   Kozikowski, A. P. The Isoxazoline Route to the Molecules of Nature. *Acc. Chem. Res* **1984**, *17*, 410–416.

(30)   Machetti, F.; Cecchi, L.; Trogu, E.; De Sarlo, F. Isoxazoles and Isoxazolines by 1,3-Dipolar Cycloaddition: Base-Catalysed Condensation of Primary Nitro Compounds with Dipolarophiles. *European J. Org. Chem.* **2007**, No. 26, 4352–4359.

(31)   Boyd, E. C. Synthetic Applications of Nitrile Oxide / Isoxazoline Chemistry. **1992**.

(32)   Kantorowski, E. J.; Brown, S. P.; Kurth, M. J. Use of Diisocyanates for in Situ Preparation of Nitrile Oxides : Preparation of Isoxazoles and Isoxazolines Requires the Use of a

Dehydrating Agent with Phenyl. *J. Org. Chem* **1998**, *63*, 5272–5274.

(33)   Trogu, E.; De Sarlo, F.; Machetti, F. Michael Additions versus Cycloaddition

Condensations with Ethyl Nitroacetate and Electron-Deficient Olefins. *Chem. - A Eur. J.*

2009, *15* (32), 7940–7948.

(34)   Guideri, L.; De Sarlo, F.; Machetti, F. Conjugate Addition versus

Cycloaddition/Condensation of Nitro Compounds in Water: Selectivity, Acid-Base

Catalysis, and Induction Period. *Chem. - A Eur. J.* **2013**, *19* (2), 665–677.

(35)   Mower, M. P.; Blackmond, D. G. Mechanistic Rationalization of Unusual Autoinductive

Kinetics in an Aqueous 1 , 3-Dipolar Cycloaddition. No. 2, 1–43.

(36)   Bernatowicz, M.; Wu, Y.; Matsueda, G. 1H-Pyrazole-1-Carboxamidine Hydrochloride:

An Attractive Reagent for Guanylation of Amines and Its Application to Peptide

Synthesis. *J. Org. Chem.* **1992**, *57*, 2497–2502.

(37)   Curran, D. P. Reduction of A2-Isoxazolines. 3.1 Raney-Nickel Catalyzed Formation of β-

Hydroxy Ketones. *J. Am. Chem. Soc.* **1983**, *105* (18), 5826–5833.

(38)   Kozikowski, A.; Ishida, H. Intramolecular [3+2] Cycloaddition Reactions in the Indole

Series "The Nitrile Oxide Route to the Ergot Alkaloids". 1. Chanoclavine I. *J.*

Am. Chem. Soc. **1980**, *102* (12), 4265–4267.

(39)   Nagireddy, J. R.; Tranmer, G. K.; Carlson, E.; Tam, W. N–O Cleavage Reactions of

Heterobicycloalkene-Fused 2-Isoxazolines. *Beilstein J. Org. Chem* **2014**, *10*, 2200–2205.

(40)   Jiang, D.; Chen, Y. Reduction of Δ 2 -Isoxazolines to -Hydroxy Ketones with Iron and

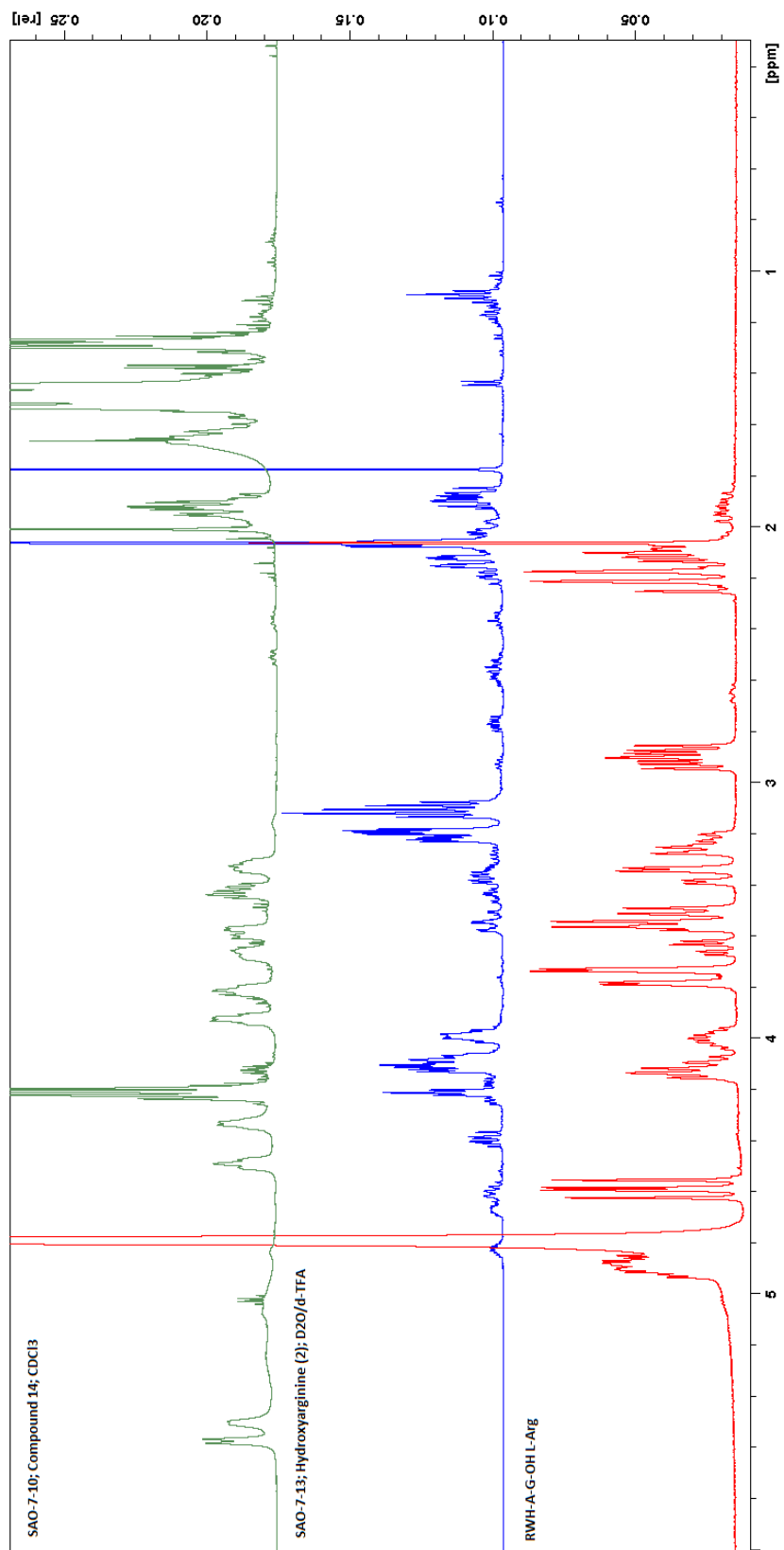Ammonium Chloride as Reducing Agent. *J. Org. Chem* **2008**, *73*, 9181–9183.

(41)   Stewart, J. M.; Young, J. D. *Solid Phase Peptide Synthesis*, 2nd ed.; Pierce Chemical
       Company: Rockford, IL, 1984.

(42)   Bergal, H. T.; Hopkins, A. H.; Metzner, S. I.; Sousa, M. C. The Structure of a BamA-
       BamD Fusion Illuminates the Architecture of the β-Barrel Assembly Machine Core.
       Structure **2016**, *24* (2), 243–251.

(43)   Hagan, C. L.; Westwood, D. B.; Kahne, D. Bam Lipoproteins Assemble BamA in Vitro.
       Biochemistry **2013**, *52* (35), 6108–6113.

(44)   Noinaj, N.; Gumbart, J. C.; Buchanan, S. K. The β-Barrel Assembly Machinery in
       Motion. *Nat. Rev. Microbiol.* **2017**, *15* (4), 197–204.

(45)   Sakai, N.; Mareda, J.; Matile, S. Artificial -Barrels. *Acc. Chem. Res* **2008**, *41* (10).

(46)   Ojima, I. Modern Molecular Approaches to Drug Design and Discovery. *Acc. Chem. Res.*
       2008, *41* (1), 2–3.

(47)   Nowick, J. S. Exploring Beta-Sheet Structure and Interactions with Chemical Model
       Systems. *Acc. Chem. Res.* **2008**, *41* (10), 1319–1330.

(48)   Pham, J. D.; Demeler, B.; Nowick, J. S. Polymorphism of Oligomers of a Peptide from β-
       Amyloid. *J. Am. Chem. Soc.* **2014**, *136* (14), 5432–5442.

(49)   Hagan, C. L.; Wzorek, J. S.; Kahne, D. Inhibition of the β-Barrel Assembly Machine by a
       Peptide That Binds BamD. *Proc. Natl. Acad. Sci. U. S. A.* **2015**, *112* (7), 2011–2016.

(50)   Xu, W.; Ren, C.; Teoh, C. L.; Peng, J.; Gadre, H.; Rhee, H.-W.; Chi-Lik, ⊥; Lee, K.;
       Chang, Y.-T. An Artificial Tongue Fluorescent Sensor Array for Identification and
       Quantitation of Various Heavy Metal Ions. *Anal. Chem.* **2014**, *86*, 8763–8769.

(51) Aragay, G.; Pons, J.; Merkoc-I, A. Recent Trends in Macro-, Micro-, and Nanomaterial-Based Tools and Strategies for Heavy-Metal Detection. *Chem. Rev.* **2011**, *1111*, 3433–3458.

(52) Järup, L. Hazards of Heavy Metal Contamination. *Br. Med. Bull.* **2003**, *68* (68), 167–182.

(53) Sensi, S. L.; Paoletti, P.; Bush, A. I.; Sekler, I. Zinc in the Physiology and Pathology of the CNS. *Nat. Rev. Neurosci.* **2009**, *10*, 780–792.

(54) Schwabacher, A.; Geissinger, P. One-Dimensional Arrays on Optical Fibers, 2007.

(55) Fenske, T.; Bathurst, B.; Schwabacher, A.; Geissinger, P.; Hagemann, T.; Oehm, S.; Henning, P. Sensor Dyes for Real-Time Sensing of Metal Ions in Aqueous Environments. WO201766672 A1, October 14, 2016.

(56) Pribil, R. Recent Developments in Chelatometry. *Analyst* **1958**, *83*, 188–195.

(57) Gough, D. S. Direct Analysis of Metals and Alloys by Atomic Absorption Spectrometry. *Anal. Chem.* **1976**, *48* (13), 1926–1930.

(58) Szurdoki, F.; Ren, D.; Walt, D. R. A Combinatorial Approach To Discover New Chelators for Optical Metal Ion Sensing. *Anal. Chem.* **2000**, *72*, 5250–5257.

(59) Radford, R. J.; Lippard, S. J. Chelators for Investigating Zinc Metalloneurochemistry. *Curr. Opin. Chem. Biol.* **2013**, *17* (2), 129–136.

(60) Keck, A.; Klein, J.; Kudlich, M.; Stolz, A.; Knackmuss, H.-J.; Mattes, R. Reduction of Azo Dyes by Redox Mediators Originating in the Naphthalenesulfonic Acid Degradation Pathway of Sphingomonas Sp. Strain BN6. *Appl. Environ. Microbiol.* **1997**, *63* (9), 3684–3690.
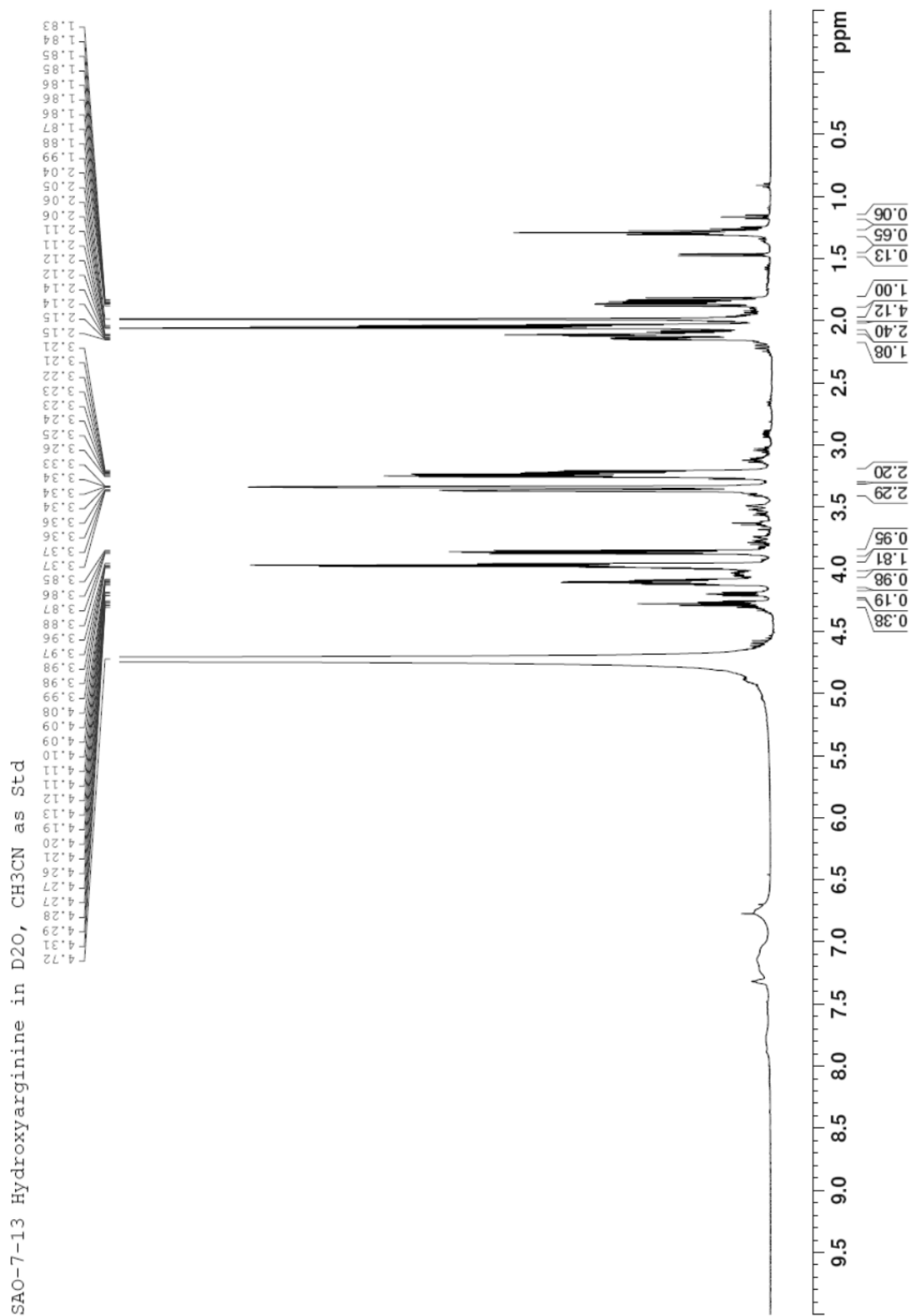
(61)   Mezohegyi, G.; Fabregat, A.; Font, J.; Bengoa, C.; Stuber, F.; Fortuny, A. Advanced

         Bioreduction of Commercially Important Azo Dyes: Modeling and Correlation with

         Electrochemical Characteristics. *Ind. Eng. Chem. Res* **2009**, *48*, 7054–7059.

(62)   Kapanidis, A. N.; Weiss, S. Fluorescent Probes and Bioconjugation Chemistries for

         Single-Molecule Fluorescence Analysis of Biomolecules. *J. Chem. Phys.* **2002**, *117* (24–

         10964), 10953.

(63)   Prince, B. J.; Schwabacher, A. W.; Geissinger, P. A Readout Scheme Providing High

         Spatial Resolution for Distributed Fluorescent Sensors on Optical Fibers. *Anal. Chem.*

         2001, *73* (5), 1007–1015.

(64)   Szurdoki, F.; Ren, D.; Walt, D. R. A Combinatorial Approach to Discover New Chelators

         for Optical Metal Ion Sensing. *Anal. Chem.* **2000**, *72* (21), 5250–5257.

(65)   Feringa, B. L. The Art of Building Small, From Molecular Switches to Motors; Univeristy

         of Wisconsin- Milwaukee, Milwaukee Wi.

(66)   Hunt, J. B.; Neece, S. H.; Ginsburg, A. The Use of 4-(2-Pyridylazo)Resorcinol in Studies

         of Zinc Release from Escherichia Coli Aspartate Transcarbamoylase. *Anal. Biochem.*

         1985, *146* (1), 150–157.

(67)   Corsini, A.; Yih, I. M.; Fernando, Q.; Freiser, H. Potentiometric Investigation of the Metal

         Complexes of 1-(2-Pyridylazo)-2-Naphthol and 4-(2-Pyridylazo)Resorcinol. *Anal. Chem.*

         1962, *34* (9), 1090–1093.

(68)   Wimpfheimer, T. A Particle in a Box Laboratory Experiment Using Everyday

         Compounds. *J. Lab. Chem. Educ.* **2015**, *3* (2), 19–21.

(69)   Ivanov, V. M.; Busev, A. I.; Nemtseva, Z. I. Ivanov-1969-Cobalt(II) Complexing with PTAR BrPTAR and QAR.Pdf. *Vestn. Mosk. Univ. Seriia Khimiia* **1969**, *24* (5), 80–85.

(70)   Mohr, G. J.; Wolfbeis, O. S. Optical Sensors for a Wide PH Range Based on Azo Dyes Immobilized on a Novel Support. *Anal. Chim. Acta* **1994**, *292* (1–2), 41–48.
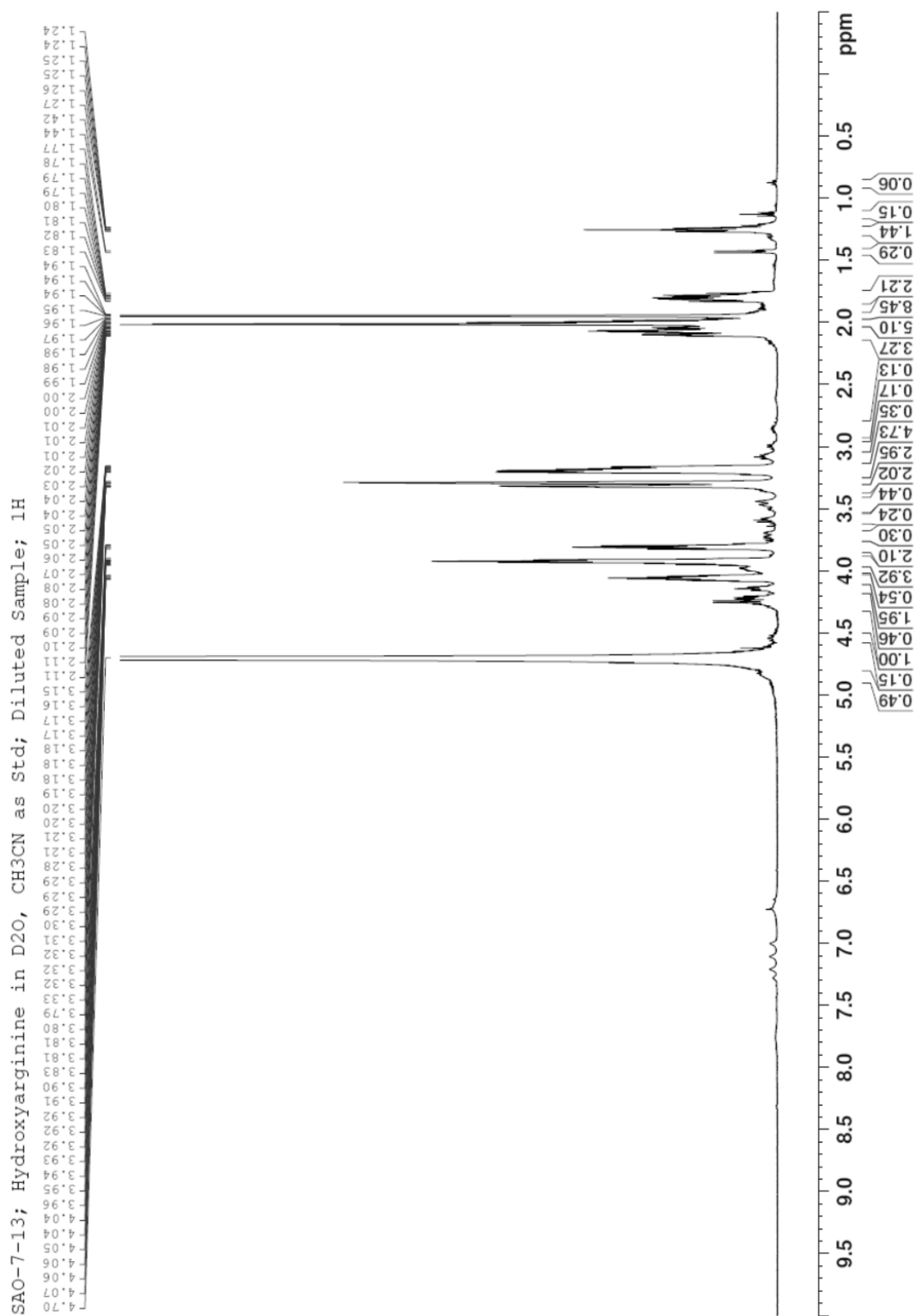
SAO-7-10; Compound 14; CDCl3

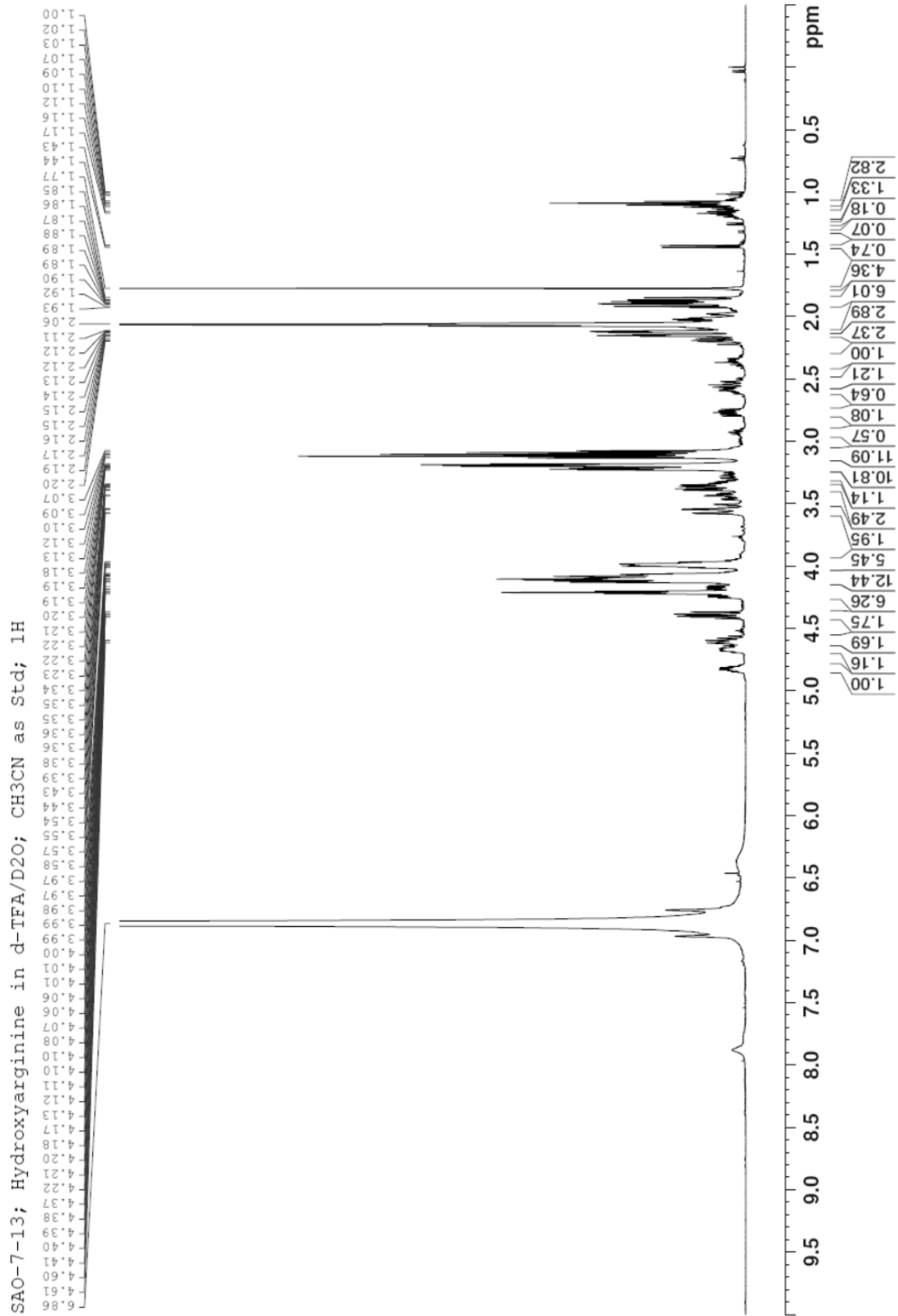SAO-7-13; Hydroxyarginine (2); D2O/d-TFA

RWH-A-G-OH L-Arg

SAO-7-13 Hydroxyarginine in D2O, CH3CN as Std

^{1}H-NMR: **2** Dilute in D2O

SAO-7-13; Hydroxyarginine in D2O, CH3CN as Std; Diluted Sample; 1H

106

^{1}H-NMR **2** in d-TFA

SAO-7-13; Hydroxyarginine in d-TFA/D2O; CH3CN as Std; 1H
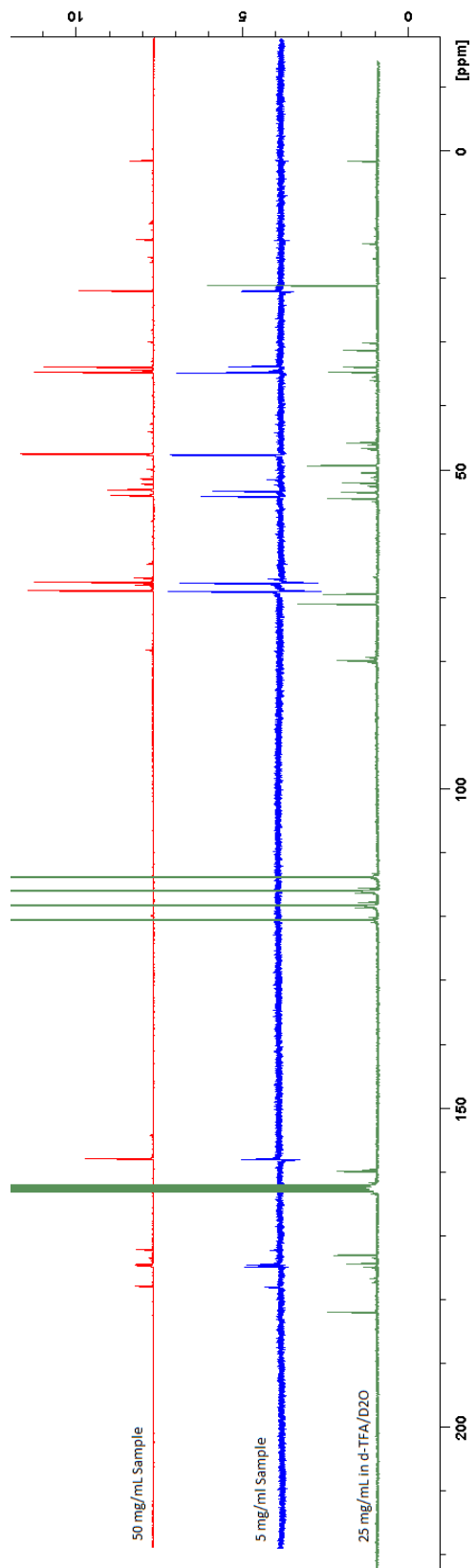
¹³C NMR **2** at Red: D₂O, Blue: Dilute D₂O, Green: dTFA

SAO-7-13 Hydroxyarginine in D2O, CH3CN as Std

0.00
9.41
9.63
9.71
9.80
10.90
12.27
12.38
12.51
15.15
15.88
20.38
22.95
26.56
27.11
28.34
30.93
31.46
31.93
32.13
32.28
32.37
32.47
32.61
32.82
32.97
33.12
33.19
33.25
34.00
36.76
36.85
39.56
41.21
41.33
42.45
43.36
44.25
44.33
45.80
45.87
45.94
46.00
46.03
46.14
46.77
48.37
49.49
49.87
50.69
51.58
52.45
56.48
58.74
58.97
63.15
65.26
65.38
65.89
66.05
66.19
66.43
66.60
66.75
67.00
67.22
67.38
67.53
76.13
76.69
76.87
77.25
89.40
118.29
152.71
152.97
156.36
156.40
168.82
170.61
171.49
171.80
171.96
172.40
172.96
173.22
174.71
176.37

SAO-7-13; Hydroxyarginine in D2O, CH3CN as Std; Diluted Sample; 13C

13.31
21.29
33.19
33.77
34.16
35.00
46.92
47.00
50.86
52.61
53.42
66.36
67.08
67.37
68.38
157.37
171.60
173.86
174.18
177.40

170 160 150 140 130 120 110 100 90 80 70 60 50 40 30 20 10 ppm

110

¹³C-NMR in dTFA **2**

COSY **2**

SAO-7-13 hydroxyarginine in D2O, CH3CN as Std; COSY

HSQC **2**

SAO-7-1.3-hydroxyarginine in D20, CH3CN as Std, HSQC 1h-13c

¹H-NMR: Isoxazoline **4** SAO-2-4Abx

SAO-2-4
Isoxazoline 4; 13C

14.13
29.42
29.94
38.64
62.18
82.33
151.48
160.65
177.76

Proton Spectrum
ethyl ester of isoxazoline ammonium chloride in DMSO with CH3CN
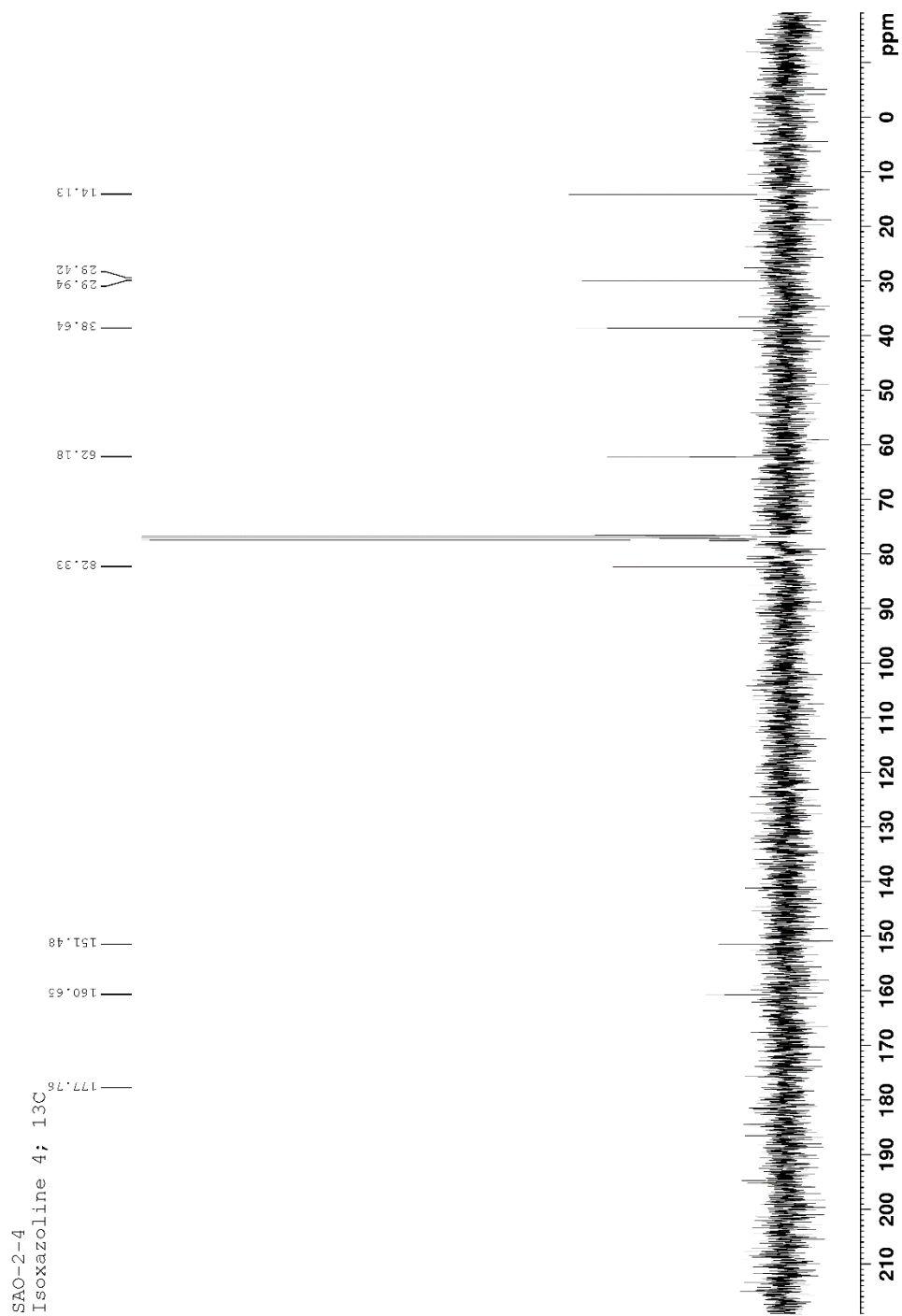
¹³C-NMR: NH3 isoxazoline ethyl ester (d6-DMSO) **5**

ethyl ester of isoxazoline ammonium chloride in DMSO with CH3CN

Current Data Parameters
NAME   SAO-5-51
EXPNO   2
PROCNO   1

F2 - Acquisition Parameters
Date_   20170525
Time   16.07
INSTRUM   spect
PROBHD   5 mm BBI 1H/19
PULPROG   zgpg30
TD   65536
SOLVENT   DMSO
NS   410
DS   0
SWH   25000.000 Hz
FIDRES   0.381470 Hz
AQ   1.3107700 sec
RG   4597.6
DW   20.000 usec
DE   6.00 usec
TE   294.2 K
D1   2.00000000 sec
d11   0.03000000 sec
DELTA   1.89999998 sec
TD0   1

====== CHANNEL f1 ======
NUC1   13C
P1   15.00 usec
PL1   -3.00 dB
SFO1   125.6697751 MHz

====== CHANNEL f2 ======
CPDPRG2   waltz16
NUC2   1H
PCPD2   100.00 usec
PL2   3.00 dB
PL12   26.26 dB
PL13   30.00 dB
SFO2   499.7319989 MHz

F2 - Processing parameters
SI   32768
SF   125.6572080 MHz
WDW   EM
SSB   0
LB   1.00 Hz
GB   0
PC   1.40

14.45

37.48
39.44
39.60
39.77
39.94
40.11
40.19
40.27
40.44
41.88

62.03

79.81

152.98

160.31

HSQC: Isoxazoline **5** SAO-5-51 exp 3

SAO-5-51, Compound 5, HSQC

^{1}H-NMR: diboc-guanidinyl Isoxazoline ethyl ester **10**

Proton Spectrum
diboc guanidinyl isoxazoline ethyl ester
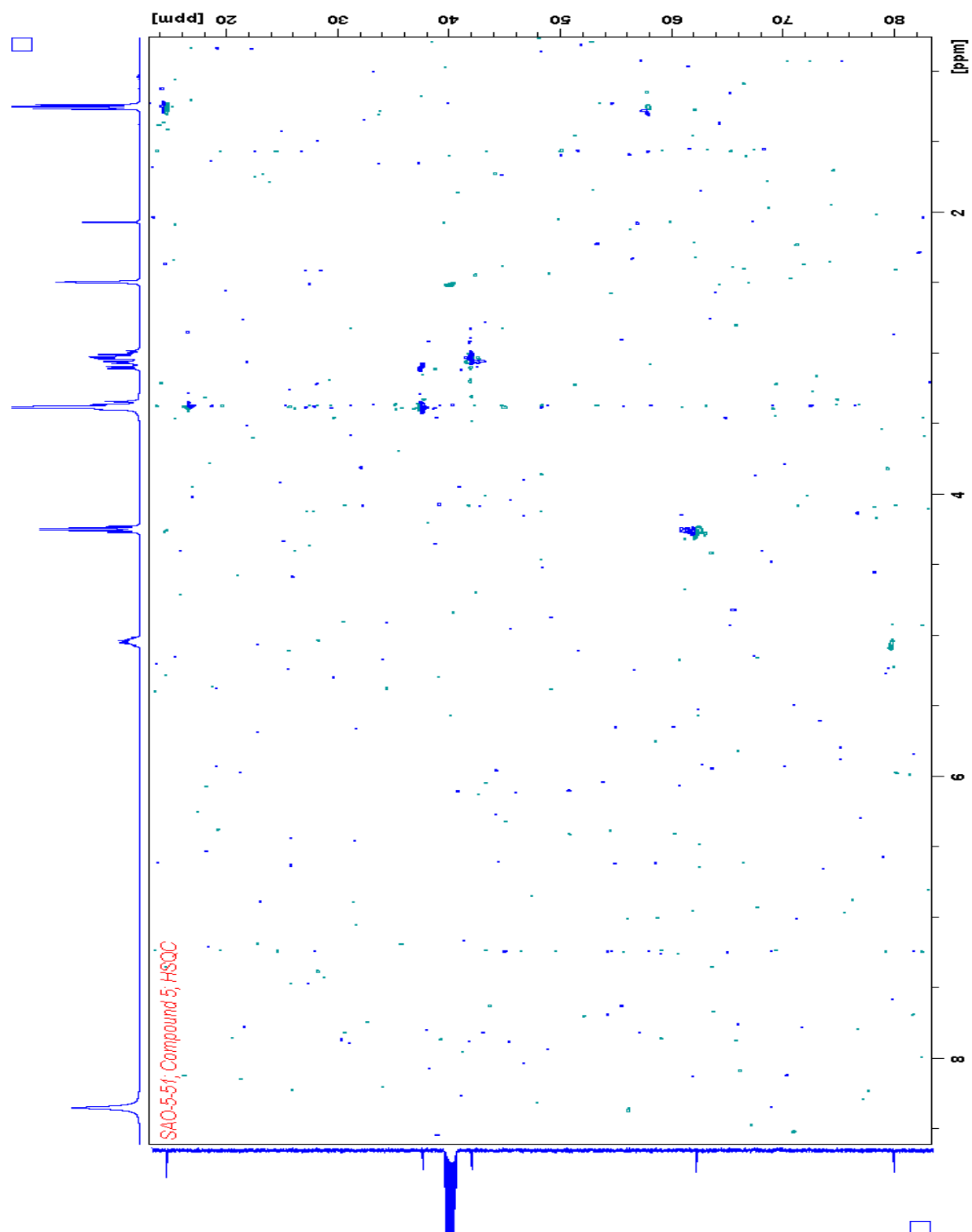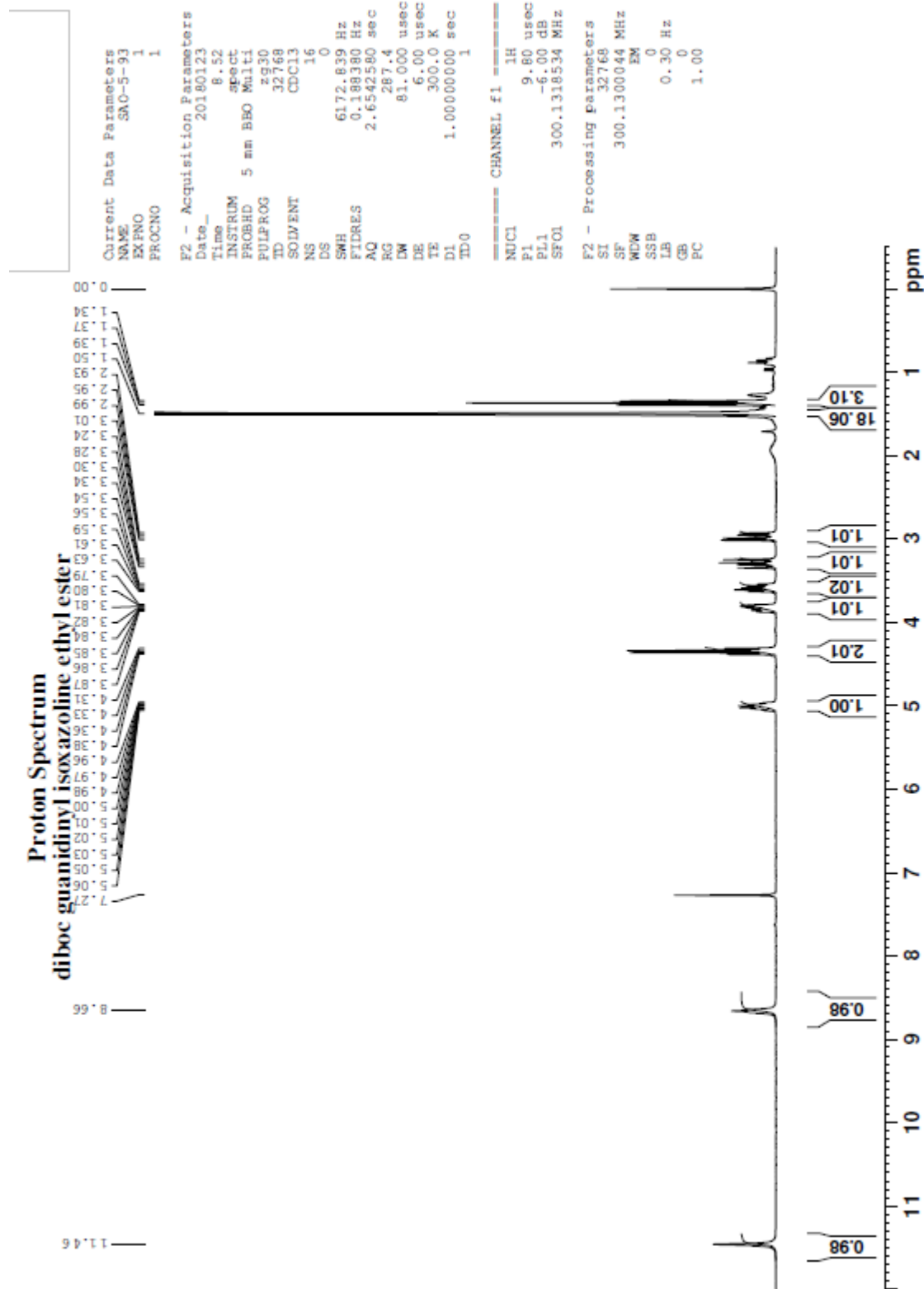
¹H-NMR: Deprotected amino Isoxazoline **11**

¹H-NMR: NaBH₄ Reduced Isoxazoline **12** SAO-2-60
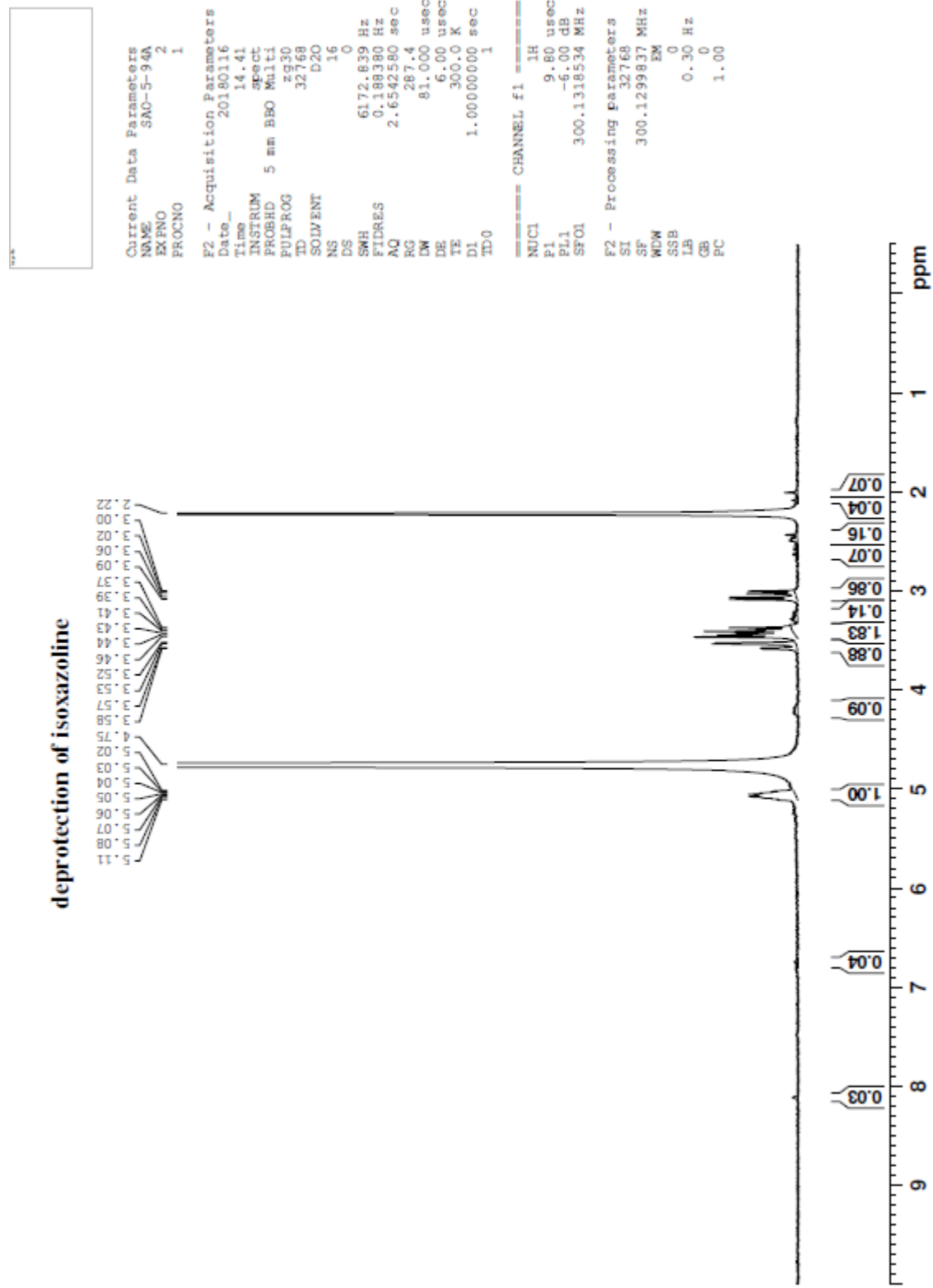
SAO-2-60
Compound 12 1H NMR Spectrum
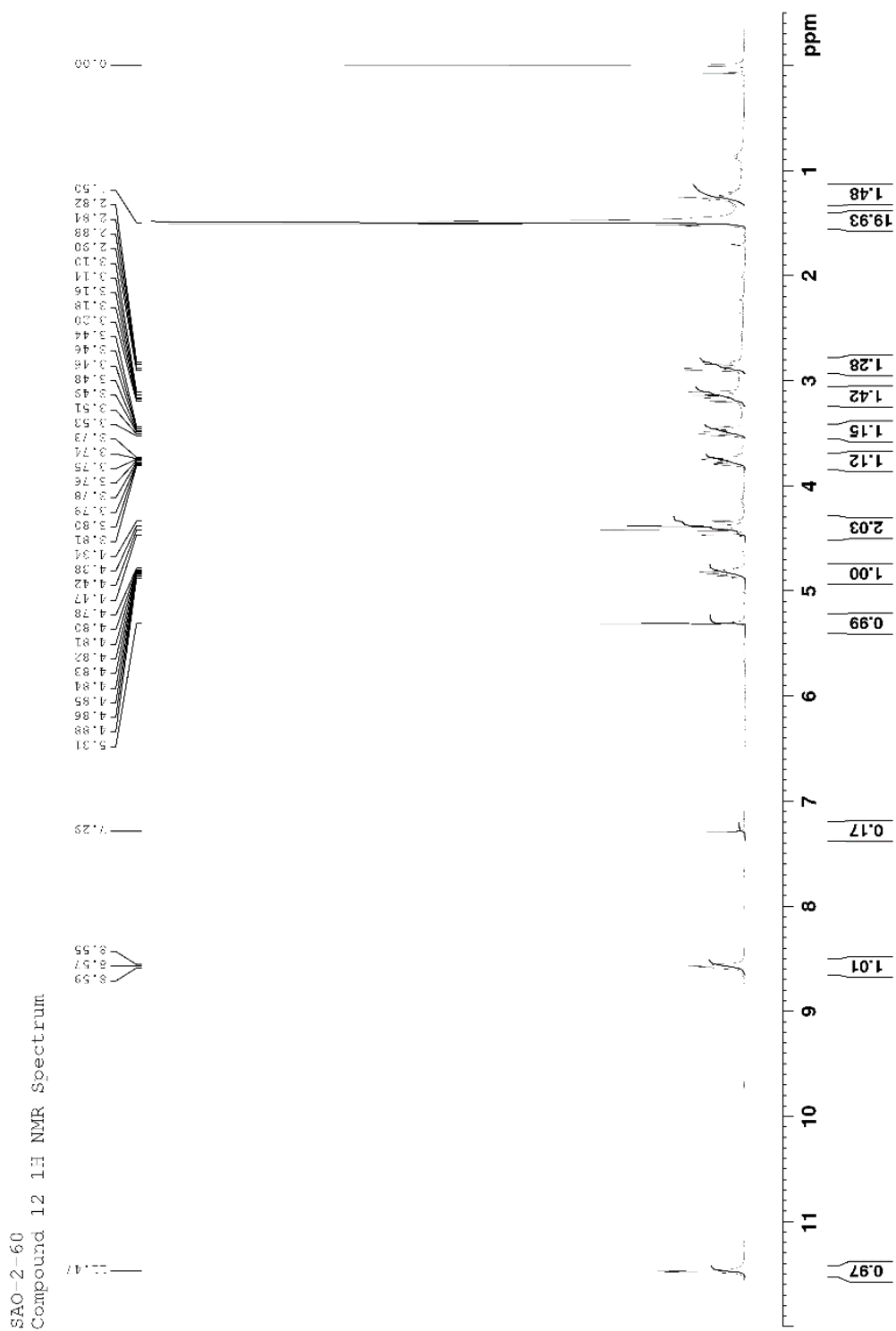
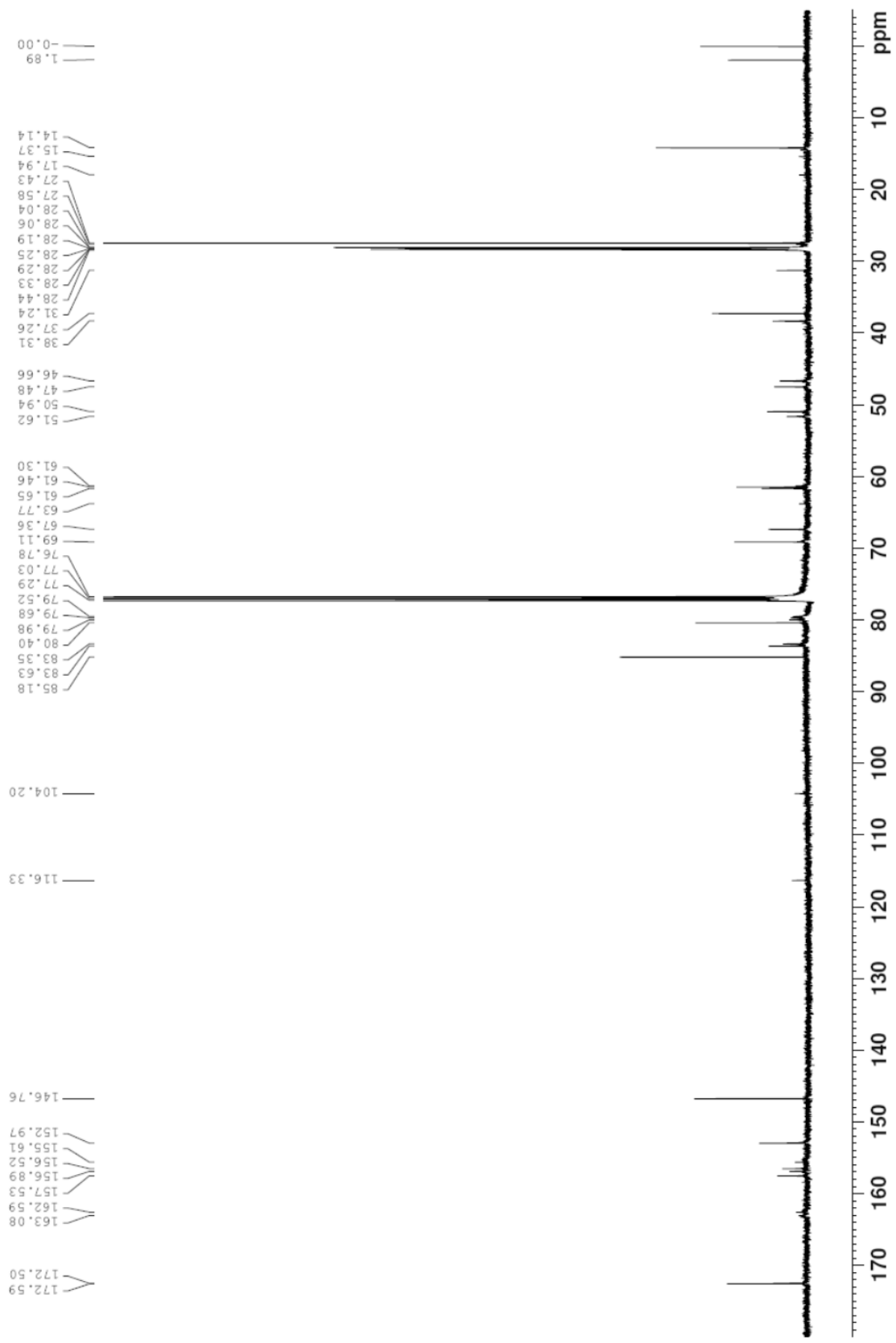# ^{13}C-NMR: NaBH$_4$ Reduced Isoxazoline **12** SAO-2-60

SAO-2-60
Compound 12; C13
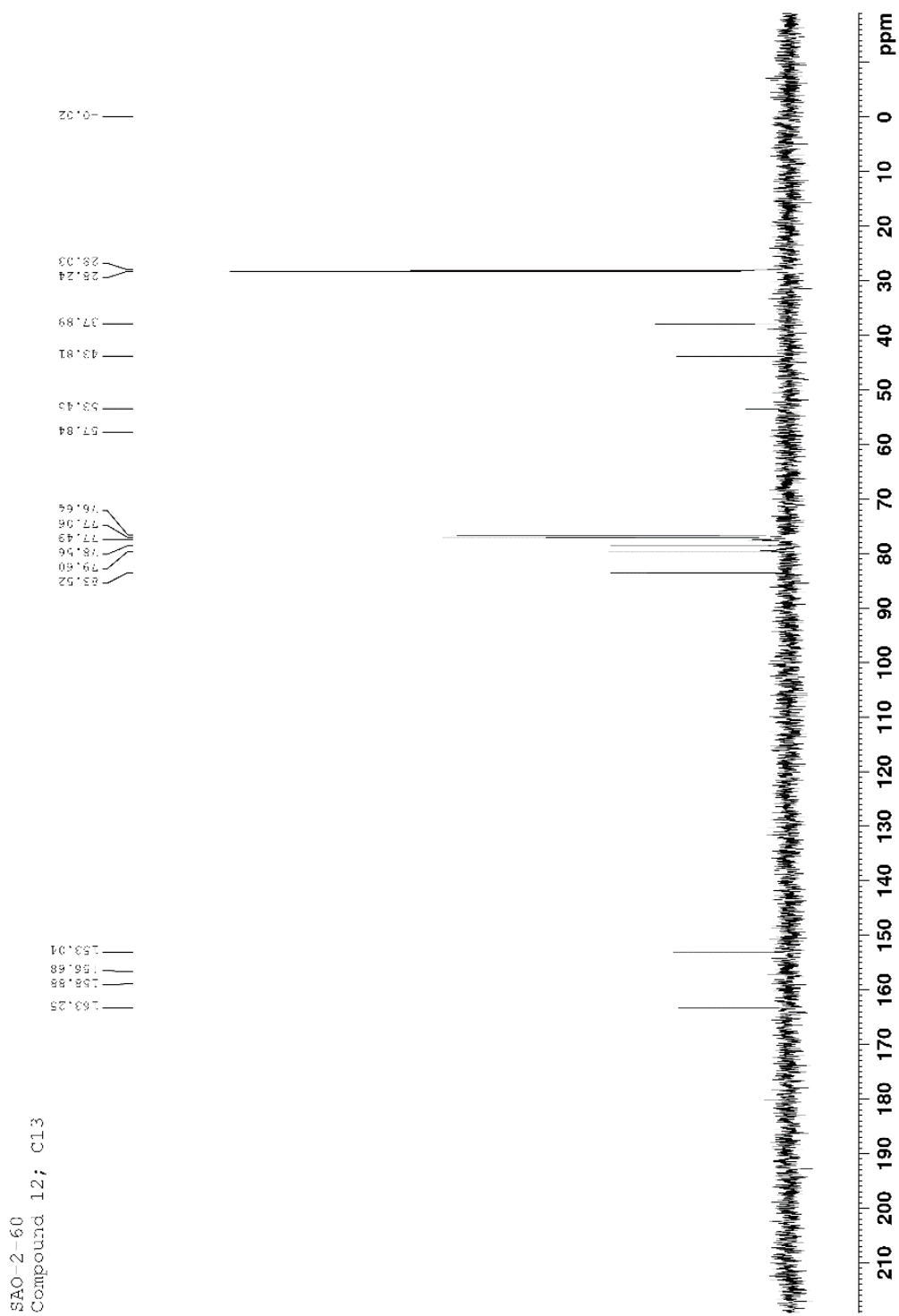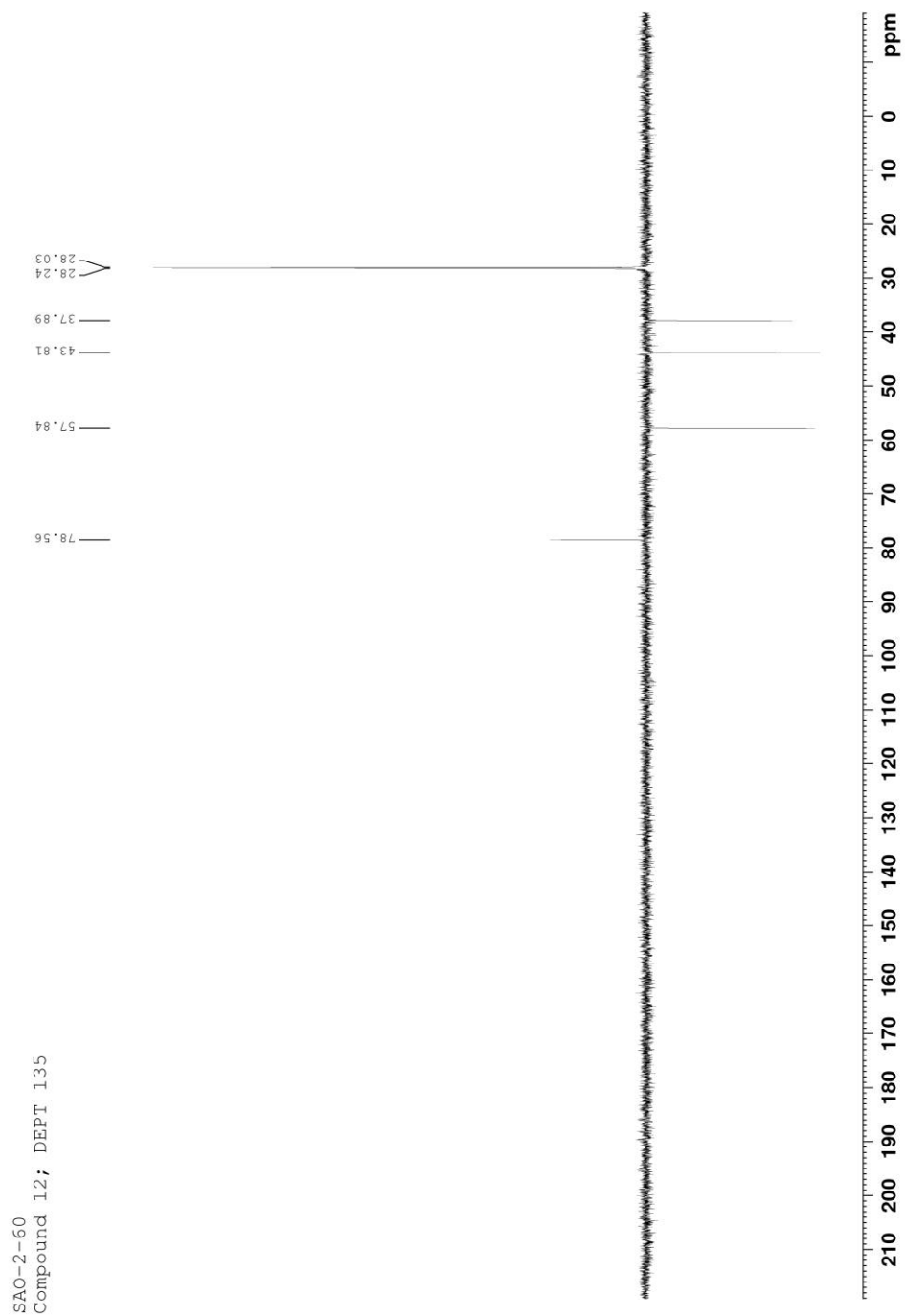
^{13}C-NMR DEPT 135: NaBH$_4$ Reduced Isoxazoline **12** SAO-2-60

123

Proton Spectrum
reduced, boc protected

124
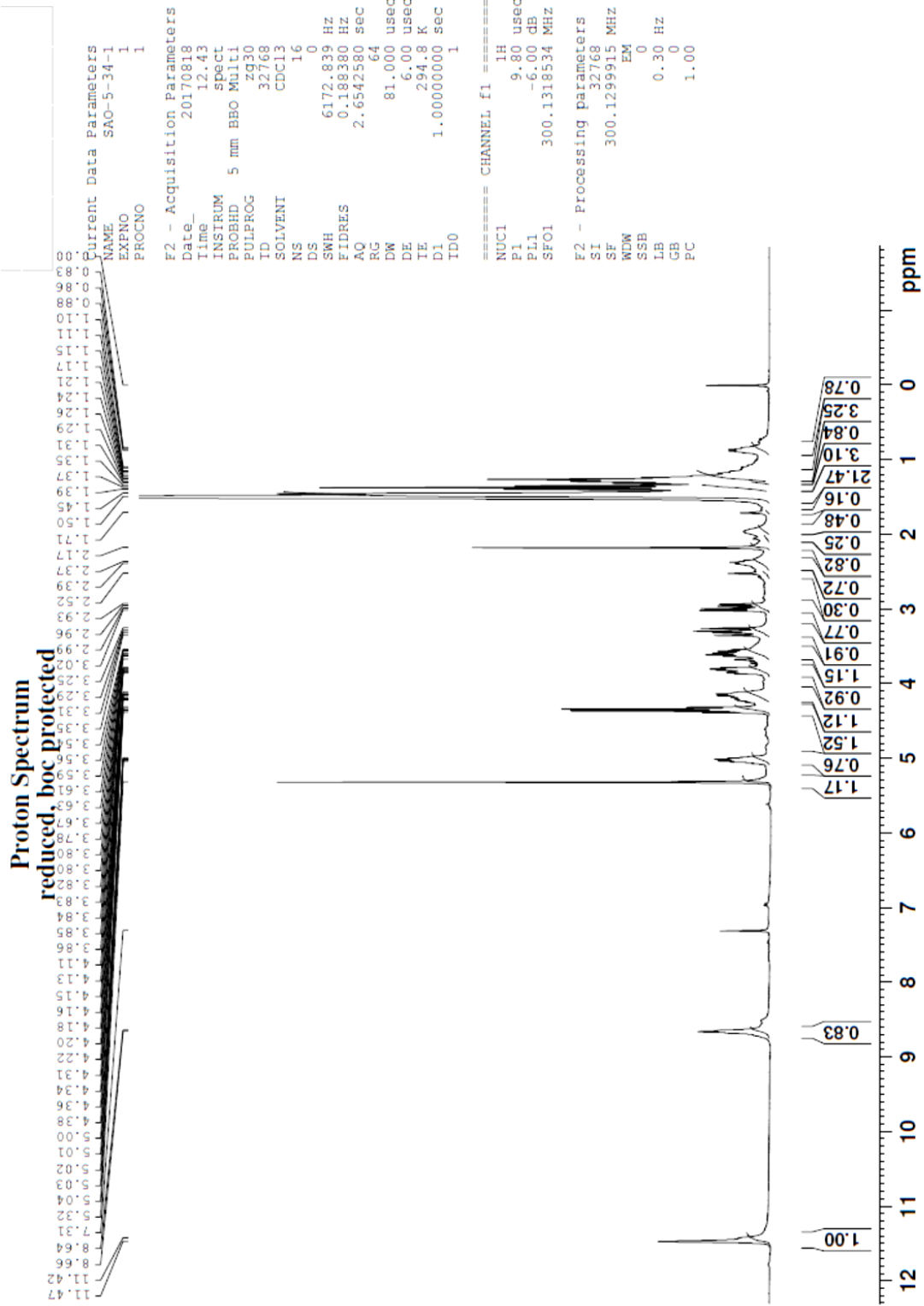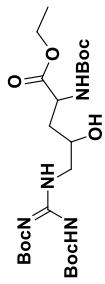
SAO-7-10; Compound 14; CDCl3; 1H

SAO-7-10; Compound 14; CDCl3; 13C

-0.00
1.89
14.14
15.37
17.94
27.43
27.58
28.04
28.06
28.19
28.25
28.29
28.33
28.44
31.24
37.26
38.31
46.66
47.48
50.94
51.62
61.30
61.46
61.65
63.77
67.36
69.11
76.78
77.03
77.29
79.52
79.68
79.98
80.40
83.35
83.63
85.18
104.20
116.33
146.76
152.97
155.61
156.52
156.89
157.53
162.59
163.08
172.50
172.59

ppm
10
20
30
40
50
60
70
80
90
100
110
120
130
140
150
160
170

126

Proton Spectrum
triboc hydroxy arginine ethyl ester

Carbon Spectrum
triboc hydroxy arginine ethyl ester

0.01

12.31
26.22
26.36
26.42
26.46
26.50
35.33
36.31
44.86
45.59
49.17
49.78
59.39
59.57
59.75
65.56
67.06
74.92
75.34
75.54
75.77
77.42
77.55
77.69
78.06
78.45
78.65
81.44
81.67

151.12
153.79
154.64
154.77
155.10
155.65
160.91
161.30
161.47
170.69
170.78

0 20 40 60 80 100 120 140 160 180 200 ppm

Mass Spectrum: tri-boc-hydroxy-arginine ethyl ester **14**

129

¹H-NMR: Aromatized-L-serine ethyl ester mono enamine **17a**
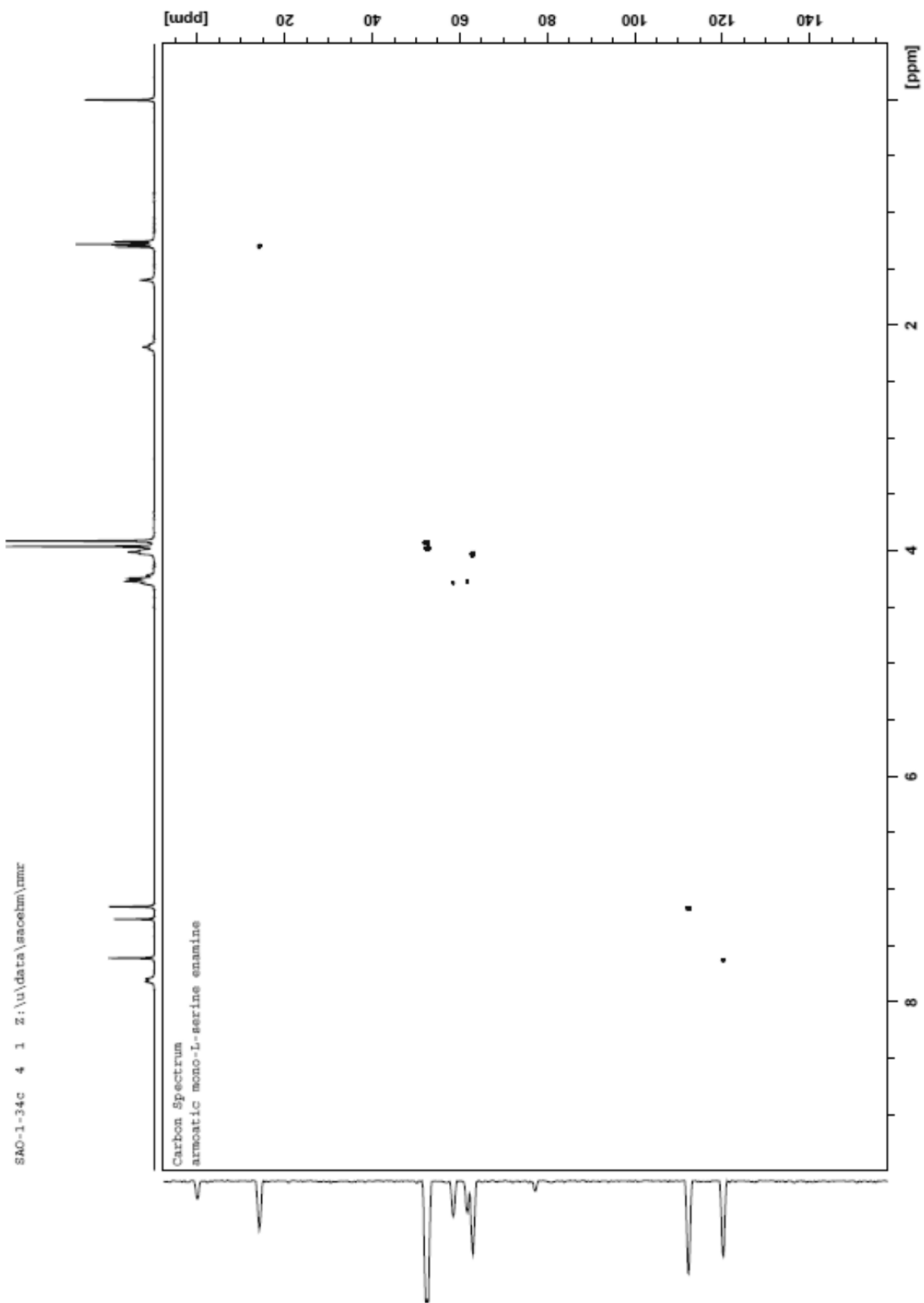

Proton Spectrum
armoatic mono-L-serine enamine
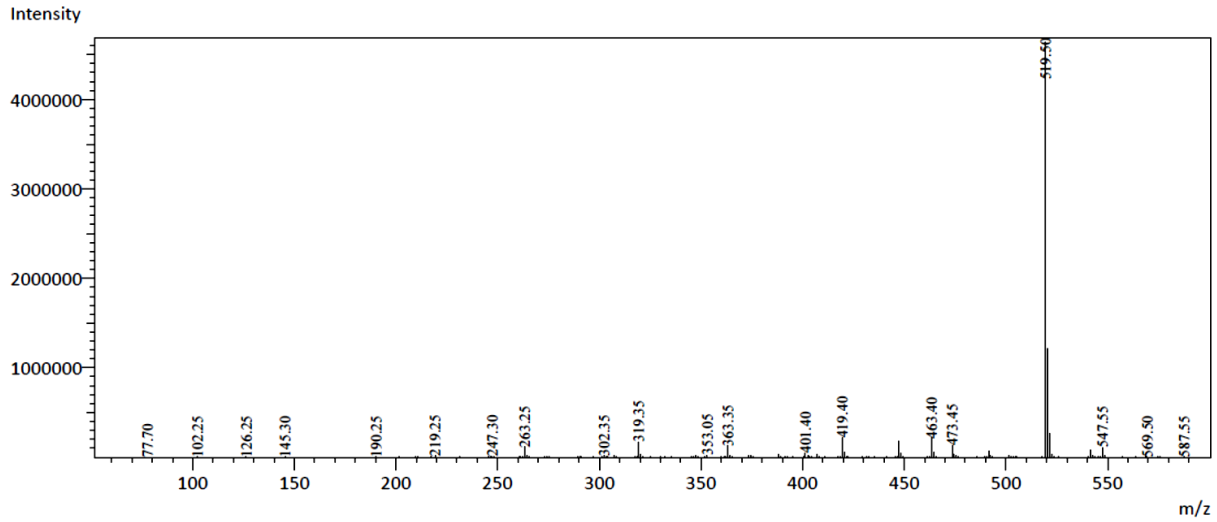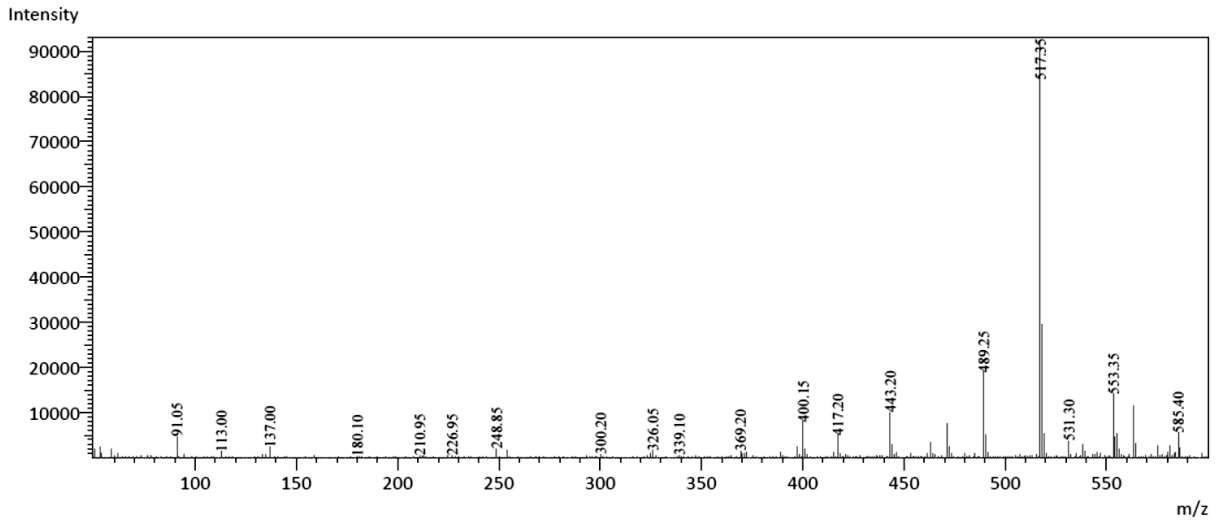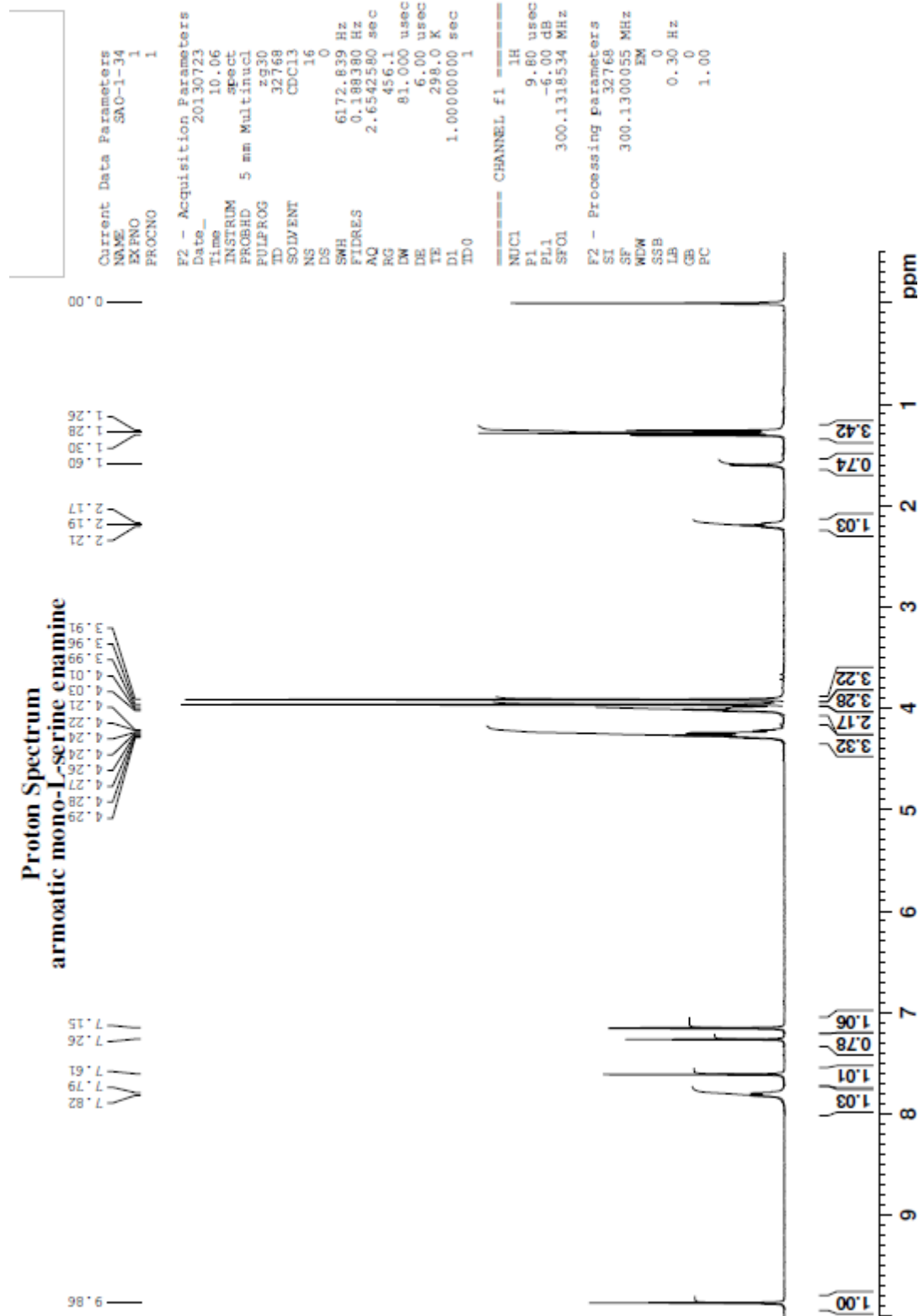
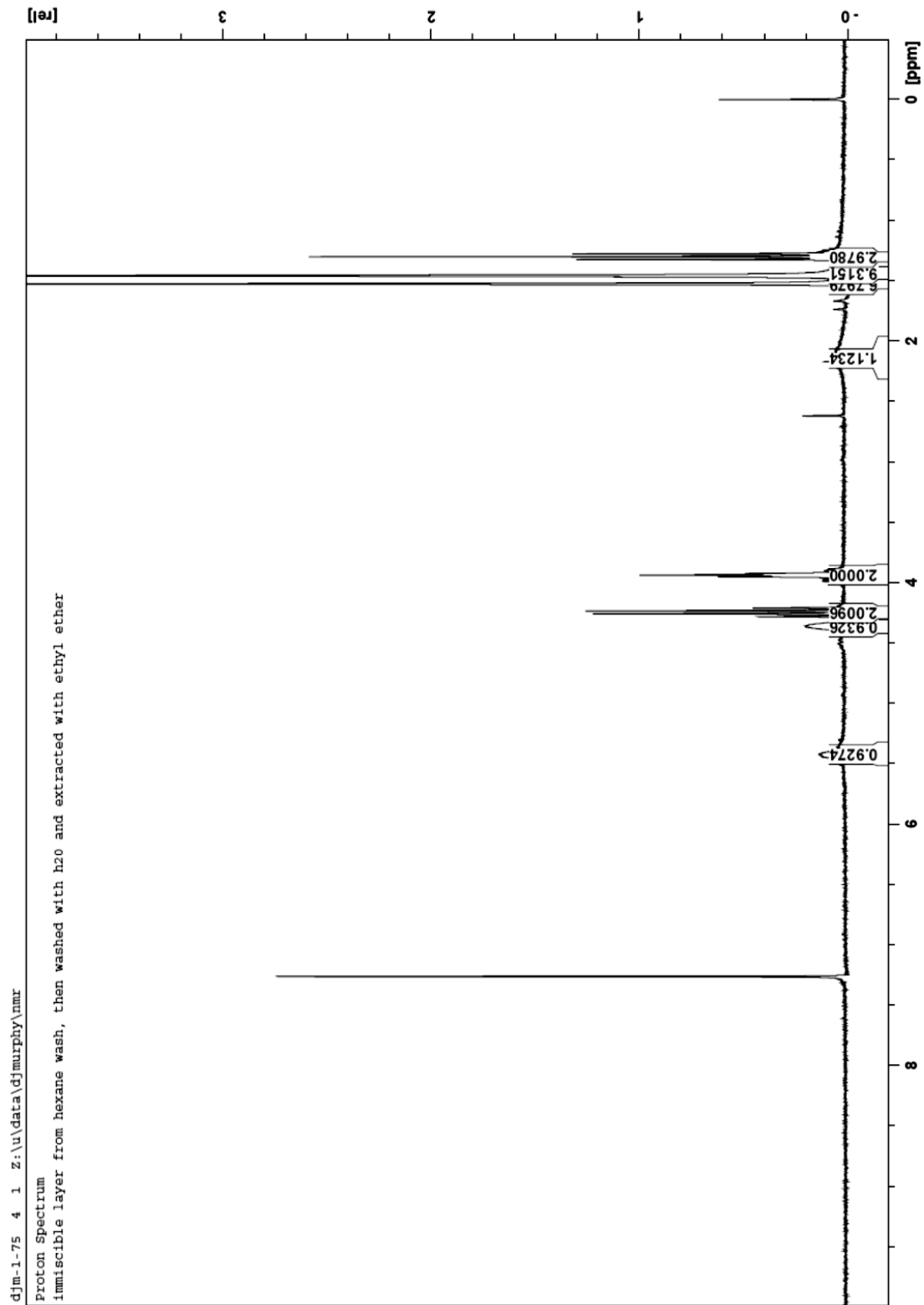¹³C-NMR: Aromatized-L-serine ethyl ester mono enamine **17a**

HSQC-NMR: Aromatized-L-serine ethyl ester mono enamine **17a**

Carbon Spectrum
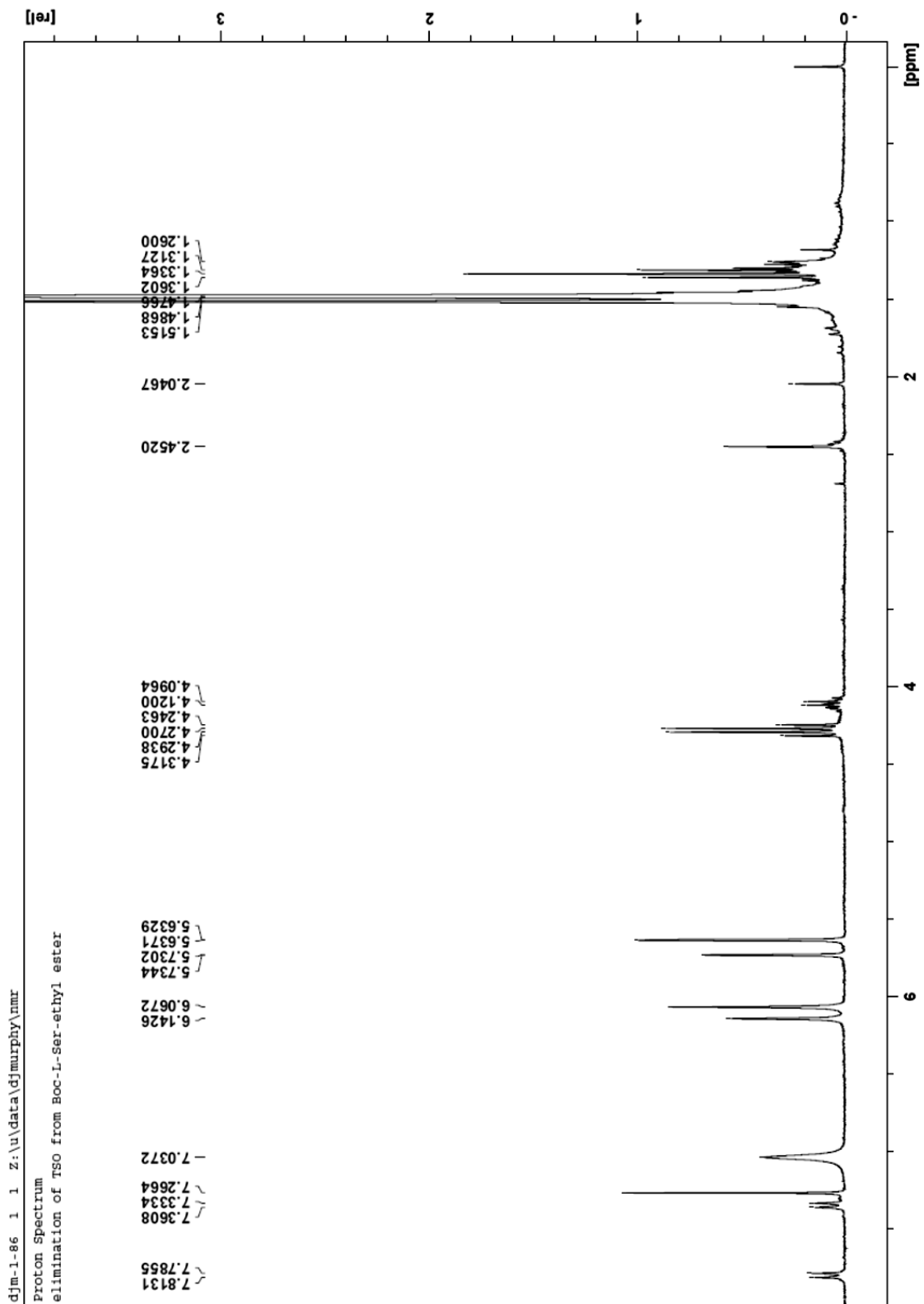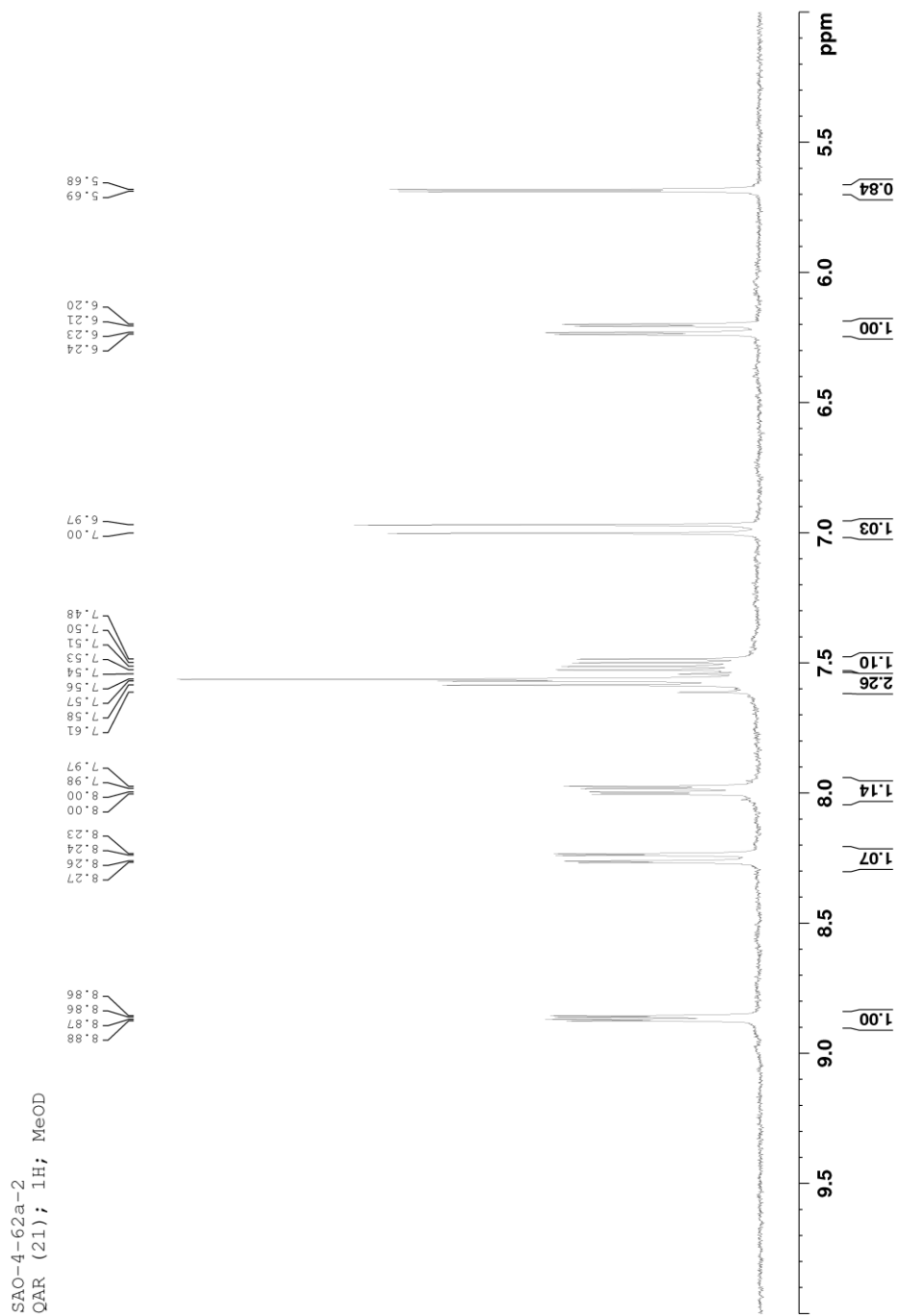armoatic mono-L-serine enamine
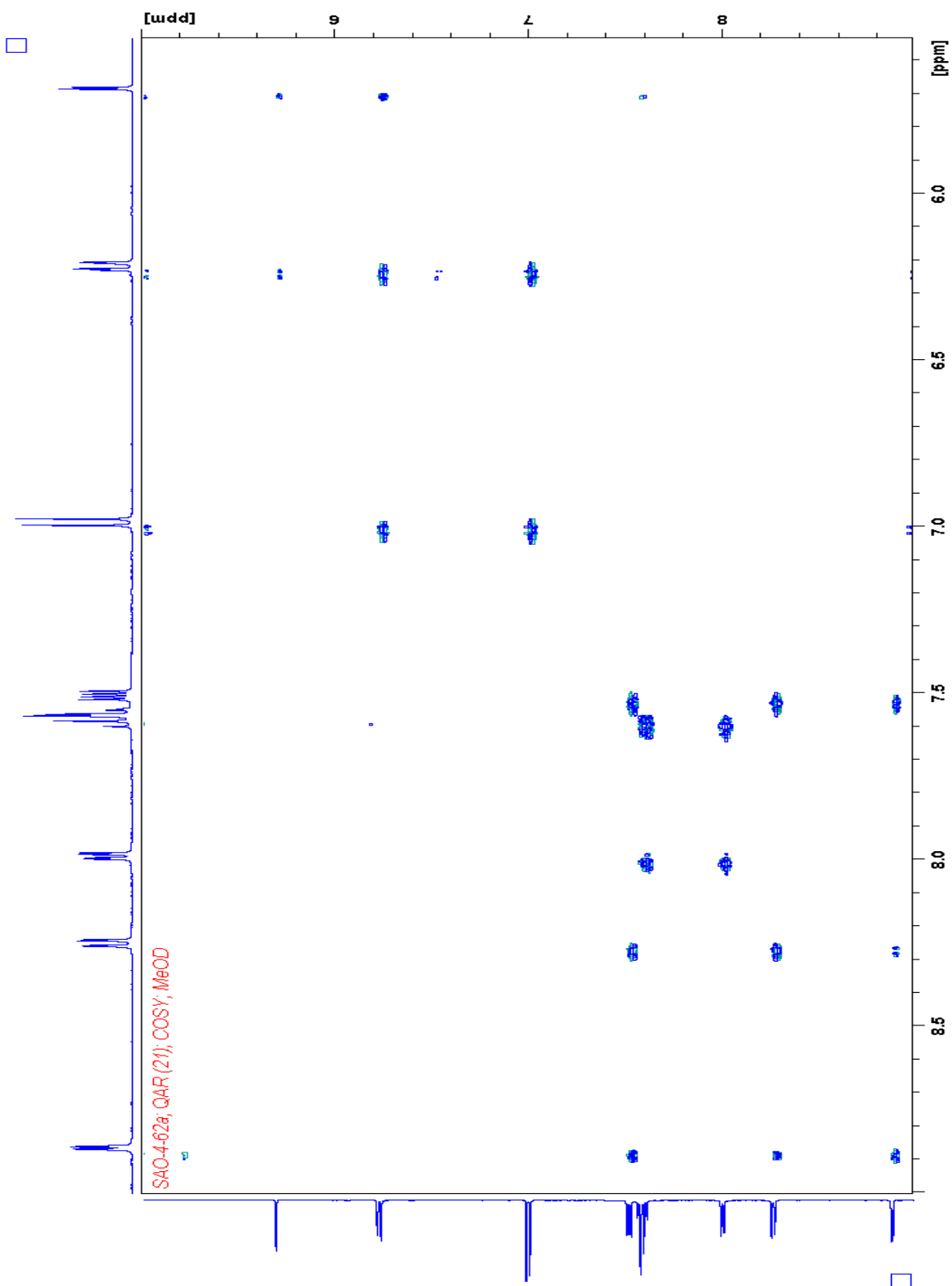
SAO-1-34c   4   1   Z:\u\data\sacehm\nmr

^{1}H-NMR: N-Boc-methylene-glycine ethyl ester **19'**

SAO-4-62a-2
QAR (21); 1H; MeOD

SAQ.4-62a, QAR (21), COSY, MeOD

Bill Watterson, Andrews McMeel Syndication

Sarah A. Oehm

Education
University of Wisconsin – Milwaukee
Doctor of Philosophy, Chemistry – Organic Chemistry and Biochemistry focused, expected May 2018
GPA: 3.927
Dissertation Title: Molecular Recognition: Non-Proteogenic Amino Acids for Antibiotic Studies and Chemosensors for Recognition and Reporting of Metal Ions
Awards:
- Gloria Moczynski Student Teacher Award, 2016
- Elected Graduate Student Senator at UW-Milwaukee Student Association
- Awarded Chemistry and Biochemistry Graduate Student Council Officer - (earned scholarship)

University of Wisconsin – Milwaukee, Milwaukee, Wisconsin
Bachelor of Science, Chemistry - (ACS Course in Chemistry), *cum laude*, 2012
GPA: 3.579
Awards:
- UWM Outstanding Senior in Chemistry and Biochemistry, 2012 - (earned scholarship)
- UWM Outstanding Student in Analytical Chemistry, 2012 - (earned scholarship)
- Chemistry Alumni Award for "New Enamine Substrate for Intramolecular Buchwald-Hartwig Indole Synthesis" Research Poster, Spring 2012 - (earned scholarship)
- Greater Milwaukee Foundation Alice C. Helland Scholarship for Women in Science, 2011-2012
- Undergraduate Research Fellowship 2010, 2011

University of Wisconsin – Fond du Lac, Fond du Lac, WI
Associate of Arts and Science, Chemistry, 2010
Awards:
- Commencement Speaker, UW-Fond du Lac Graduation, 2010
- American Chemical Society Scholastic Achievement Award, 2010

Experience
Accelerated Analytical Labs, Milwaukee, WI
Consultant, June 2017- Present
- Optimization of analyte extraction procedures
- Separation and quantitation of analytes using Liquid Chromatography – Mass Spectrometry

University of Wisconsin – Milwaukee, Milwaukee, WI
Graduate Research Assistant, 2013 - Present
- Synthesis, analysis, and characterization of small molecules and polymers
- Literature review and contributing author on patent, grants, and academic publications
- Group Safety Representative responsible for lab safety, training, documentation and compliance
- Inventory management and purchasing

Teaching Assistant, 2010 – Present
- Developed curricula in organic chemistry, implementation of new supplemental instruction
- Experienced instructor in laboratory and lecture formats

Undergraduate Research Assistant, 2009-2012
- Synthesis of natural products, method development in catalysis

Patents & Publications

- Han, L.; Vuksanovic, N.; Oehm, S.; Fenske, T.; Schwabacher, A.; Silvaggi, N., "Streptomyces wadayamensis MppP is a PLP-Dependent Oxidase, Not an Oxygenase." Biochemistry. 2018, Article ASAP. DOI: 10.1021/acs.biochem.8b00130

- Bathurst, Fenske, Geissinger, Hagemann, Henning, Oehm, and Schwabacher. "Sensor Dyes for Real-Time Sensing of Metals in Aqueous Environments." US patent WO 2017066672 A1. 2016.

- Todd, R.; Huisman, M.; Uddin, N.; Oehm, S.; Hossain, M., "One-Pot Enantioselective Synthesis of Tryptophan Derivatives via Phase-Transfer Catalytic Alkylation of Glycine Using a Cinchona-Derived Catalysts." Synlett., 2012, 23, 2687-2691. DOI: 10.1055/s-0032-1317382

Speaking Engagements

- "Monitoring Metal Pollutants in Waste Water" Research Lunch Talks with Nobel Laureate Ben Feringa, Milwaukee, WI, Fall 2017.

- "Monitoring Metal Pollutants in Waste Water" Presented original research to general audience at Wisconsin Science Fest, Milwaukee, WI, Spring 2017.

- "Lipopolysaccharide Transport Proteins: A 'Molecular Pez Dispenser' and Potential Antibiotic Target" Chemistry and Biochemistry Department Seminar, Milwaukee, WI, Fall 2014.

- Presented research posters at National Conference of Undergraduate Research in Ithaca, NY 2011 and Ogden, UT 2012.

Publications in Preparation

- **Oehm, S.,** Eggert, M., Silvaggi, N., Schwabacher, A., "Oxidized Arginine Derivatives: Intermediates on Pathways to Enduracididine." *Manuscript in Preparation.*

- **Oehm, S.**, Hagemann, T., Henning, P., Fenske, T., Labeots, J., Geissinger, P., Schwabacher, A., "Design, Synthesis, and Binding of a New Set of Metal-Selective Azo Dyes." *Manuscript in Preparation.*